ธรณีวิทยาเชิงโครงสร้างในพื้นที่อำเภอวังน้ำเขียว จังหวัดนครราชสีมา

นายถิรวุฒิ ณ ลำปาง



วิทยานิพนธ์นี้เป็นส่วนหนึ่งของการศึกษาตามหลักสูตรปริญญาวิทยาศาสตรมหาบัณฑิต
สาขาวิชาธรณีวิทยา ภาควิชาธรณีวิทยา
คณะวิทยาศาสตร์ จุฬาลงกรณ์มหาวิทยาลัย
ปีการศึกษา 2558

# STRUCTURAL GEOLOGY IN AMPHOE WANG NAM KHIAO AREA, CHANGWAT NAKHON RATCHASIMA

Mr. Tirawut Na Lampang


A Thesis Submitted in Partial Fulfillment of the Requirements
for the Degree of Master of Science Program in Geology
Department of Geology
Faculty of Science
Chulalongkorn University
Academic Year 2015

| | |
|---|---|
| Thesis Title | STRUCTURAL GEOLOGY IN AMPHOE WANG NAM KHIAO AREA, CHANGWAT NAKHON RATCHASIMA |
| By | Mr. Tirawut Na Lampang |
| Field of Study | Geology |
| Thesis Advisor | Assistant Professor Pitsanupong Kanjanapayont, Dr.rer.nat. |

Accepted by the Faculty of Science, Chulalongkorn University in Partial Fulfillment of the Requirements for the Master's Degree

.....Dean of the Faculty of Science
(Associate Professor Polkit Sangvanich, Ph.D.)

THESIS COMMITTEE

.....Chairman
(Professor Montri Choowong, Ph.D.)

.....Thesis Advisor
(Assistant Professor Pitsanupong Kanjanapayont, Dr.rer.nat.)

.....Examiner
(Assistant Professor Vichai Chutakositkanon, Ph.D.)

.....Examiner
(Sukonmeth Jitmahantakul, Ph.D.)

.....External Examiner
(Assistant Professor Krit Won-in, Ph.D.)

ถิรวุฒิ ณ ลำปาง : ธรณีวิทยาเชิงโครงสร้างในพื้นที่อำเภอวังน้ำเขียว จังหวัดนครราชสีมา (STRUCTURAL GEOLOGY IN AMPHOE WANG NAM KHIAO AREA, CHANGWAT NAKHON RATCHASIMA) อ.ที่ปรึกษาวิทยานิพนธ์หลัก: ผศ. ดร.พิษณุพงศ์ กาญจนพยนต์, 120 หน้า.

วิวัฒนาการทางธรณีวิทยาแปรสัณฐานในอดีตบริเวณพื้นที่ศึกษาส่งผลทำให้เกิดลักษณะธรณีวิทยาเชิงโครงสร้างปรากฏ ในบริเวณพื้นที่อำเภอวังน้ำเขียว ซึ่งตั้งอยู่ระหว่างแผ่นทวีปสืบูมาสุแผ่นทวีปสุโขทัย-จันทบุรี และแผ่นทวีปอินโดไชน่า การลำดับชั้นหินในพื้นที่ศึกษา จากหินที่มีอายุแก่กว่าไปอายุอ่อนกว่า สามารถจำแนกออกเป็นห้ากลุ่ม ประกอบด้วย หินตะกอนยุคเพอร์เมียน หินตะกอนภูเขาไฟยุคเพอร์โม-ไทรแอสซิก หินอัคนีแทรกซอนยุคไทรแอสซิก หินฮอร์นเบลนด์แกรนิตยุคไทรแอสซิก และหินตะกอนชุดโคราชมหายุคมีโซโซอิก ธรณีวิทยาเชิงโครงสร้าง ริ้วขนาน การวางตัวของหิน ถูกนำมากำหนดตำแหน่งในตาข่ายสเตอริโอร่วมกับการลำดับชั้นหิน แสดงถึงแนวการวางตัวของหินสองกลุ่ม กลุ่มแรกประกอบด้วย หินตะกอนยุคเพอร์เมียน หินตะกอนภูเขาไฟยุคเพอร์โม-ไทรแอสซิก หินแกรนิตยุคไทรแอสซิกบริเวณตะวันออกเฉียงเหนือในพื้นที่ศึกษา และหินฮอร์นเบลนด์แกรนิตยุคไทรแอสซิก มีการวางตัวในแนวตะวันออกตะวันออกเฉียงเหนือ-ตะวันตกตะวันตกเฉียงใต้ ตะวันออกตะวันออกเฉียงใต้-ตะวันตกตะวันตกเฉียงเหนือ จนถึงตะวันออกเฉียงเหนือ-ตะวันตกเฉียงใต้ กลุ่มที่สอง ประกอบด้วยหินอัคนีแทรกซอนแกรนิตยุคไทรแอสซิกบริเวณตะวันตกเฉียงใต้ในพื้นที่ศึกษา และหินตะกอนชุดโคราช มหายุคมีโซโซอิก ซึ่งวางตัวในแนว ตะวันตกเฉียงเหนือ-ตะวันออกเฉียงใต้ การศึกษาโครงสร้างจุลภาค แสดงการเปลี่ยนลักษณะของหินเป็นแบบเปราะ และแบบยืดหยุ่น ผลจากการวิเคราะห์วางตัวของหินประกอบกับการลำดับชั้นหินในพื้นที่ศึกษา แสดงการเกิดการการเปลี่ยนลักษณะสอง ครั้ง โดยการเปลี่ยนลักษณะครั้งแรก ($D_1$) ทำให้เกิดชั้นหินคดโค้ง ($F_1$) วางตัวในแนวตะวันออกตะวันออกเฉียงเหนือ-ตะวันตกตะวันตกเฉียงใต้ ตะวันออกตะวันออกเฉียงใต้ ตะวัน-ตกตะวันตกเฉียงเหนือ จนถึงตะวันออกเฉียงเหนือ-ตะวันตกเฉียงใต้ และการเปลี่ยนลักษณะครั้งที่สองเกิดการคดโค้งซ้อนทับ ของการแปรสภาพครั้งที่สอง ($D_2$) ทำให้เกิดชั้นหินคดโค้งในแนวที่สอง ($F_2$) ตะวันตกเฉียงเหนือ-ตะวันออกเฉียงใต้ และเกิดเป็นโครงสร้างที่มีลักษณะเป็นโดมและแอ่งปรากฏในพื้นที่อำเภอวังน้ำเขียว

ภาควิชา ธรณีวิทยา ลายมือชื่อนิสิต .....

สาขาวิชา ธรณีวิทยา ลายมือชื่อ อ.ที่ปรึกษาหลัก .....

ปีการศึกษา 2558

# # 5771994523 : MAJOR GEOLOGY

KEYWORDS: STRUCTURAL GEOLOGY / MICROSTRUCTURES / AMPHOE WANG NAM KHIAO

TIRAWUT NA LAMPANG: STRUCTURAL GEOLOGY IN AMPHOE WANG NAM KHIAO AREA, CHANGWAT NAKHON RATCHASIMA. ADVISOR: ASST. PROF. PITSANUPONG KANJANAPAYONT, Dr.rer.nat., 120 pp.

Tectonic evolution in study area all along had been effected to bring about the apparent geological structure in Amphoe Wang Nam Khiao Area, where situated between the Sibumasu terrane, the Sukhothai-Chanthaburi terrane and the Indochina terrane. The rocks stratigraphy in study area in term of age form older to younger can be recognized to be five groups, including the Permian sedimentary rocks, the Permo-Triassic volcanic rocks, the Triassic Intrusive rocks in NE part of the study area, the Triassic hornblende granite and the Mesozoic in the Khorat group. Structural geology studies by measuring the orientations of apparent structure in outcrops such as foliations, bedding which plotted in stereonet diagrams and complied with stratigraphy, suggests two groups of trend. The first group includes the Permian sedimentary rocks, the Permo-Triassic volcanic rocks, some part of the Triassic intrusive rocks and the hornblende granite illustrated trend ENE-WSW to ESE-WNW and NE-SW. The second group consists of the Triassic intrusive rocks in SW part of the study area illustrated NW-SE orientation trends. Microstructures study further show evidence of brittle and ductile deformation mechanism. The orientations analysis of structural geology obtain and stratigraphy from the study area are indicated two deformations, as a result the former deformation ($D_1$) generated first fold ($F_1$) in ENE-WSW to ESE- WNW and NE-SW directions. The first fold was superimposed by the later deformation ($D_2$) generated second fold ($F_2$) in NW-SE direction. The resulting of two deformations caused structure like dome and basin apparent in Amphoe Wang Nam Khiao Area.



| | | | |
|---|---|---|---|
| Department: | Geology | Student's Signature | ..... |
| Field of Study: | Geology | Advisor's Signature | ..... |
| Academic Year: | 2015 | | |

# ACKNOWLEDGEMENTS

This thesis would not be all over and done with if the author did not have supports from persons and organizations. The author would like to express his gratitude to persons and organizations who supported everything in this thesis.

The first of all, the author would like to thank to my family who help financial for my study in master's degree and budget for field works. Mr. Somkiat and Mrs. Pailin Na Lampang, who have been exemplary persons and being his role model moreover they are inspiration for his life. Miss Jirattikarn Na Lampang is his younger sister, who gives encouragement. The author's proud to be a member in his family.

On the other hand his adviser, Assistant Professor Dr. Pitsanupong Kanjanapayont from Department of Geology, Chulalongkorn University who advices in structural geology and gives an opportunity him to study microstructures and including students master's degree and staff. It's really appreciated.

In addition the author obliged to Mr. Noppadol Poomvises director of geology division, office of Topographical and geotechnical survey the royal irrigation department who give an change to him. The author's really appreciate that.

Finally, the author would like to thank to the participant who do not mention and Department of Geology, Faculty of Science, Chulalongkorn University.

**CONTENTS**

Page

Page

Page

# LIST OF FIGURES

**Figure** **page**

# GLOSSARY

| | | |
|---|---|---|
| Ban | = | Village |
| Amphoe | = | District |
| Changwat | = | Province |
| Permo-Triassic | = | Boundary of the Permian and Triassic periods together or the system of rocks deposited during them |
| PPL | = | Plane polarized light |
| CPL | = | Cross polarized light |
| NW-SE | = | Northwest-southeast |
| NE-SW | = | Northeast-southwest |
| ENE-WSW | = | East northeast-west southwest |
| ESE-WNW | = | East southeast-west northwest |
| ID12 | = | Identity outcrop and number |
| L1 | = | Location of photograph under the same thin section. |

# CHAPTER I
## INTRODUCTION

### 1.1 Preface

Structural geology in Amphoe Wang Nam Khiao, Changwat Nakhon Ratcahasima at the southwestern part of the Khorat plateau has a complex feature, because this area has evidence of fold and thrust appear on outcrops in study area. Study area situates between the Sibumasu terrane, the Sukhothai-Chanthaburi terrane and the Indochina terane (Metcalfe, 2013). Stratigraphy within of the study area consists of Permian rocks to Triassic rocks that are surrounded by the Mesozoic Khorat group. Permian rocks in study area are a member of Saraburi group. Also landform and structural geology reflect tectonic evolution of opening and closing of Tethyan oceans in the past. Tethyan oceans were separated from the Gondwanaland to be three scenarios. These events include the formation of Palaeo-Tethys (Devonian-Triassic), Meso-Tethys (Late Early Permian-Late Cretaceous) and Ceno-Tethys (Late Triassic-Late Cretaceous). These Tethys illustrated in sutures in Southeast Asia present-day. During closed the Palaeo-Ththys conduce to collision among the Sibumasu terrane with the Sukhothai Arc and the Indochina terrane (Metcalfe, 2013). In Permian, Indochina terrane rifted before the Indosinian orogeny. Results from collision of these terranes are illustrated major trends of the structural geology approximately N-S direction. Rifting of the Indochina terrane in Permian before the Indosinian orogeny (Booth and Sattayarak, 2011) generated structure trends in ENE-WSW, ESE-WNW to NE-SW directions. Trend NW-SE direction from an effect in The Cenozoic strike-slip faults in Permian rocks (Arboit et al., 2014; Morley et al., 2013; Ridd, 2012; Ridd and Morley, 2011). In the northern part of study area appears Permian rocks that continue from Permian of Saraburi group. Structural geology and microstructures provided by measurement orientations of rocks for instance foliation, bedding, folding for plotting in stereonet diagram and correct oriented hand specimens combine with stratigraphy for analysis trend of each rock age for study the evolution structural geology in this area.

## 1.2 Objective and scope of study

An objective studies structural geology and microstructures in Amphoe Wang Nam Khiao area, Changwat Nakhon Ratchasima.

Scope of study is term of structural analysis orientation by stereonet diagrams in each rock units in study area and microstructures. Thin-sections prepare for microstructure study in deformation from evolution of structural geology. The study area covered about 525 square kilometers (Figure 1.1). Expected results are study structural geology and microstructures and construct evolutionary structure model in Amphoe Wang Nam Khiao area.

## 1.3 Location and accessibility

Study area is located at Amphoe Wang Nam Khiao in the Southwestern part of Nakon Ratchasima province where far from Bangkok about 250 kilometers in the northeastern direction. Extent of study area is composed of four topographic maps sheets of the Royal Thai Survey RTSD (1999b) at scale 1:50,000 follow as sheet 448-5338III (Ban Sup Noi) and 449-5338II (Ban Sukhang), 516-5337IV (Ban Thawang Sai) and 517-5337I (Amphoe Wang Nam Khiao) (Figure 1.1). Study area is accessed by using Highway Number1 Bangkok to Rangsit district then turn right in NE direction along road number 305 until to Nakhon Nayok province and turn right to SE direction for go alone road number 33 to Krabin Buri district in Prachin Buri province and turn left to road number 304 go to north to the Amphoe Wang Nam Khiao.

## 1.4 Terrain features and Climate

Morphology of terrain in study area is characterized undulating hills where site like domes and basins. Whereabouts in central part are high about 300-500 meters from mean sea level. From feature like undulating landform caused generate many narrow creeks in terrain. Consequently, almost stream patterns illustrate in dendritic and radiate patterns. Terrains are appropriated for resorts and residence as well as are suitable agriculture to illustrate corn, flower and fruit. Fringe areas are braced by hills high about 600-700 meters from mean sea level. The minor roads in study area almost are dirt roads and rugged ways. Amphoe Wang Nam Khiao

encompass by mountain range. The climate is comfortable temperature and beauty of the nature which three seasons composed of the winter season during middle of October-middle of February, whereas in summer season during middle of February-middle of May, while rainy season during middle of May-middle of October. The average temperature in each year is 27.4 degrees Celsius. The low range average temperature is about 22.7 degrees Celsius. While, the high range average temperature is about 33.0 degrees Celsius and the peak temperature in April about 42.7 degrees Celsius. The lowest temperature in January is about 6.2 degrees Celsius. The relative humidity is about 71% in a year. The average of rainfall is about 1,019.2 millimeters/ year (Nakhonratchasima, 2016).

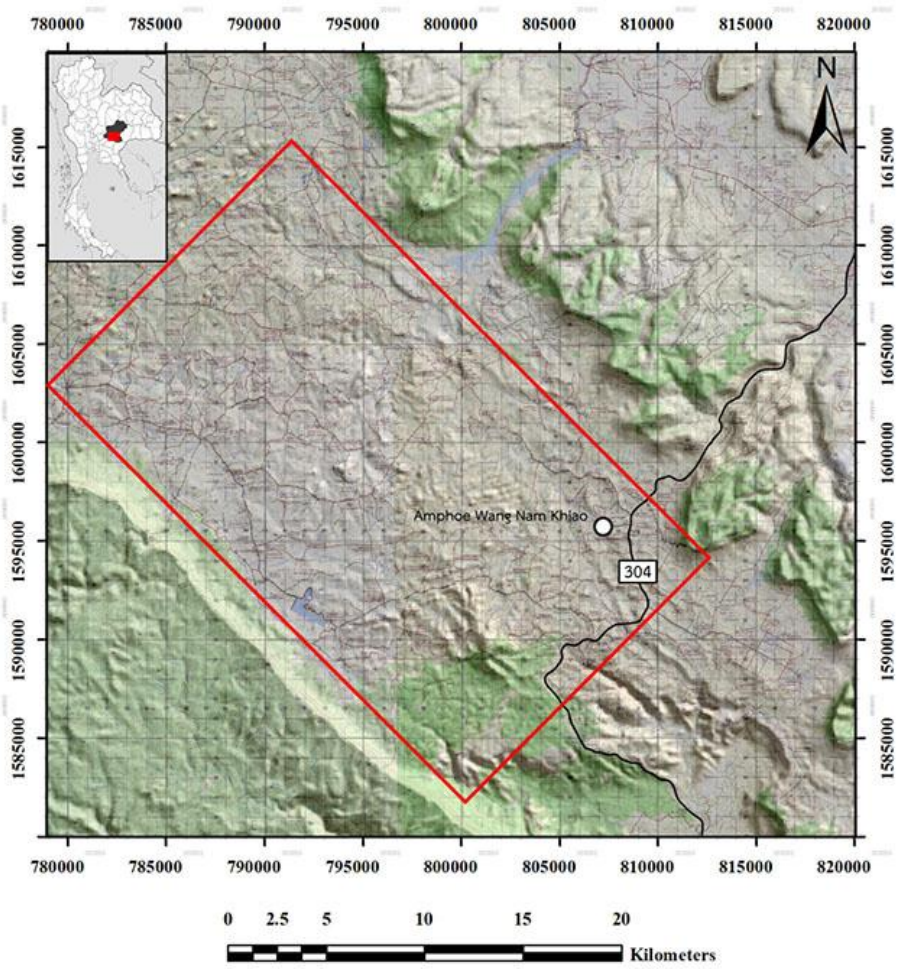


Figure 1.1 Topographic map showing study area in red rectangle area long 30 km and wide 17.5 km. Modified from RTSD (RTSD, 1999a, b, c, d).

## 1.5 Previous geologic studies

In adjacent areas around Wang Nam Khiao have been geological studies. Their studies focus on interpretation of tectonic evolution in Thailand. Bunopas (1981) firstly proposed tectonic evolution in Thailand and Southeast Asia that comprise of Shan-Thai block, Sukhothai, Loei and Indochina block (Figure 1.2). The Indosinian orogeny (Figure 1.3) generate first structural trend in Permian and the second is the tectonic evolution in the Cenozoic strike-slip faults of the Mae Ping fault zone (Arboit et al., 2014; Morley et al., 2013; Ridd, 2012; Ridd and Morley, 2011).

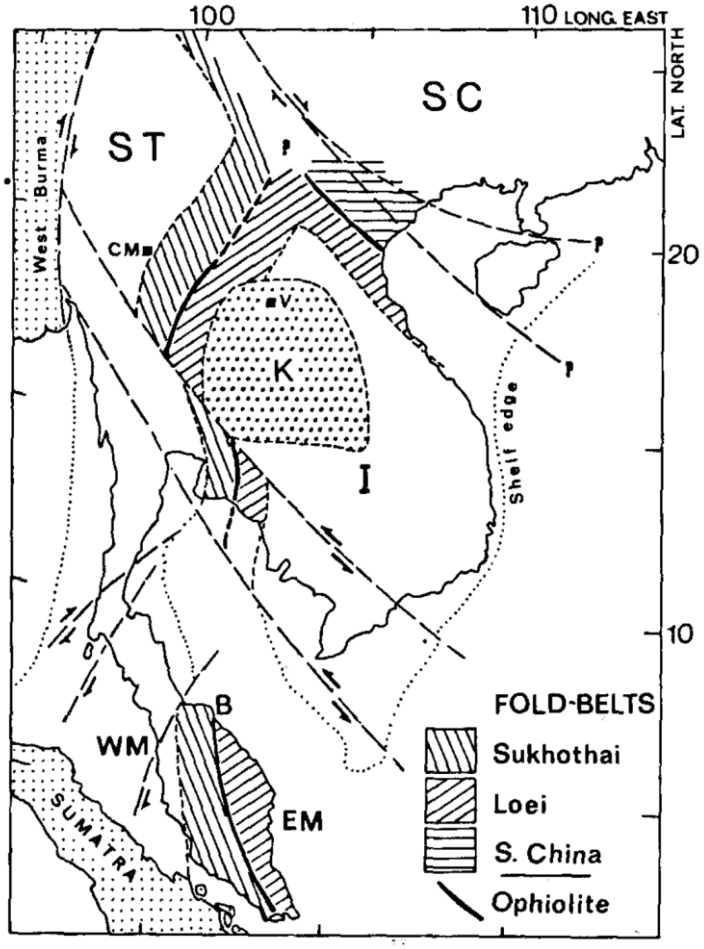


Figure 1.2 Map showing ancient cratonic areas; ST= Shan-Thai (including eastern Burma, Western Thailand and Northestern Malay Peninsula), I=Indochina (estern Thailand), SC=South china, K=Khorat basin, CM=Chiangmai, V=Vientiane, WM=West Malay Peninsula, EM=East Malay Peninsula, B=Bentong ophiolite line. (Modified after Bunopas, 1981)

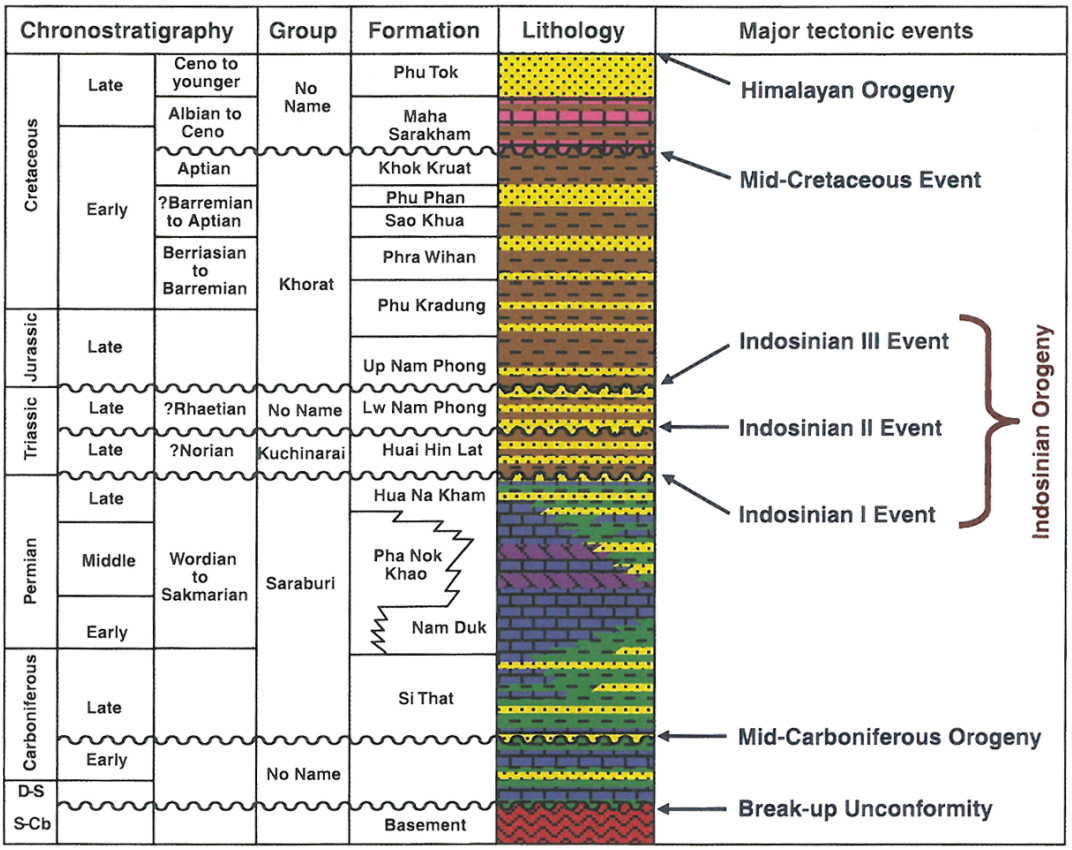


Figure 1.3 Chronostratigraphic of the Indosinian orogeny.(After Booth and Sattayarak, 2011)

Metcalfe (2013) studies about dispersion of the Gondwana and Asian accretion by tectonic and palaeogeographic evolution of eastern Tethys and proposed that mainland of Southeast Asia comprises of heterogeneous of continental blocks which derived from the eastern margin of the Gondwana then collision by subduction volcanic arcs and closure of Tethyan. Now the evolution is represented by suture zones  Figure 1.4). In addition, Tethyan separate in three intervening Tethyan oceans such as Palaeo-Tethys (Devonian-Triassic), Meso-Tethys (Late early Permian-Late Cretaceous) and Ceno-Tethys (Late Triassic-Late Cretaceous). In Palaeo-Tethys continental blocks separated from Gondwana in the Devonian, Palaeo-Tethys was opened, including the North China, Tarim, South China and Indochina blocks (including West Sumatra and West Burma). Now suture zones

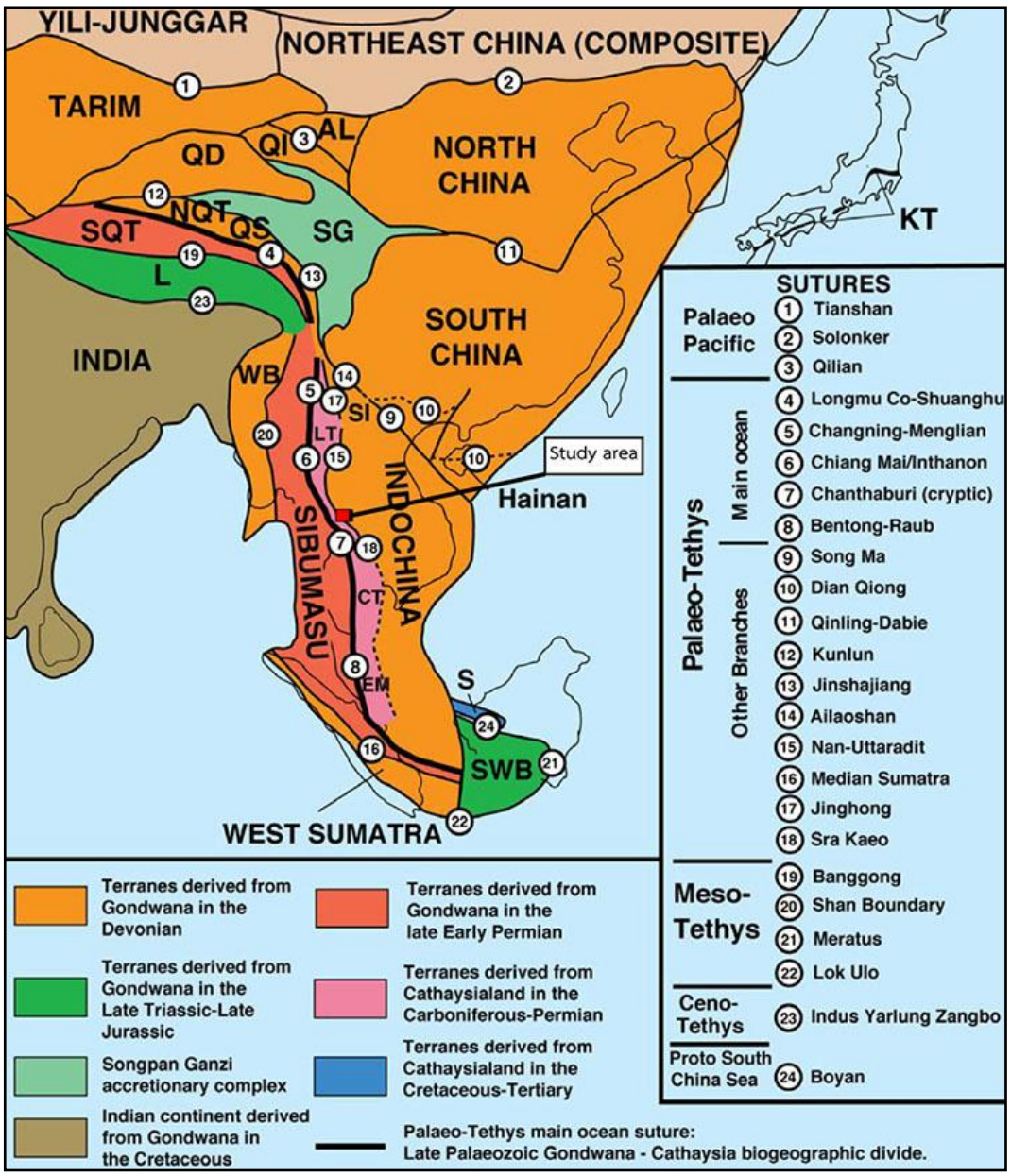


Figure 1.4 Map Showing distribution of principal continental blocks, arc s and sutures of eastern Asia. WB = West Burma, SWB = South West Borneo, S = Semitau, L = Lhasa, SQT = South Qiangtang, NQT = North Qiangtang, QS = Qamdo–Simao, SI = Simao, SG = Songpan Ganzi accretionary complex, QD = Qaidam, QI = Qilian, AL = Ala Shan, KT = Kurosegawa, LT = Lincang arc , CT = Chanthaburi arc , EM = East Malaya. (After Metcalfe, 2013).

from Palaeo-Tethys are consist of the Longmu Co-Shuanghu, Changning-Menglian, Chiang Mai/Inthanon and Bentong-Ruab suture zones. During northwards subduction of the Palaeo-Tethys, the Sukhothai arc was constructed on the edge of South China-Indochina, The Sukhothai arc is a shot-life back-arc basin can be separated from those is represented by the Jinghong, Nan-Uttaradit and Sra Kaeo sutures. Meso-Tethys are opened by rifted and separated of a second continental silver of collage of blocks (Cimmerian continent) from the northern part of the Gondwana. The Sibumasu terrane (including the Baoshan and Tengchong blocks of Yunnan) collided with the Sukhothai arc and South China/Indochina in the Triassic, closing the Palaeo-Tethys. Ceno-Tethys were opened in the Late Triassic and closed in Late Cretaceous. Nan-Uttaradit sutures consist between the Sukhothai arc and the Indochina terrane in eastern part of Thailand. The suture is composed of ophiolite of the Permian to the middle Triassic (Metcalfe, 2013). The Phasom metamorphic rocks include blueschist metamorphic rocks, thick bed of chert and basic/ultrabasic rocks. Moreover, the actinolite in mafic schist rocks indicats age in middle Permian age dating by K-Ar indicates 269±12 Ma of middle the Triassic (Anisian) (Barr and Macdonald, 1987) and illustrated Radioralian in chert (Saesaengseerung et al., 2008b) The rocks in the suture is overlaid by the Jurassic to the Cretaceous continent sediments. The Nan-Uttaradit suture is a part of the Sukhothai back-arc, open in the Carboniferous and closed in late Triassic (Metcalfe, 2002; Sone and Metcalfe, 2008; Ueno and Hisada, 1999; Wang et al., 2000). The Sa Kaeo suture is a part of the Sukhothai back-arc and continues from the Nan-Uttaradit to the Chanthaburi and the western of the Indochina. The ophiolites are exposed in Thung Kabin mélange and cherts bed, limestone, serpentinite, gabbros and pillow lavas. The radiolarian cherts in Permian age and late middle-early late Permian from radiolarians and conodonts (Saesaengseerung et al., 2008a) occurred in chert clastic sequence (Hada et al., 1999) age in Middle Triassic (Sashida et al., 1997).

Morley et al. (2013) proposed development of the Khao Khwang fold and thrust belt during the Indosinian Orogeny. Fold and thrust belt developed trend approximately N-S direction and disrupted by the Cenozoic strike-slip faults. The Khao Khwang platform part of the Saraburi group where consist on the SW rim of the Indochina terrane. Fold and thrust belt illustrate trend in ENE-WSW to NE-SW striking (Figure 1.5). Reversal movement clockwise from the Mae Ping Fault zone showing trend of folds and thrust belt in NW-SE and continue to Cambodia. Data from the hydrocarbon exploration on the Khorat plateau imply the Saraburi group is the part of the Indochina terrane. The Khorat plateau was a series of continental blocks were separated by Permian rifting (Booth and Sattayarak, 2011). The rifting of basins were thrust and inverted later when Sibumasu collided with Sukhothai zone-Indochina terrane during the Late Triassic.

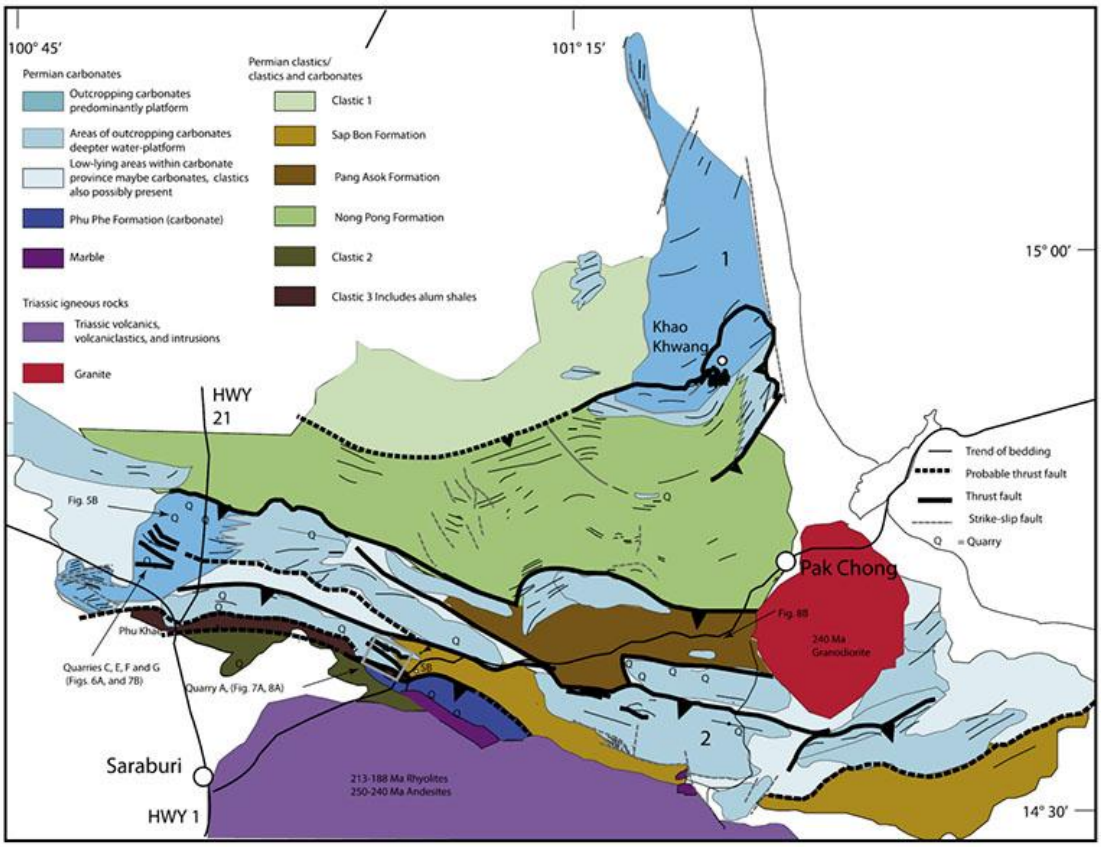


Figure 1.5 Geological map showing trend of fold and thrust belt of the Khao Khwang fold and thrust belt. Trend show ENE-WSW to NE-SW striking. (After Morley et al., 2013)

Arboit et al. (2014) studied a section through the Khao Khwang Fold and thrust belt along Highway number 21 (Figure 1.5). They suggest that the Khao Khwang area represents a thin-skined fold and thrust, with the fold and thrust belt illustrate E-W to WNW-ESE striking thrusts. The thrust direction is to northwards transport. structural evolution and can be separated to be six ridges separated by thrust faults (Figure 1.6).

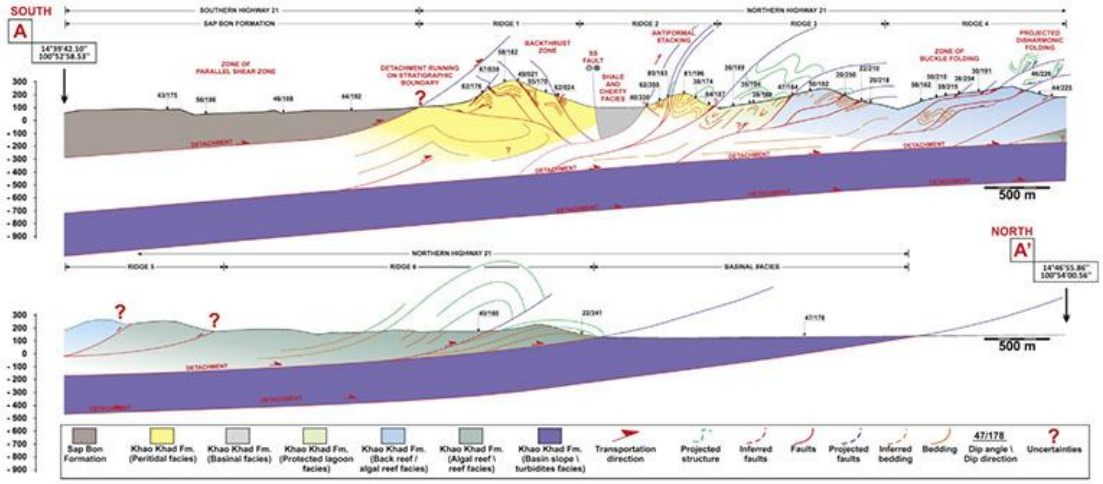


Figure 1.6 Sections showing six ridges and thrust faults along high way 21. (After Arboit et al., 2014)

Ridd and Morley (2011) suggested the Khao Yai Fault on the southern margin of the Khorat Plateau (Figure 1.7). The lineament, confirmed by Digital elevation model (DEM) images, lineament is at least 130 km long and coincides with a dip reversal of the Mesozoic Khorat Group. It is interpreted here as a fault, named the Khao Yai Fault, and it has characteristics which make it unusual within the Khorat plateau. Fault in the northern boundary of a belt of several ENE-WSW trending fault splays which link with the Mae Ping Fault further south; this is interpreted as a left-stepping, sinistral strike-slip duplex about 50 km, wide and 150 km long. From apatite fission track indicate the exhumation began during the earliest Palaeogene. The Khao Yai Fault includes the Cardamomes Mountains of Cambodia, the offshore Phuquoc-Kampot Basin and the Khao Thalai Red beds. The latter is interpreted as a down faulted sliver of the Khorat Group in the Thamai Fault.

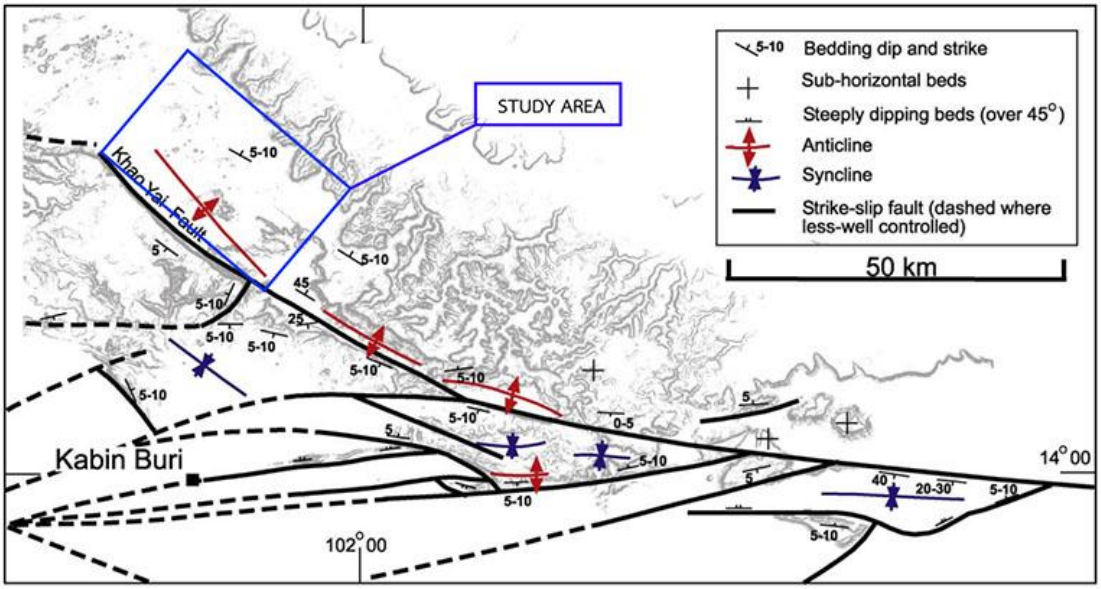


Figure 1.7 Map showing the Khao Yai fault and the study area. (After Ridd and Morley, 2011)

Ridd (2012) proposed the role of strike-slip faults in the displacement of the Palaeo-tethys suture zone in Southeast Thailand. Six N-S tectono stratigraphic belts (Figure 1.8) can be defined by stratigraphy and igneous history. belt (I) in the western most is throught to be a part of the Sibumasu block, the easternmost belt (V) includes part of the Indochina block; belt (II) consists of mylonite and apparently the lower Ordovician schist , the middle Silurian shale, chert and sandstone, the Permian chert, sandstone and shale, red-beds sedimentary rocks and granite. belt (III) comprises acid volcanic rocks, volcanic clastics and the Carboniferous to Triassic sedimentary rocks with distinctive faunas, interpreted to be a volcanic arcs; belt (IV) comprises of the Triassic rocks of back-arc basin origin; belt (V) in interpreted as a Permian accretionary complex on the western border of the Indochina; belt (VI) is an unconformable cover of Jurassic-Cretaceous red-beds correlation with the Khorat group. The Devonian-Triassic Palaeo-tethys (the Inthanon zone) disappears in southeastern Thailand because a phase of post-Indosinian oblique to longitudinal, sinistral, strike-slip faulting which offset the tectono-stratigraphic belts and faults of the earlier phase.

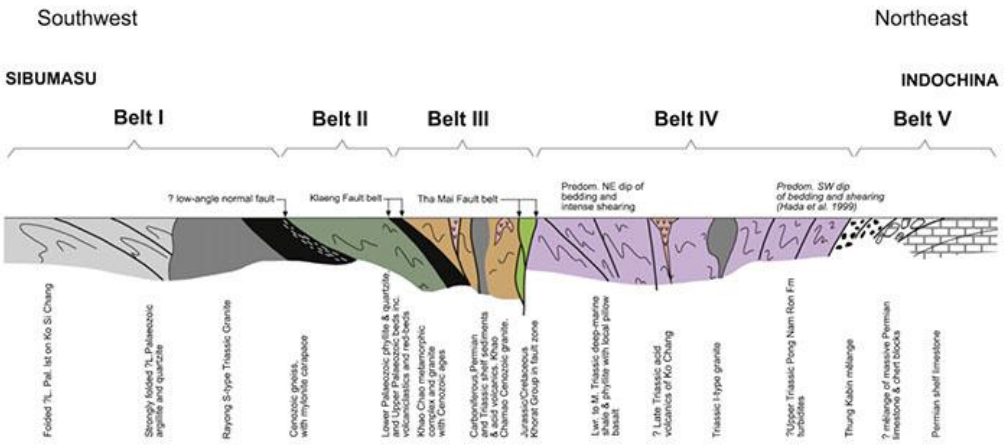


Figure 1.8 Schematic section Six N-S tectono stratigraphic belts between Sibumasu terrane and Indochina terrane. (After Ridd, 2012)

The previous study (Arboit et al., 2014; Metcalfe, 2013; Morley et al., 2013; Ridd, 2012; Ridd and Morley, 2011) in the adjacent area suggests that the study area were affected by the tectonic in the past. Structural geology in adjacent area show trend ENE-WSW to NE-SW striking (Morley et al., 2013) E-W to WNW-ESE striking thrusts (Arboit et al., 2014) and NW-SE trend from the Mae Ping fault (Arboit et al., 2014; Morley et al., 2013; Ridd, 2012; Ridd and Morley, 2011). In study area, structural geology studies recognized rocks ages for interpretation trend of structural geology in each age. The geological maps in study area were compiled by Department of Mineral Resources (2013). Rocks can be divided by age to the Permian, the Permo-Triassic, the Triassic, and the Mesozoic of the Khorat Group.

**1.6 Methodology**

The processes for this study geological structure in Amphoe Wang Nam Khiao area are composed of 5 processes.

1.6.1 Literature review and field investigation plan

This process is studies previous works (Arboit et al., 2014; Metcalfe, 2013; Morley et al., 2013; Ridd, 2012; Ridd and Morley, 2011) in the study area for understanding the tectonic and the structural evolution in the study area. Also, to prepare topographic maps and geological maps with scale 1:50,000. Topographic map of Royal Thai Survey (RTSD, 1999a, b, c, d) and geologic map data were compiled for studies the stratigraphy of the rock units in the study area and geomorphology for estimation in field investigation plan for determine boundary of study area. Also, preparing tools for field investigation and correcting samples such as topographic maps, compass, field Note, GPS, geological hammer, hand lens, sampling tools, field trips, field camp, weather in study area and budget. Method in obtain the orientation of rocks and orientate sampling for microstructural study.

1.6.2 Field investigation

After accessed to the study in field investigation can be provided in methods involve the structural geology acquisition and sampling the hand specimens. Method in structural geology acquisition by measure the orientation for instance; the foliation, bedding, folding, faulting which relate to interpretation structural geology in the study area. Stereonet plots are applied to data for structural analysis. In addition, oriented sample hand specimens are sufficient to description rock and thin sections.

1.6.3 Data analysis

Measurement structural geology in each rock units (Permian rocks, Permo-Triassic rock, Triassic granite rock, Triassic hornblende granite and Mesozoic Khorat group) such as bedding and foliation plot in the stereonet analysis the structural. The program for stereonet plot is Stereonet 9.5 which was written by from Department of Earth & Atmospheric Sciences, Cornell University, Ithaca, USA. Program plots foliations, bedding and faulting. Program is easy for graphics presentation. Plot planes (Figure 1.9) and $\pi$(pi) diagram (Figure 1.10) for determine folding style (Figure 1.1)

Microstructures study under the polarized-light microscope in deformation of rocks in the study area.

1.6.3.1 Plotting planes in stereonet

Plot plane of bedding and plane of foliation in stereonet plot (Rowland et al., 2007) for study structural orientation each rock unit in study area.

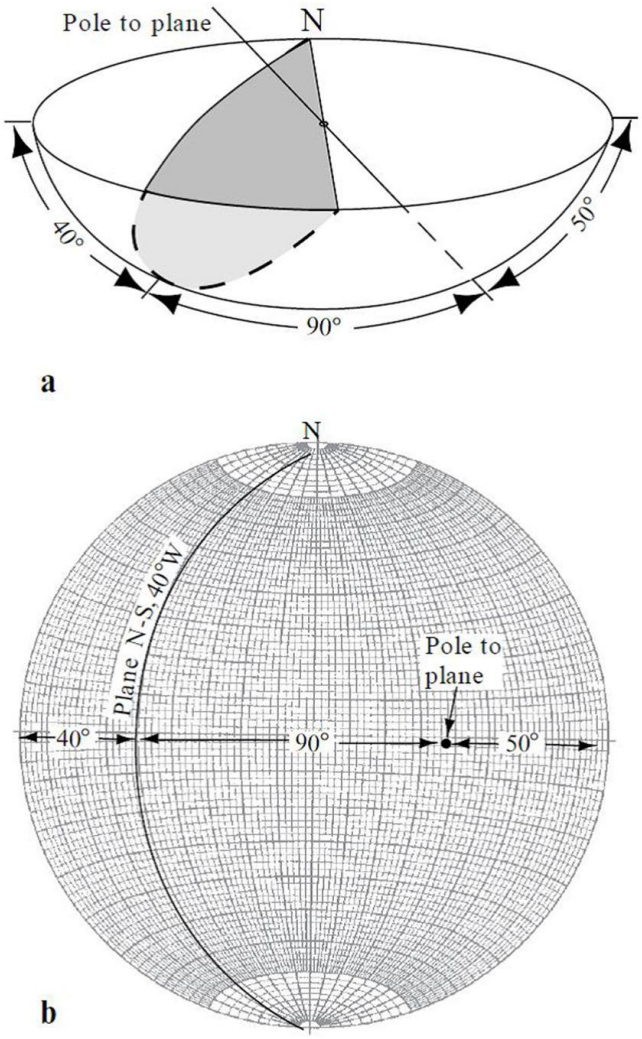


Figure 1.9 Photograph showing stereonet projection of plane strike 180° dip 40° and dip direction to 270°. (a) Oblique view. (b) Top view of stereonet projection. (Modified after Rowland et al., 2007)

1.6.3.2 Plotting $\pi$ diagram

After plot planes in stereonet in each rock unit then plot pole for generate $\pi$ diagram (Figure 1.10). $\pi$ diagram plot use determine fold style (Figure 1.11) in each rock unite.

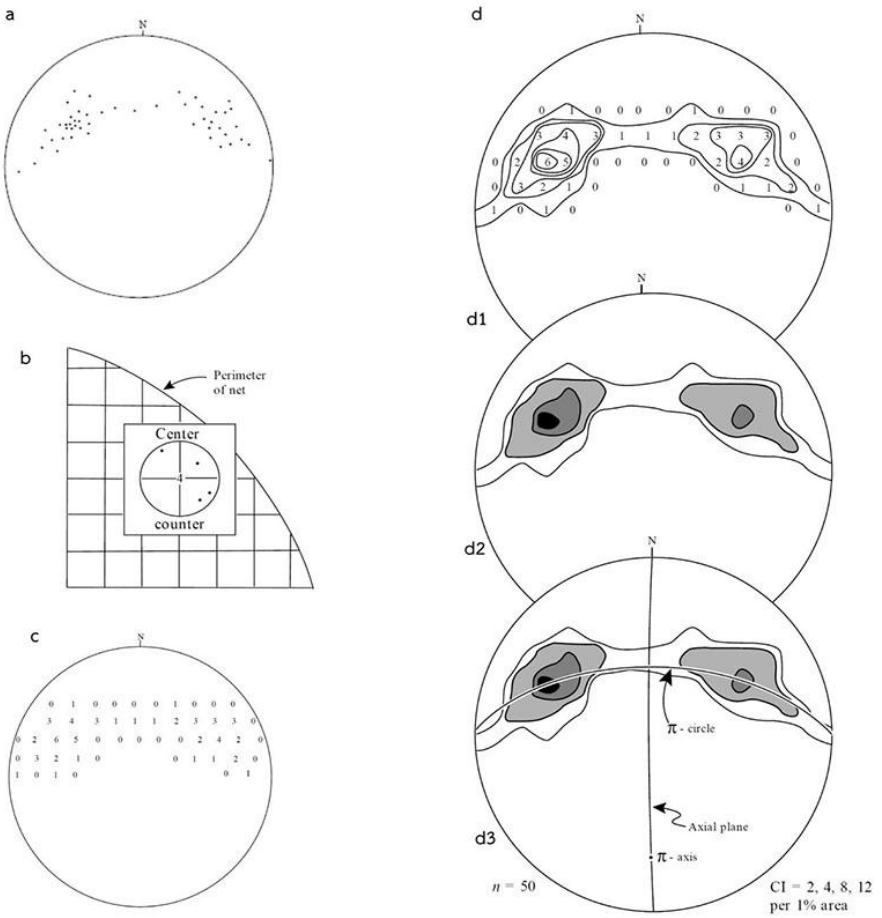


Figure 1.10 Method in generate $\pi$ diagram. (a) Point diagram form poles plot bedding and foliation planes. (b) Technique for counting points for the purpose of contouring. Using center counter. (c) Counting points. (d) Procedure generate $\pi$ diagram. (d1) contour plot of counting points. (d2) selected shade of contours. (d3) plot $\pi$ circle and $\pi$ axis on diagram. n=number of attitude plot. CI=contour interval. (Modified after Rowland et al., 2007).

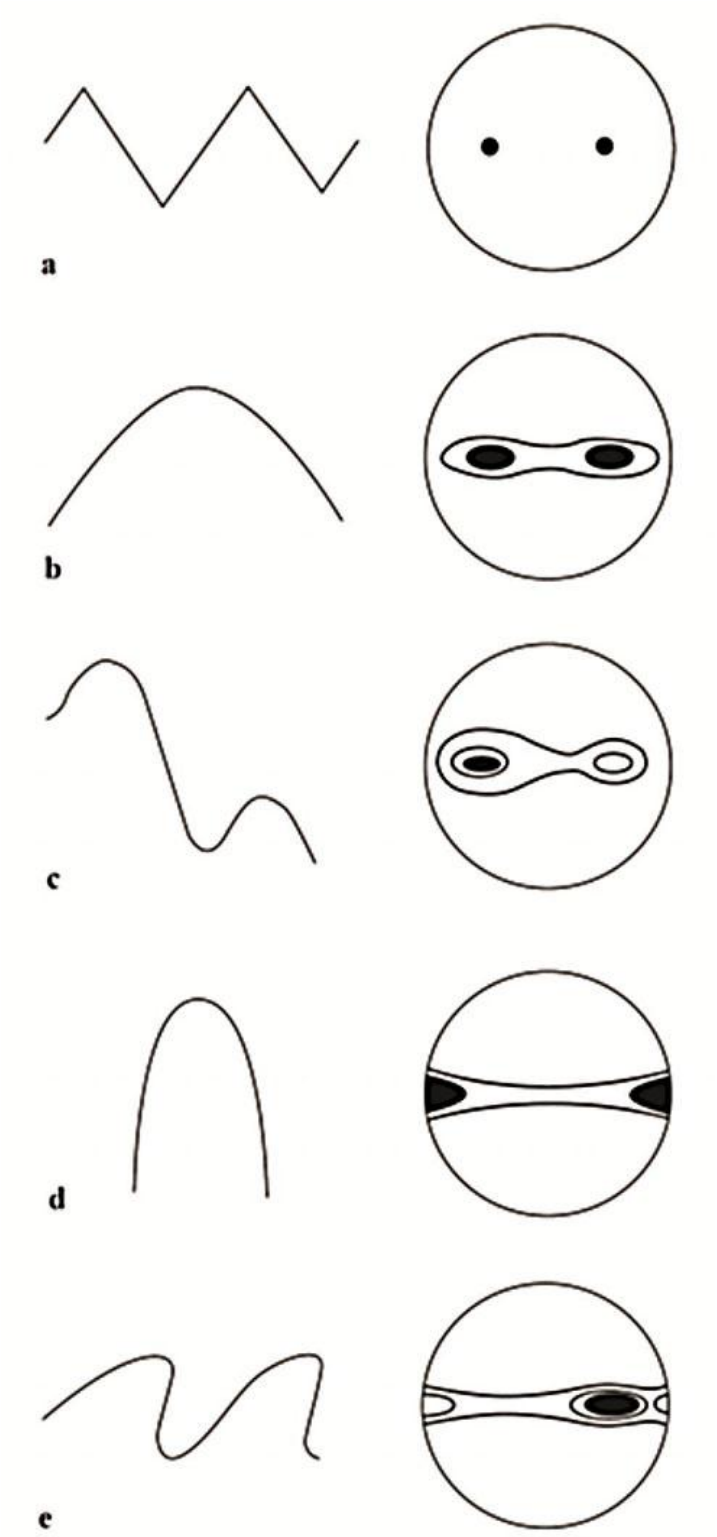


Figure 1.11 Profiles and corresponding contoured $\pi$-diagrams determine variously shaped folds. (Modified after Rowland et al., 2007)

1.6.3.1 Microstructures study

Microstructures study about the deformation in outcrop. Oriented samples cut for make thin section. Thin sections use in determine deformation in outcrops (Figure 1.12). Deformations recognize to marker and foliation deflection, porphyroclast systems and sigmoids, deformation of twin, c-type shear bands, oblique foliation, stair stepping, boudins, deformation behavior and three type of fragmented porphyroclast. More detail of microstructures study is in Appendix B.

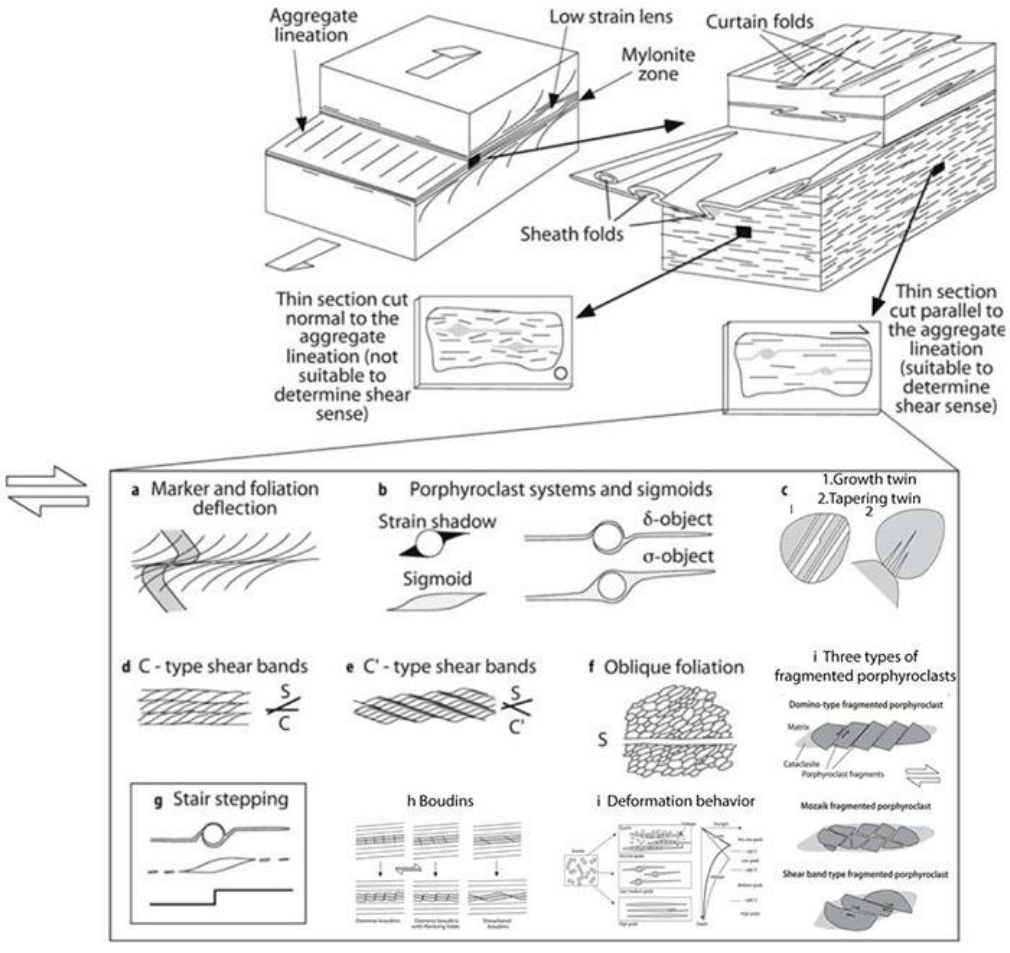


Figure 1.12 Schematic diagram showing the geometry of a mylonite zone and the nomenclature used. For thin sections parallel to the aggregate lineation, the most common types of shear sense indicators are shown. (Modified after Passchier and Trouw, 2005)

1.6.4 Structural evolutionary model

After, Plotting planes and $\pi$diagram in each rock unit are prepared for constructing the structural evolutionary model. Because, in each rock unit is preserve structural trend. The structural evolution model can be constructed base on the stratigraphy combine to the structural analysis plots. The structural evolutionary model corresponds with tectonic evolution in study area. Times of tectonic events effect to structural model. Ramsay and M.I. (1987) proposed superposition of shear folds which recognize to four types such as Type 0, Type 1, Type2 and Type3 (Appendix A).

1.6.5 Discussion and conclusion

The structural evolutionary model is discusses with the other previous works in the adjacent areas; in subject the orientation trends and the structural evolution and structural geology style in study area. At last, all structural data be concluded the structural trend in each rock unit, microstructures and structural evolutionary model in the study area.

The methodology study the geological structure in Amphoe Wang Nam Khiao area composes of 5 processes (Figure 1.13).

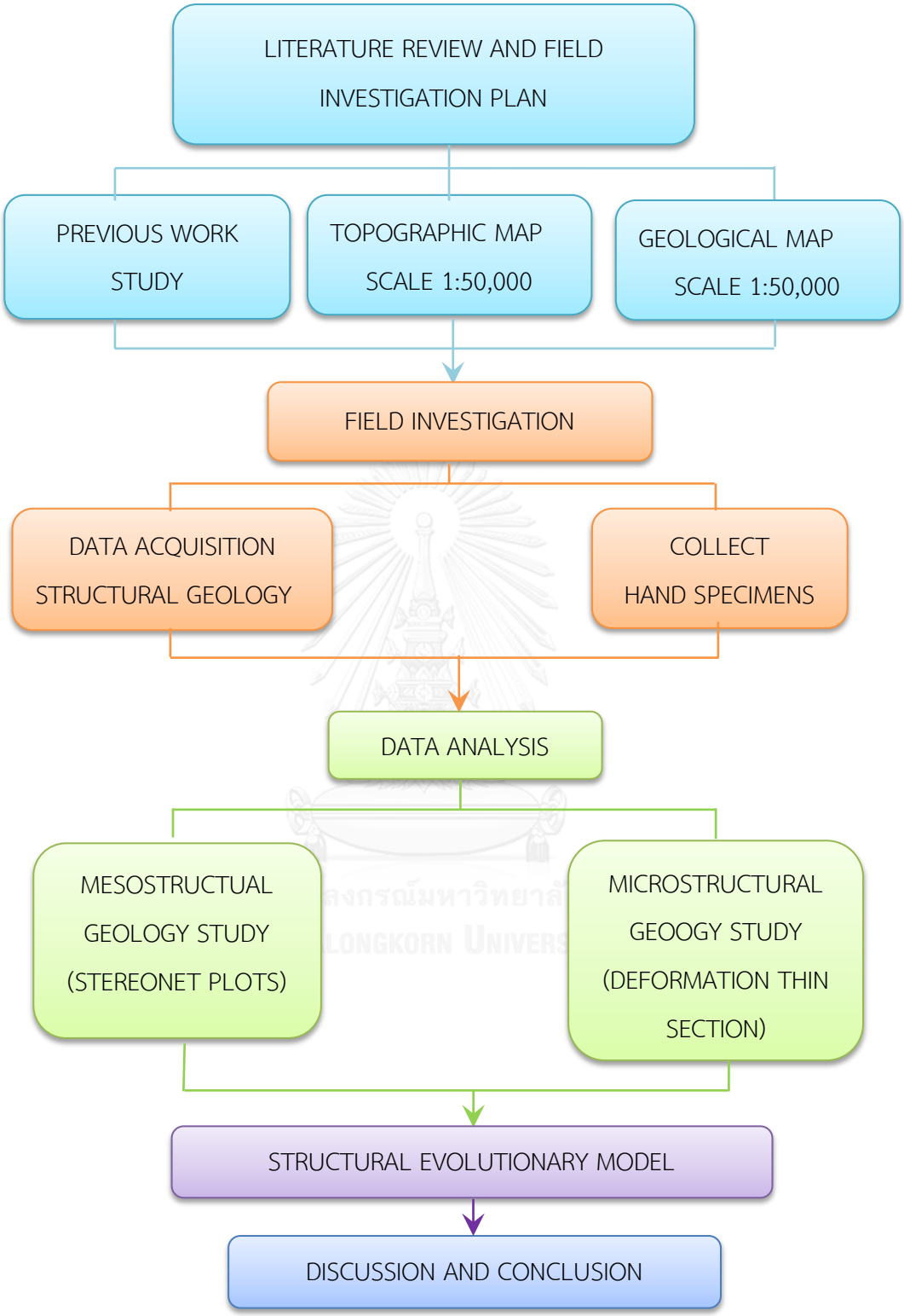


Figure 1.13 Methodology of the study.

# CHAPTER II

# REGIONAL GEOLOGY

This chapter presents in detail of the regional geology that important because it is the overview of the geology and structural geology in the study area. On the other hand, the evolution in regional scale is effect to the mesoscopic scale structure. Also microscopic structure can be explained by the feature of regional geology. The regional geology is associated with the tectonic framework (Figure 2.1) and tectonic evolution, lithology, stratigraphy and the structural trend in macroscopic scale.

## 2.1 Tectonic framework

### 2.1.1 Sibumasu Terrane

Sibumasu Terrane (Figure 2.1) is composed of the Shan stage of Myanmar, NW of Thailand, Peninsular Myanmar and Thailand, Western Malaya and Sumatra (Metcalfe, 2013). The terrane is bounded by the Mogok metamorphic belt to the Andaman Sea and the medial Sumatra tectonic zone (Baber and Crow, 2009) and the eastern to northeastern boundary by sutures are composed of the Changning-Menglian suture in SW China, Chiang Mai-Inthanon suture in Thailand and the Bentong-Raub suture in Malaysia Peninsula. The oldest sedimentary rocks Sibumasu is middle Cambrian to Early Ordovician clastics.

### 2.1.2 Sukhothai terrane

Sukhothai terrane (Figure 2.1) comprising the Linchang, Sukhothai and Chanthaburi terrane and the central eastern belts of the Malaysia Peninsula (Metcalfe, 2013). The western part is bonded by Changning-Menglian, Chiang Mai-Inthanon, and Bentong-Raub palaeo-Tethyan suture zone. While, in the eastern part is bonded by the back-arc basin Jinghong, Nan-Uttaradit and Sra Kaeo suture zone. Sukhothai terane was constructed in the Late Carboniferrous-Early Permian on the margin along the South China-the Indochina super terrane by northward subduction

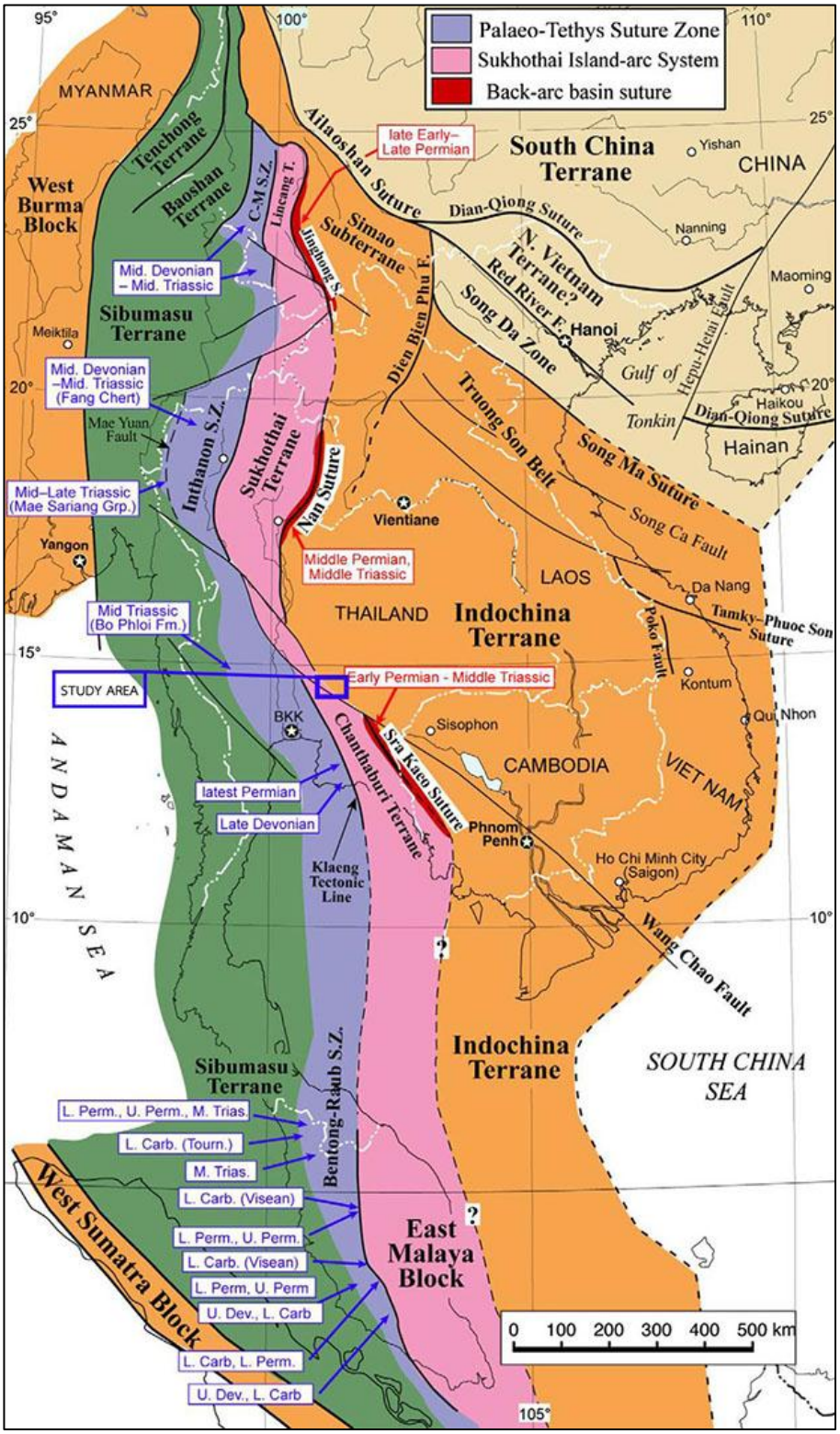


Figure 2.1 Map showing terranes and sutures zone in Southeast Asia. (modified after Metcalfe, 2013)

of the Palaeo-Tethys. It is separated by back-arc spreading in the Early-Middle Permian and then accreted back to South China-Indochina terrane by back-arc collapse in the Triassic. The oldest rocks in the East Malaysia segment of the Sukhothai terane are the Carboniferous siliciclastic and Carbonates (Chakraborty and Metcalfe, 1995).

2.1.3 Nan-Uttradit suture

Nan-Uttradit suture zone (Figure 2.1) forms boundary between the Sukhothai arc and Indochina block in eastern Thailand. The Sutures are composed of ophiolite of the Permian-Middle Triassic age. Pha Som metamorphic complex in the suture included blueschist, bedded cherts and basic/ultrabasic igneous rocks. Actinolite in mafic schist age in early middle Permian K-Ar age 269±12 Ma is a minimum of metamorphic age (Barr and Macdonald, 1987). Middle Triassic bedded radiolarian cherts are described from the suture zone by Saesaengseerung et al. (2008b) and suture rocks are overlain by Jurassic-Cretaceous continental sediments. The Nan-Uttradit suture is interpreted a segment of the Sukhothai back arc basin which opened in the Carboniferous and closed in the Late Triassic (Metcalfe, 2002; Ueno and Hisada, 1999; Wang et al., 2000)

2.1.4 Sra Kaeo suture

Sra Kaeo suture (Figure 2.1) is interpreted as the segment of the Sukhothai back arc basin in the southern Thailand. Also, a southward extend of the Nan-Uttradit suture. It was formed between the Chanthaburi terrane (Sukhotiai terrane) in the west and in the east of Indochina block. The ophiolites in the suture were found in the Tung Kabin mélange and include chert beds, limestone, serpentinites, gabbros and pillow lava. Bedded radiolarian cherts associated with pillow basalts (Metcalfe, 2013). Clasts in the Tung Kabin mélange have been date Early Permian and Late Middle to Early Late Permian by radiolarians and conodonts (Saesaengseerung et al., 2008a). Morover, chert from the chert clastic sequence (Hada et al., 1999) have been dated as Middle Triassic (Sashida et al., 1997).

2.1.5 Indochina terrane

Indochina terrane (Figure 2.1) in the NE boundary is the Song Ma suture zone in Vietnam and in the western bound with the Jinhong, Nan-Uttradit, Sra Kaeo to a cryptic offshore eastern Malaysia. Eastern of Indochina terrane bound to the South China Sea. The basement of the Indochina block composed of a metamorphic core (Kontum massif) of granulite facies (Metcalf, 2013) Two thermotectonic events by U-Pb (Monazite and zircon) and Ar-Ar (mica) age of the granulites from Kontum massif, one in the Middle Ordovician (470-465 Ma) and the other in the Early Triassic (250-245 Ma) (Roger et al., 2007).

## 2.2 The tectonic evolution

The tectonic evolution of the mainland Southeast Asia was proposed by Bunopas (1981) Thailand composed of two terranes collision between The Shan-Thai and The Indochina block. The previous workers (Arboit et al., 2014; Metcalfe, 2013; Morley et al., 2013; Ridd, 2012; Ridd and Morley, 2011) interpret the tectonic evolution model (Figure 2.2) that fit to the new evidences. Metcalfe (2013) suggested that the Southeast Asia was accreted by the closure of Tethyan in three intervening Tethyan oceans, composed of the Palaeo-Tethys (Devonian-Triassic) continental blocks separated from Gondwana in the Devonian, Palaeo-Tethys was opened included the North China, Tarim, South China and Indochina blocks. Now Suture zones from Palaeo-Tethys are consist of the Longmu Co-Shuanghu, Changning-Menglian, Chiang Mai/Inthanon and Bentong-Ruab suture zones, During northwards subduction of the Papaeo-Tethys, the Sukhothai Arc was constructed on the edge of South China-Indochina, The Sukhothai Arc is a shot-lived back-arc basin can be separated from those terranes is represented by the Jinghong, Nan-Uttaradit and Sra Kaeo Sutures. The Meso-Tethys (Late early Permian-Late Cretaceous) are opened by rifted and separated of a second continental silver of collage of blocks (Cimmerian continent) from the northern part of the Gondwana. The eastern Cimerian continent, including the South Qiangtang block and Sibumasu terrane (Including the Baoshan and Tengchong blocks of Yunan) collided with the Sukhothai Arc and South China/Indochina in the Triassic, Closing the Paleao-Tethys.

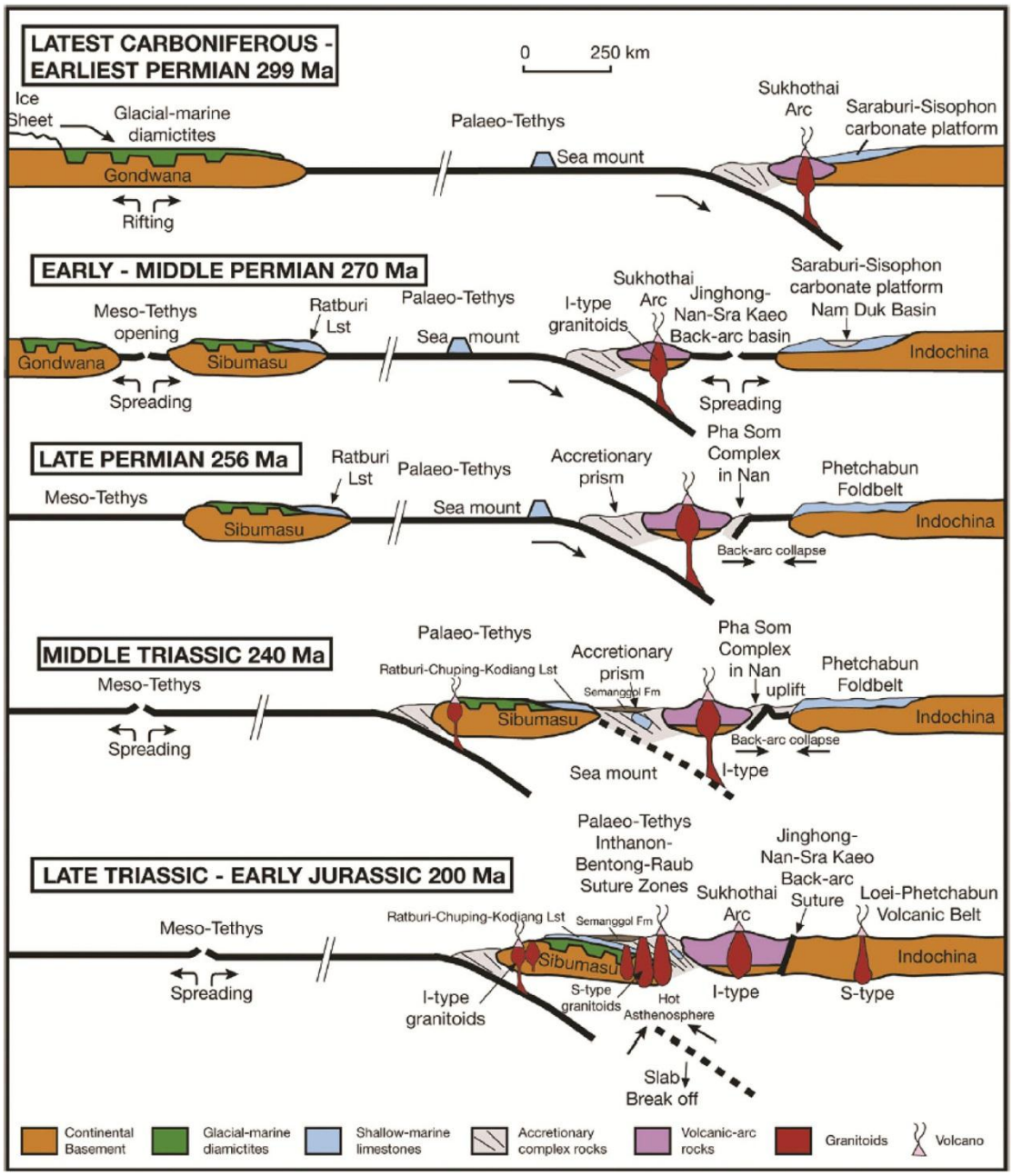


Figure 2.2 Tectonic evolution of Thailand and evolution of the Sukhothai Arc System during Late Carboniferous–Early Jurassic times (After Metcalfe, 2013)

The third collision including the Lhasa block, South West Borneo and East Java-West Sulawesi were separated from NW Australia during the Late Triassic-Late Jurassic by opening Ceno-Tethys (Late Triassic-Late Cretaceous) and accreted to SE of Sundaland by subduction of the Meso-Tethys in the Cretaceous. Now represent sutures in Southeast Asia and Paleogrographic. The sutures have trend about N-S direction (Figure 2.1). In study area is located in the part of the Sukhothai Arc and the Indochina. The Sukhothai Arc is a shot-lived back-arc basin can be separated from those terranes is represented by the Jinghong, Nan-Uttaradit and Sra Kaeo sutures (In the southern part of the study area). The Khorat Plateau is that the part of the Indochina terrane was a series of continental blocks were separated by Permian rifting (Figure 2.3) about ENE-WSW to E-W trend and closed during the Triassic there was closure the back arc between the Sukhotiai zone and Indochina terrane (Booth and Sattayarak, 2011). Also, The Permian rifting of basins thrust and inverted later Sibumasu terrane collided with the Sukhothai zone/Indochina terrane during the Late Triassic. Thrusting evidence was illustrated in E-W trending (Arboit et al., 2014; Morley et al., 2013). Not only thrust in from south to north direction but also this area was disturbed by the Cenozoic strike-slip of Mae Ping faults zone (Arboit et al., 2014; Morley et al., 2013; Ridd, 2012; Ridd and Morley, 2011).

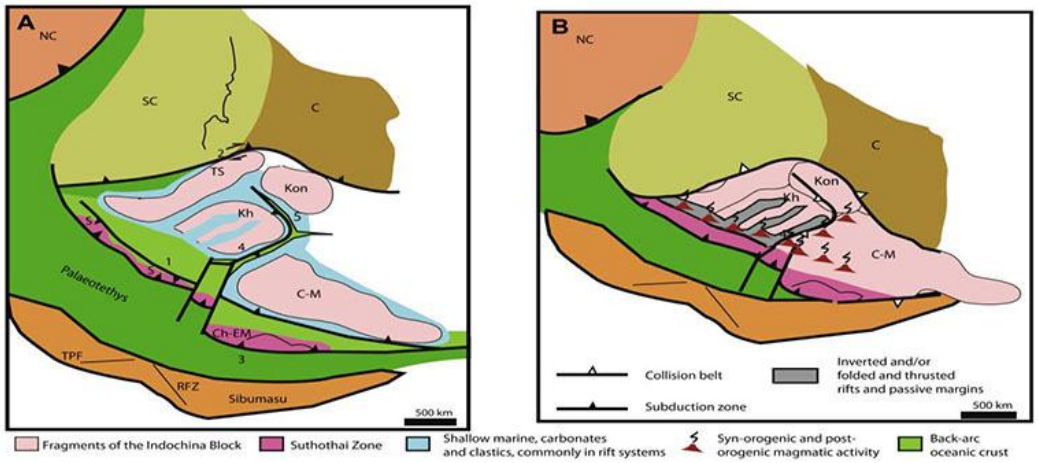


Figure 2.3 Rifting in the Khorat (A) Early Triassic (B) Middle Triassic, NC=the North China, SC=the South China, C= Cathasian Block, TS=Truong Son, Kon=Kontum, Kh=Khorat, C-M=Cambodia, offshore Malaysia, S=Shkhothai, Ch-EM= Chanthaburi-East Malaysia. (after Morley et al., 2013)

**2.3 Lithology and stratigraphy**

The geological maps in Amphoe Wang Nam Khiao were mapped by Putthapiban et al. (1989b) sheet Amphoe Wang Nam Khiao Quadrangle, Ban Tha Wang Sai Quadrangle and Kemlheg and Vichidchalermpong (1992b) sheet Ban Sap Noi Quadrangle, Ban Sukhang Quadrangle in 1st edition and 2nd edition in year 2013. The Geological map (Figure 2.4) four sheets were combined for study regional geology and stratigraphy in the study area (Figure 2.5).

2.3.1 Permian rocks

Permian rocks (Figure 2.5) in the study area are dominant by sedimentary rocks. These sedimentary of Permian distributes in the northwestern, the middle and rare in southern of study area. The Permian rocks were recognized to be P (Putthapiban et al., 1989a, b), $P_3$, $P_2$ and $P_1$ (Kemlheg and Vichidchalermpong, 1992a, b).

Rocks P are consisted of phyllitic shale, siltstone, sandstone illustrated thin bedded, colored light brown, brownish gray, gray and black intercalated with hornfels and quartzite, thin bedded, gray cherts locally contact metamorphosed.

Rocks $P_1$ are composed of Limestone color dark gray to black also illustrated thin to thick-bedded and some part are interbedded with chert bed and lenses, fossiliferous limestone; partialy sandstone and shale intercalated, locally marble, recrystalline, skarn and hornfels, fusulinids, ostracods, corals, gastropods algaes, bryozoan and pellets.

Rock $P_2$ are consisted of the Limestone is color light-gray and showed laminated to thick-bedded, interbedded with chert bedded and lenses, the argillaceous limestone colored gray to pinkish brown interbedded in upper part, fusulinids, smaller forams, crinoid stems, algaes and gastropods.

Rocks $P_3$ are comprised of Shale colored greenish gray to dark greenish gray illustrated laminated and dark limestone, dark gray limestone lenses intercalated in lower part, partially tuffaceous limestone and pebbly shale; locally spotted phyllitic shale, slaty shale and schist colored greenish gray.

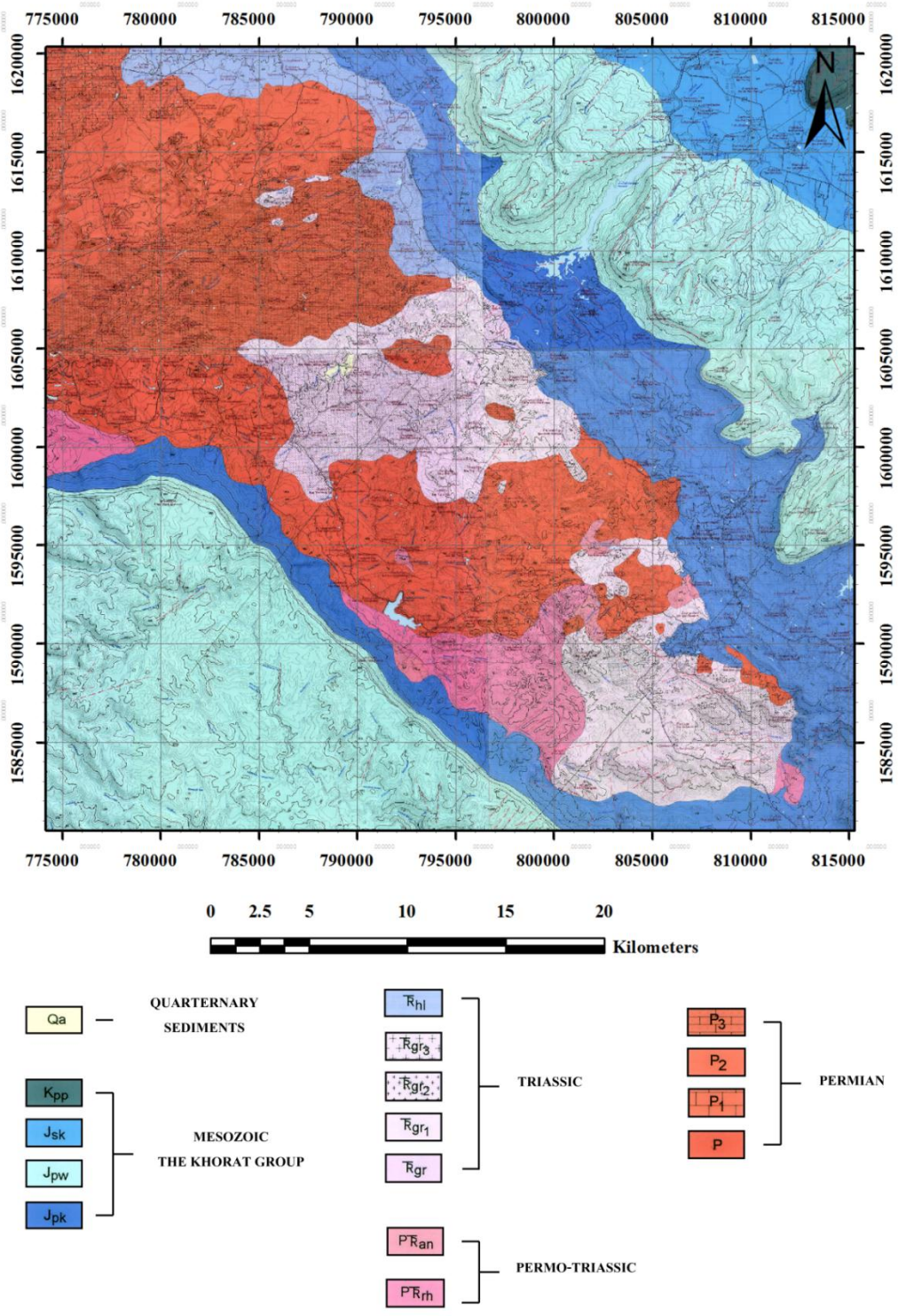


Figure 2.4 The geological map in the study area. (Modifieded after Kemlheg and Vichidchalermpong, 1992a, b; Putthapiban et al., 1989a, b)

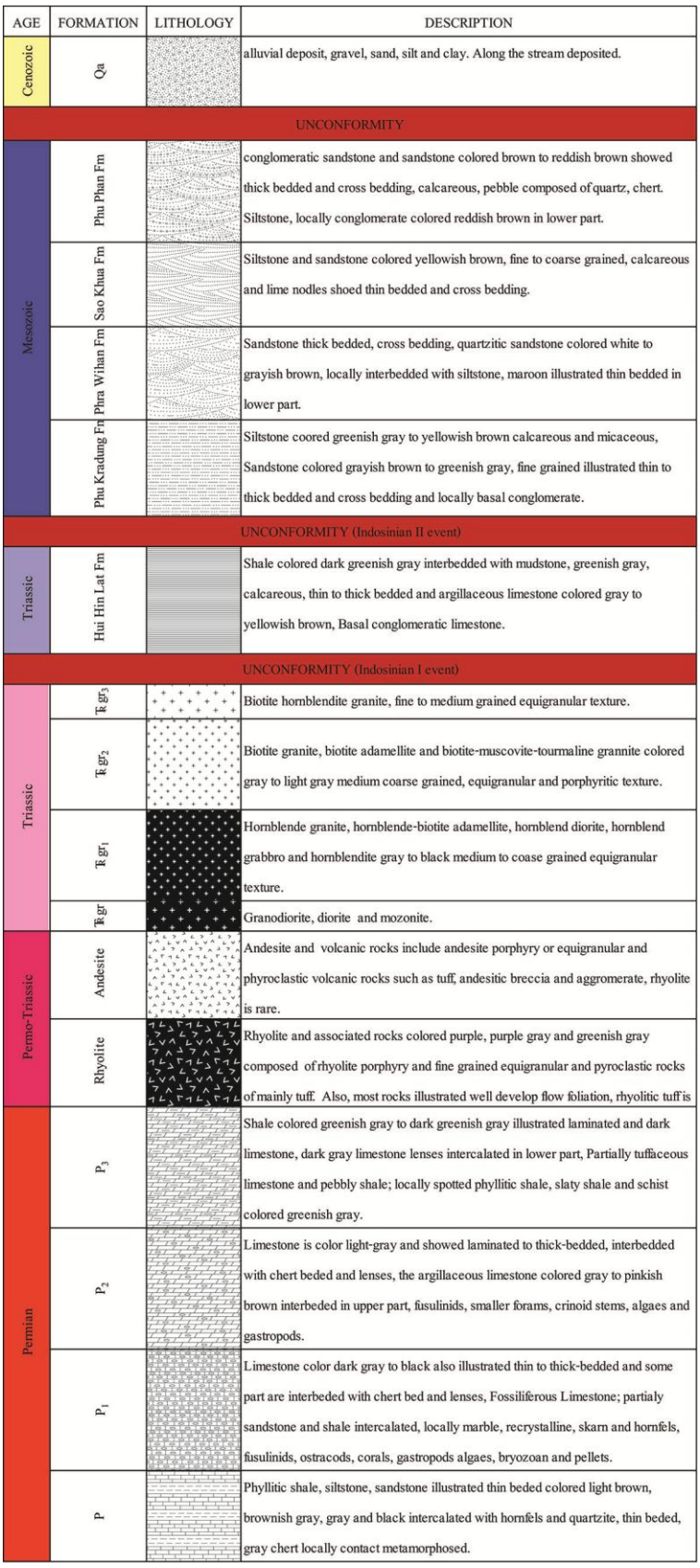


Figure 2.5 Statigraphy rock units in the study area.

2.3.2 Permo-Triassic rocks

Permo-Triassic rocks (Figure 2.5) in the study area were dominant by the volcanic and pyroclastic rocks. In the study area, the Permo-Triassic rocks distribute in the western and the lower central part of the study area and rare in the eastern. The Permo-Triassic rocks were divided to two groups (Putthapiban et al., 1989a, b).

Permo-Triassic rocks ($PTR_{rh}$) are comprised of rhyolite and associated rocks colored purple, purple gray and greenish gray composed of rhyolite porphyry and fine grained equigranular and pyroclastic rocks of mainly tuff. Also, most rocks illustrated well develop flow foliation, rhyolitic tuff is always present.

The Permo-Triassic rocks ($PTR_{an}$) are consisted of andesite and associated volcanic rocks include andesite porphyry or equigranular and phyroclastic volcanic rocks such as tuff, andesitic breccia and aggromerate, rhyolite is rare.

2.3.3 Triassic rocks

Triassic rocks (Figure 2.5) in the study area are dominant by the intrusive rocks such granodiorite, diorite, biotite granite and hornblendite granite. Also, the intrusive rocks are distributed in the north of the central part, the southeastern part and rare in the north part of the study area. The Triassic intrusived rocks were divided in $TRgr$ , $TRgr_1$, $TRgr_2$ and $Tgr_3$ and the Huai Hin Lat Formation of the Khorat group (Kemlheg and Vichidchalermpong, 1992a, b; Putthapiban et al., 1989a, b).

Triassic rocks ($TRgr$) are dominant by the granodiorite, diorite and monzonite.

Triassic rocks ($TRgr_1$) are consisted of the hornblende granite, hornblende-biotite adamellite, hornblend diorite, hornblend grabbro and hornblendite gray to black medium to coase grained equigranular texture.

Triassic rocks ($TRgr_2$) are composed of the biotite granite, biotite adamellite and biotite-muscovite-tourmaline grannite colored gray to light graymedium coarse grained, equigranular and porphyritic texture.

Triassic rocks ($TRgr_3$) are composed of the biotite hornblendite granite, fine to medium grained equigranular texture.

Triassic rocks ($TRhl$) Huai Hin Lat Formation are sedimentary rocks comprised of shale colored dark greenish gray interbedded with mudstone, greenish gray,

calcareous, thin to thick bedded and argillaceous limestone colored gray to yellowish brown, basal conglomeratic limestone.

2.3.4 Mesozoic Khorat group

Mesozoic Khorat group (Figure 2.5) in the study area are distributed in the northeastern part and southwestern part. The Khorat group is composed of the Phu Kradung Formation, the Phra Wihan Formation, the Sao Khua Formation and the Phu Phan Formation. The Khorat group is dominant by the non-marine sedimentary rocks. Also, low dip angles (Kemlheg and Vichidchalermpong, 1992a, b; Putthapiban et al., 1989a, b).

Phu Kradung Formation ($J_{Pk}$) is consisted of the siltstone color red greenish gray to yellowish brown calcareous and micaceous, sandstone colored grayish brown to greenish gray, fine grained illustrated thin to thick bedded and cross bedding and locally basal conglomerate.

Phra Wihan Formation ($J_{pw}$) is composed of the sandstone thick bedded, cross bedding, quartzitic sandstone colored white to grayish brown, locally interbedded with siltstone, maroon illustrated thin bedded in lower part.

Sao Khua Formation ($J_{sk}$) is comprised of Siltstone and sandstone colored yellowish brown, fine to coarse grained, calcareous and lime nodules shoed thin bedded and cross bedding.

Phu Phan Formation ($J_{pp}$) is dominant by the conglomeratic sandstone and sandstone colored brown to reddish brown showed thick bedded and cross bedding, calcareous, pebble composed of quartz, cherts, siltstone, locally conglomerate colored reddish brown in lower part.

2.3.5 Quaternary sediments

The quaternary sediments (Q) are comprised of the alluvial deposit, gravel, sand, silt and clay and stream deposited (Figure 2.5).

# CHAPTER III

# STRUCTURAL GEOLOGY AND MICROSTRUCTURES

This chapter includes the structural geology and the microstructures in study area. The content of structural geology studies with deformed rocks respond to the stresses. The results from the stresses and directions are illustrated various natures such as folds, faults, foliations, lineation, and joints. Field investigation in structural geology methods obtains data orientations of apparent structure at the outcrop and sampling hand specimens for microstructures study. In field investigation, outcrops in the study area are emerged at road cut and in creek, canal and abandon mine. In the study area, 39 outcrops were found and measure of the orientation (Figure 3.1) such as folding, foliation and bedding and plot those planes and poles in stereonet diagram. For avoidance obscuring in recognized structural, rocks unit in study area can be divided into five groups are composed of the Permian rocks, the Permo-Triassic rocks, the Triassic rocks, the Triassic hornblende granite and the Mesozoic of the Khorat group. Orientation of rocks in the study area are not only the Permian rocks are illustrated orientation in ESE-WNW, ENE-WSW and NE-SW direction, but also were illustrated these trend in the Permo-Triassic rocks, some part of the Triassic granite rocks and the Triasic hornblende granite. On the other hand, Triassic granite rocks in the southwest part of study area and the Mesozoic of the Khorat group are illustrated trend in NW-SE direction. Subsequently, the hand specimens were kept by orientated sampling for thin sections in study deformation under the polarized microscopic in texture, of microstructure (Blenkinsop, 2000; Passchier and Trouw, 2005; Trouw et al., 2009) such as c-type shear bands, strain shadow, synthetic micro-faulting, micro-folding, kinking, boudins and tapering edges of twin were illustrated . Consequently, the structural analysis (Grasemann et al., 2004; Ramsay, 1976; Ramsay and M.I., 1987; Rowland et al., 2007) stratigraphy and the deformation in microstructure are combined and construct the structural evolution in Amphoe Wang Nam Khiao area.

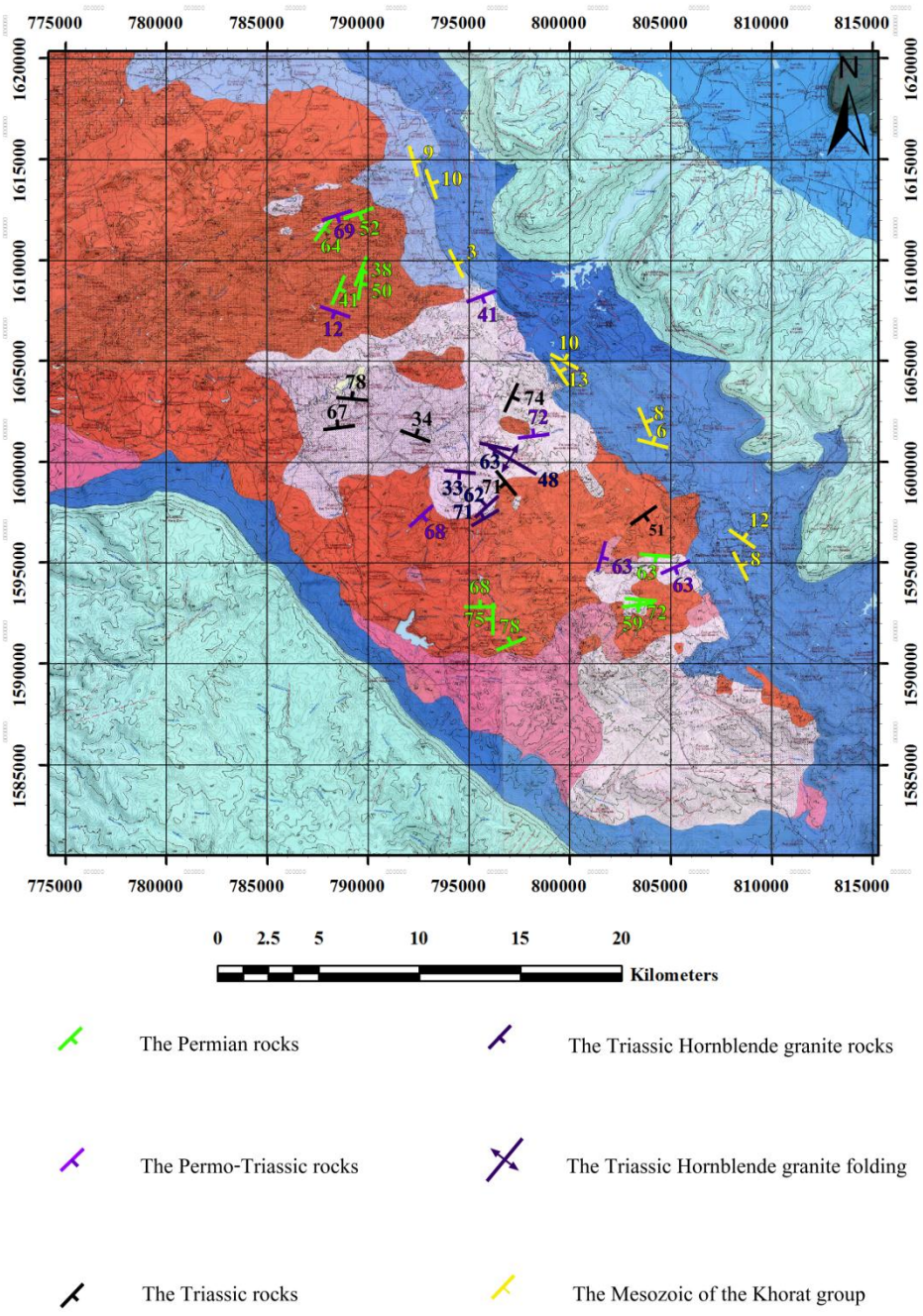


Figure 3.1 Geological map showing distibution and orientation of outcrops in the study area. (Modifieded after Putthapiban et al., 1989; Kemlheg and Vichidchalermpong, 1992)

### 3.1 Permian rocks

The Permian rocks in the study area disperse at the northern part and the southern part in the study area. Outcrops are dominant by the clastic sedimentary rocks such siltstone, shale, and shale interbedded limestone (Figure 3.2).

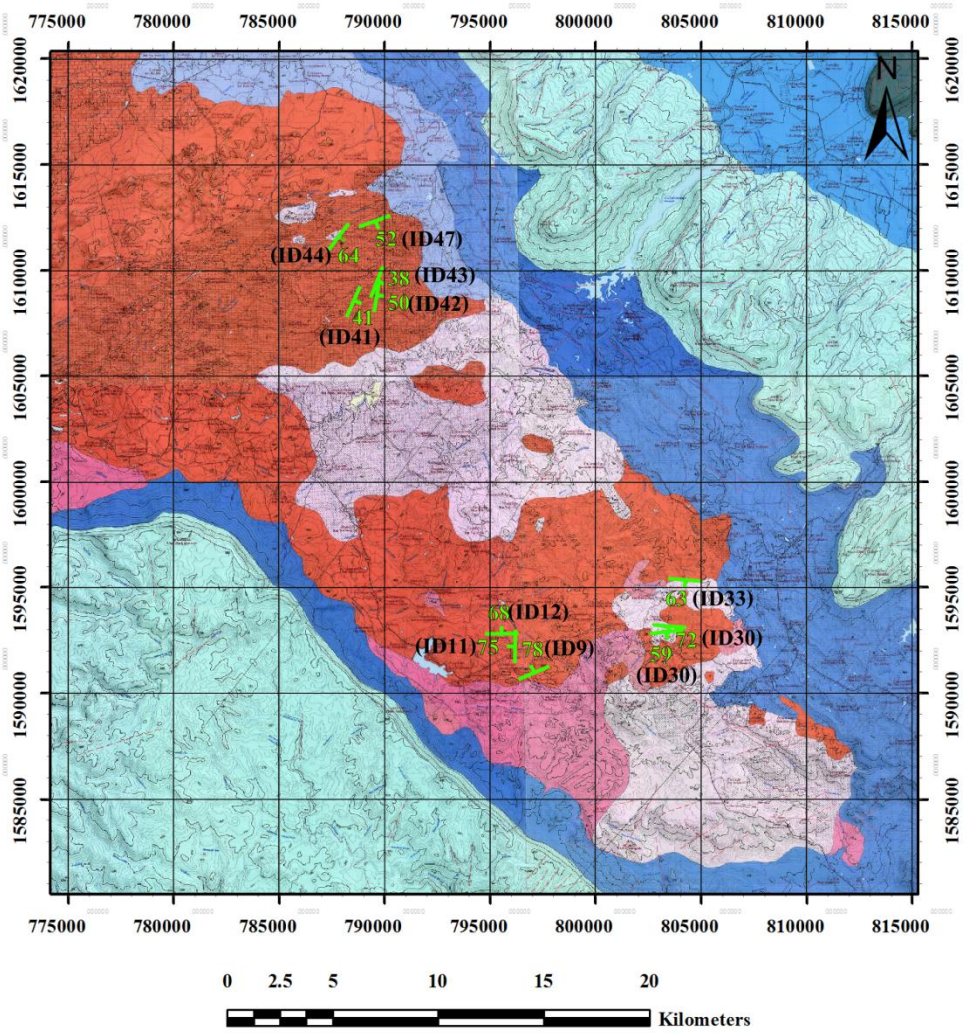


Figure 3.2 Map shows dispersion and orientation of Permian outcrops.

Siltstone outcrop ID12 (Figure 3.2) illustrates foliation plane 267°/68° and dip direction to NW (Figure 3.3). Outcrop ID44 (Figure 3.2) of shale shows bedding plane 038°/64° dip direction to SE (Figure 3.4). Also, siltstone outcrop ID11 (Figure 3.2) exhibits foliation plane 181°/75° dip direction to W (Figure 3.5). Slab is moderately weathered (Figure 3.6), microstructures are illustrated c-type shear bands on plane polarized light magnification 10× (Figure 3.7a) and c-type shear bands showing dextral shear scene (Figure 3.7b). Shale outcrop ID41 (Figure 3.2) illustrates foliation plane 023°/41° dip direction to SE (Figure 3.8). Slab sample is moderately weathered (Figure 3.9). Microstructures showing oblique foliation on crossed polarized light magnification 5× (Figure 3.10a) and showing exposition of oblique foliation (Figure 3.10b). Furthermore, shale outcrop ID42 (Figure 3.2) shows foliation plane 009°/50° dip direction to SE (Figure 3.11) and microstructure appear porphyroclasts of quartz start strain shadow $\emptyset$ (phi) type (Appendix B) on plane polarized light magnification 10× (Figure 3.13a) and drafting strain shadow illustrates no stair stepping in porphyroclasts 10× (Figure 3.13b). In addition, siltstone interbedded limestone outcrop ID43 (Figure 3.2) presents bedding plane 022°/38° dip direction to SE (Figure 3.14). Slab sample is low weathered (Figure 3.15), microstructures display strain shadow of porphyroclast of feldspar crossed polarized light magnification 5× (Figure 3.16a) and drafting porphyroclasts shows strain shadow $\sigma$ (sigma) type (Appendix B) which indicates sinistral shear scene on crossed polarized light magnificent 5× (Figure 3.16). Furthermore, two feldspar porphyroclasts illustrates $\sigma$ type in Figure 3.17a and drafting sinistral shear scene in Figure 3.17b. Accordingly, Figure 3.18a shows $\sigma$ type of feldspar porphyroclasts and drafting Figure 3.18b illustrates sinistral shear scene. Moreover, Figure 3.19a porphyroclasts of polycrystal exhibit sinistral shear scene and Figure 3.19b showed drafting of sinistral shear scene, while shale outcrop ID47 (Figure 3.2) exhibits foliation plane 068°/52° dip direction to SE (Figure 3.20), Slab sample is highly weathered (Figure 3.21). Microstructures are manifested strain shadow of porphyroclasts $\sigma$ type was sheared in sinistral scene on crossed polarized light magnification 5× (Figure 3.22a) and porphyroclasts drafting sinistral shear scene crossed polarized light magnificent 5× (Figure 3.22).

Porphyroclast illustrates strain shadow of $\sigma$ type in sinistral shear scene on plane polarized light magnification 10× (Figure 3.23a) and drafting sinistral shear scene on plane polarized light magnificent 10× (Figure 3.23b). Moreover, porphyroclast illustrates dissolution in dark horizontal seams on crossed polarized light magnification 10× (Figure 3.24a) and porphyroclasts drafting of sinistral shear scene with on crossed polarized light magnificent 10× (Figure 3.23b). Almost of microstructure of the Permian rocks are illustrated strain shadow and some part showed c-type shear bands, shear scene demonstrated in both dextral and sinistral.

Likewise, in the structural analysis plots of Permian rocks can recognized to two groups, such as the first group is bedding planes plot and second group is foliation planes plot. Bedding planes plot composed of outcrop ID9, ID18, ID43 and ID44. Over all bedding plane plot is 28 planes (Figure 3.25A). Foliation planes plot composed of outcrop ID11, ID12, ID29, ID30, ID31, ID33, ID41, ID42 and ID47. Total of foliation plane plot is 48 planes (Figure 3.26A).

Bedding planes plot (Figure 3.25A) shows orientation in NE-SW. In addition poles plot $\pi$(pi) diagram (Figure 3.25B) to determining the orientation of folding feature demonstrated $\pi$-circle (curve line cross point 1 and 2 in Figure 3.25B) trend axial plane about NE-SW and $\pi$-axis (point 3 in Figure 3.25B) that imply axial plane plunges to NE.

Foliation planes plot illustrates the orientation of the Permian rocks recognizes to two set such as set I foliation plane shows trend in ENE-WSW to ESE-WNW (Figure 3.26A). In addition poles plotted $\pi$diagram (Figure 3.26B) to determining the orientation of folding feature demonstrated $\pi$-circle (curve line cross point 1 and 2 in Figure 3.26B) trend axial plane about E-W and $\pi$-axis (point 3 in Figure 3.26B) that imply axial plane plunges to E. Set II foliation planes orientates trend in NE-SW (Figure 3.27a). Poles plotted $\pi$diagram (Figure 3.27B) to determining the orientation of folding feature demonstrated $\pi$-circle (curve line cross point 1 and 2 in Figure 3.27B) trend axial plane about N-S and $\pi$-axis indicates axial plane plunges to S (point 3 in Figure 3.27B)

Figure 3.3 Photograph shows outcrop ID12 of siltstone (Looking to E) foliation plane 267°/68°, dip direction to NW. Coordinate 795544E/1593082N. Hammer has length 16.5 inches.

Figure 3.4 Photograph shows outcrop ID44 of shale (Looking to SW) illustrates bedding plane 038°/64° dip direction to SE. Coordinate 787959E/1611504N.

Figure 3.5 Photograph shows outcrop ID11 of siltstone (Looking to SE) shows foliation plane 181°/75° dip direction to W. Coordinate 795973E/1592226N.


Figure 3.6 Photograph shows slab sample of outcrop ID11.

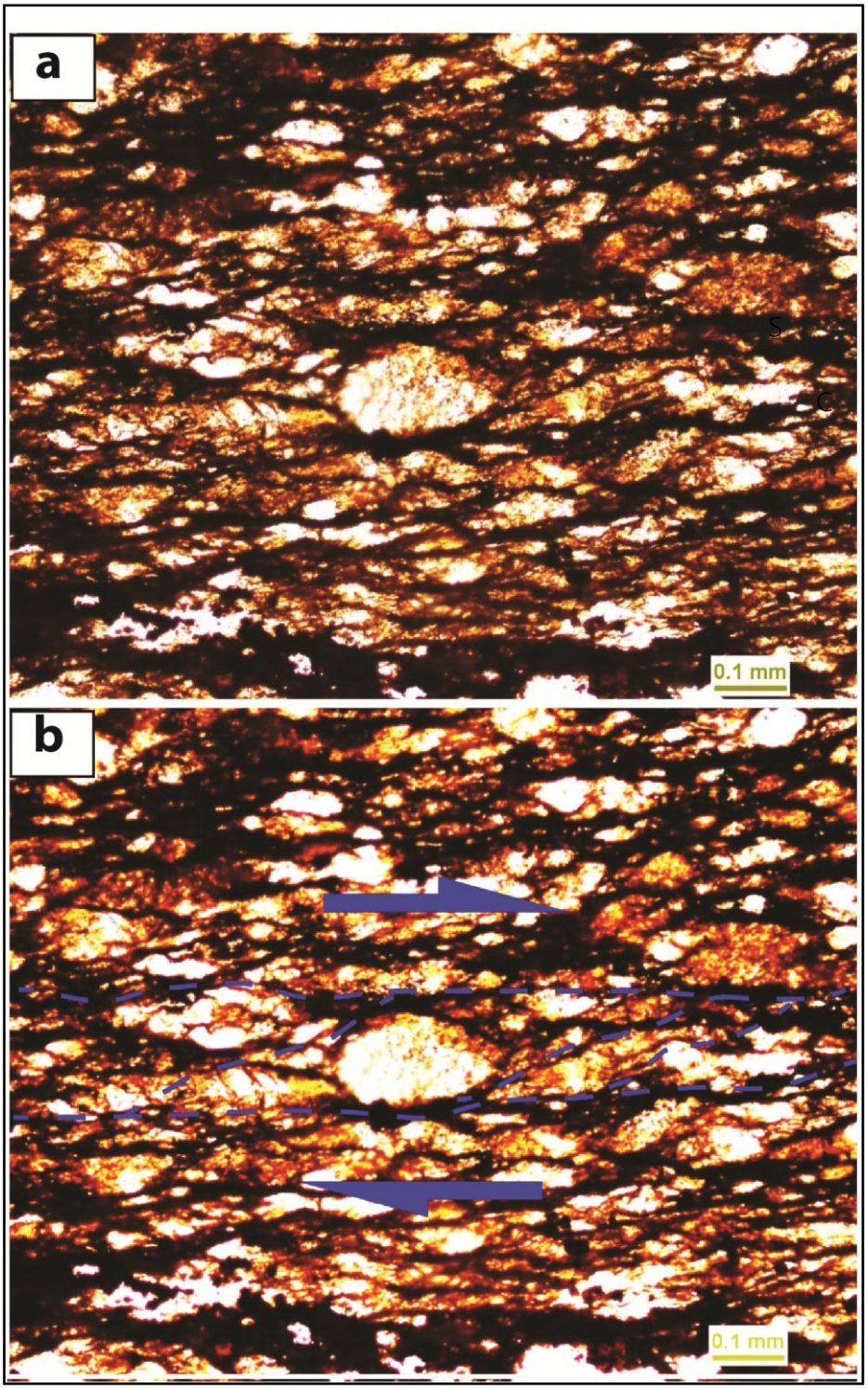


Figure 3.7 Photograph of microstructure shows (a) c-type shear bands of quartz. (b) Microstructure shows dextral shear scene of c-type shear bands of outcrop ID11, L1, PPL 10×.

Figure 3.8 Photograph exhibits shale outcrop ID41 (Looking to SW) foliation plane 023°/41° dip direction to SE. Coordinate 788804E/1608429N.

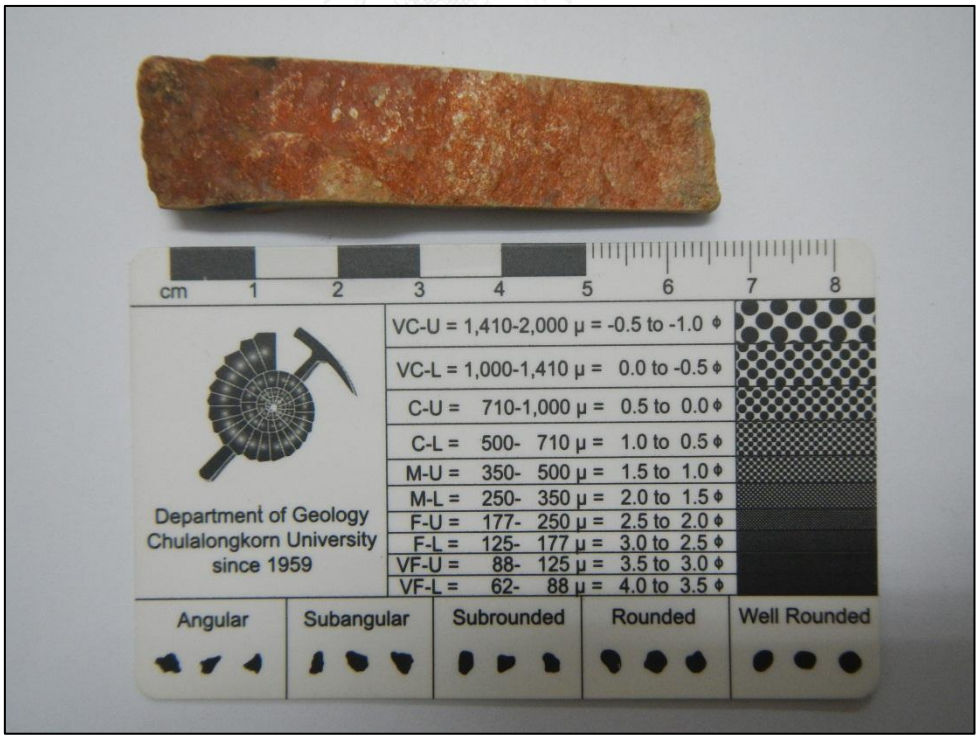


Figure 3.9 Photograph shows slab sample of outcrop ID41.

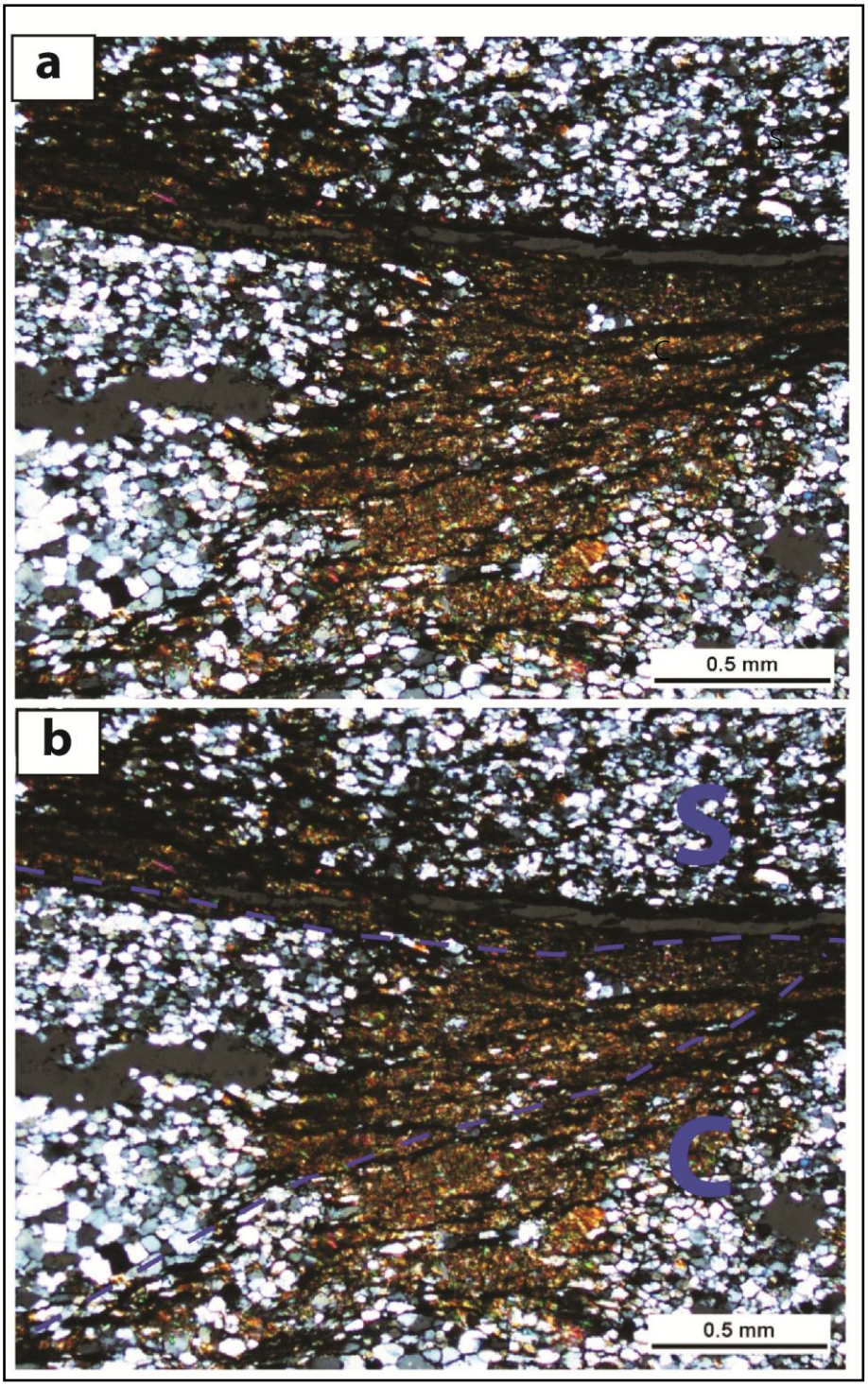


Figure 3.10 Photograph of microstructures shows (a) Oblique foliation. (b) Dashed lines showing exposition of oblique foliation. Outcrop ID41, L1, CPL 5×.

Figure 3.11 Photograph of shale outcrop ID42 (Looking to NW) foliation 009°/50° dip direction to SE. Coordinate 789880 E/1608813 N.

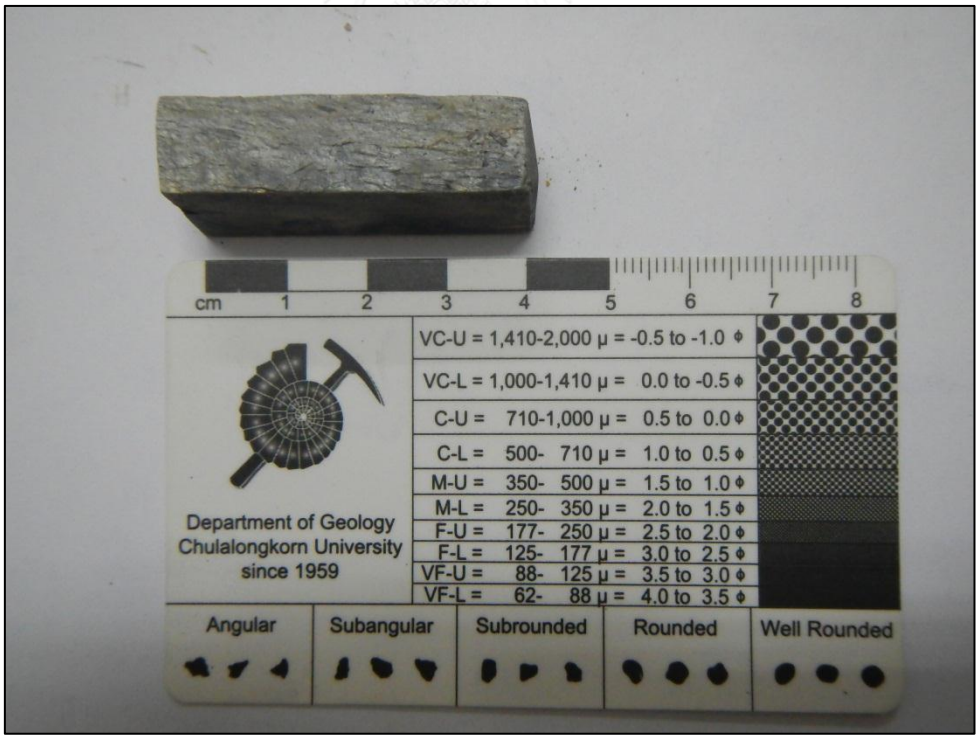


Figure 3.12 Photograph shows slab sample of outcrop ID42.

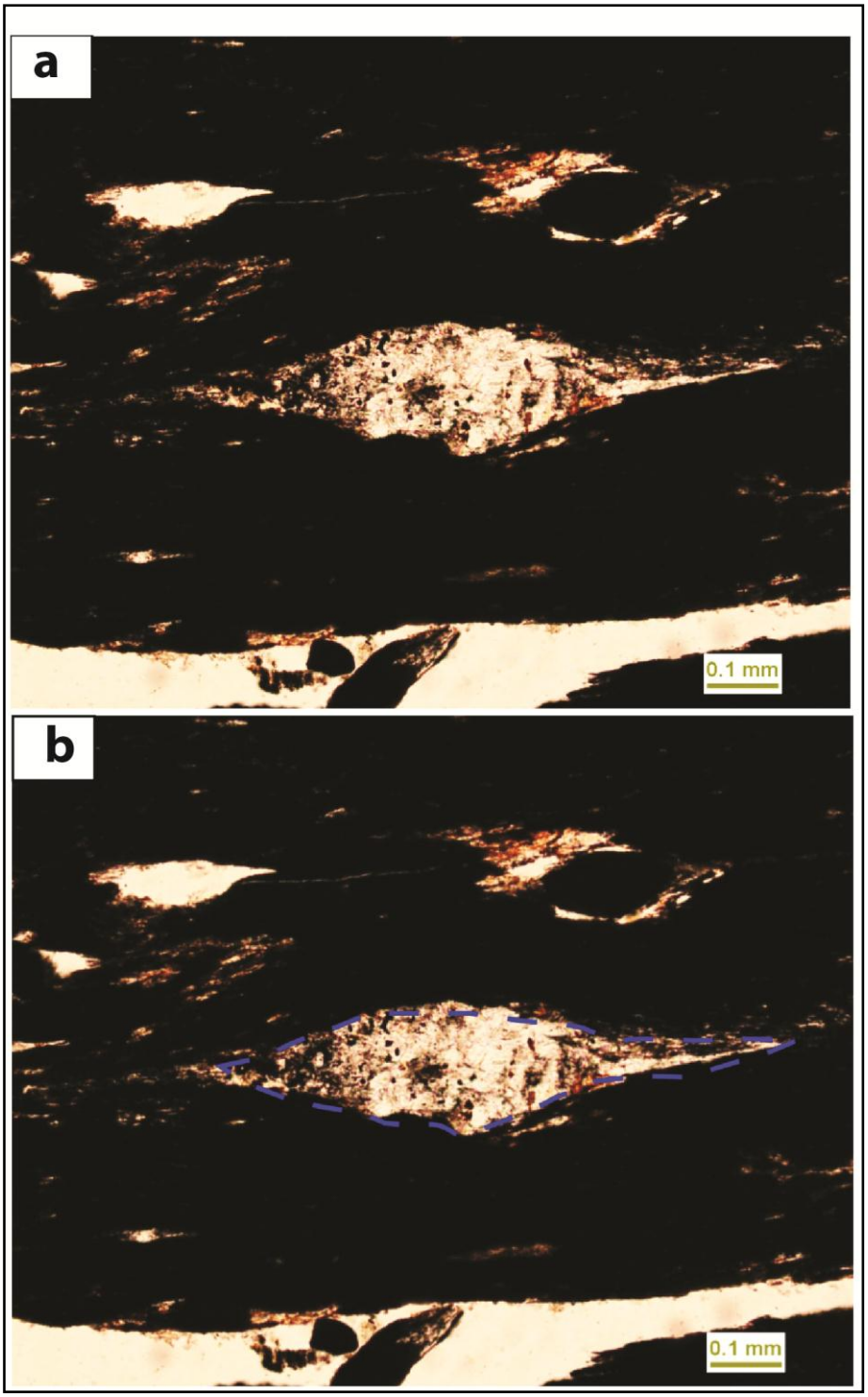


Figure 3.13 Photograph of microstructures shows (a) Quartz porphyroclasts Ø type start strain shadow. (b) Drafting of quartz porphyroclasts Ø type start strain shadow. Outcrop ID42, L1, PPL 10×.

Figure 3.14 Photograph shows outcrop of siltstone interbedded limestone ID43 (Looking to SE) bedding plane 022°/38° dip direction to SE. Coordinate 789830E/1609385N.


Figure 3.15 Photograph shows slab sample of outcrop ID43.

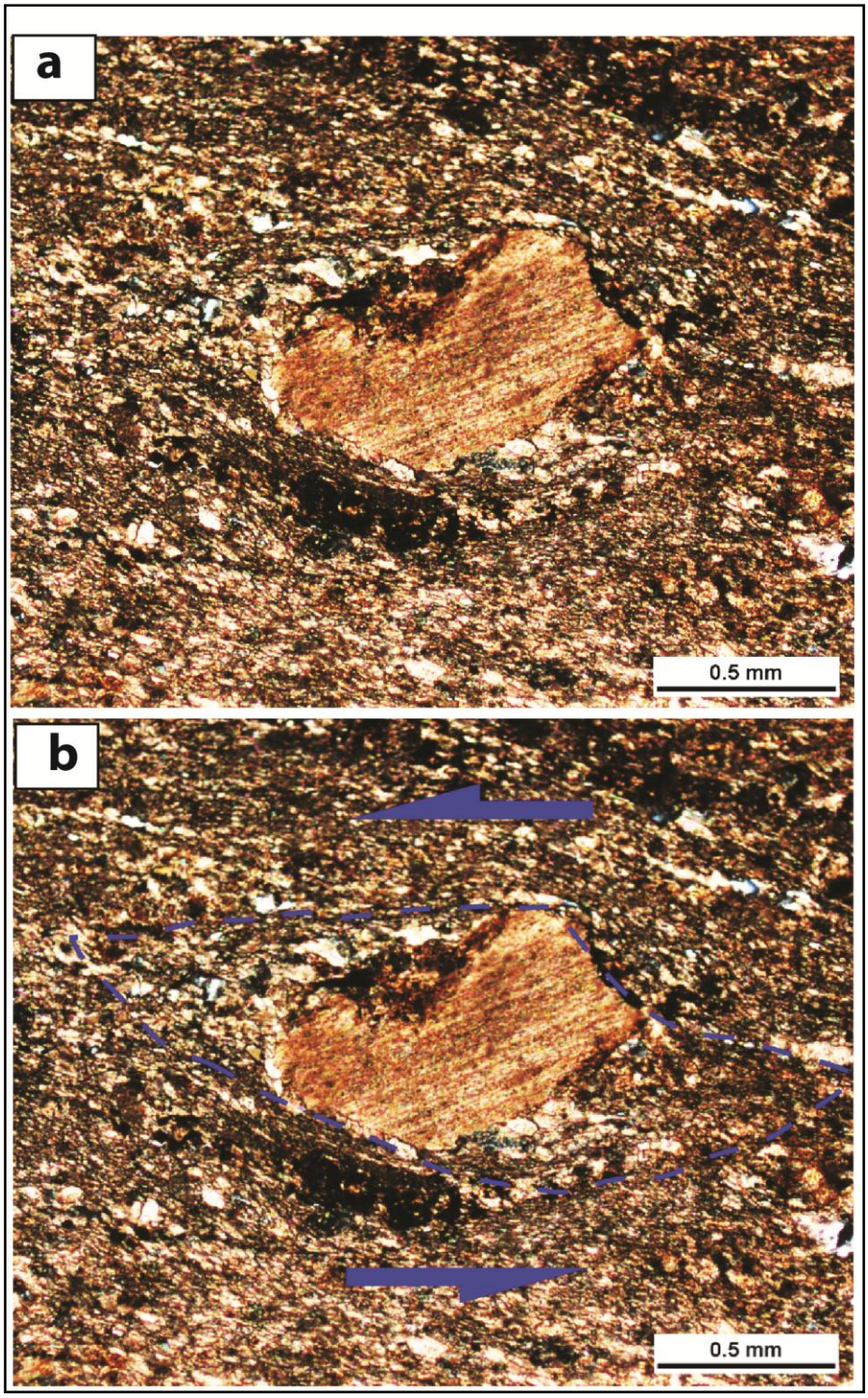


Figure 3.16 Photograph of microstructure shows (a) Feldspar porphyroclasts $\sigma$ type. (b) drafting strain shadow of porphyroclasts $\sigma$ type in sinistral shear scene. Outcrop ID43, L1, CPL 5×.

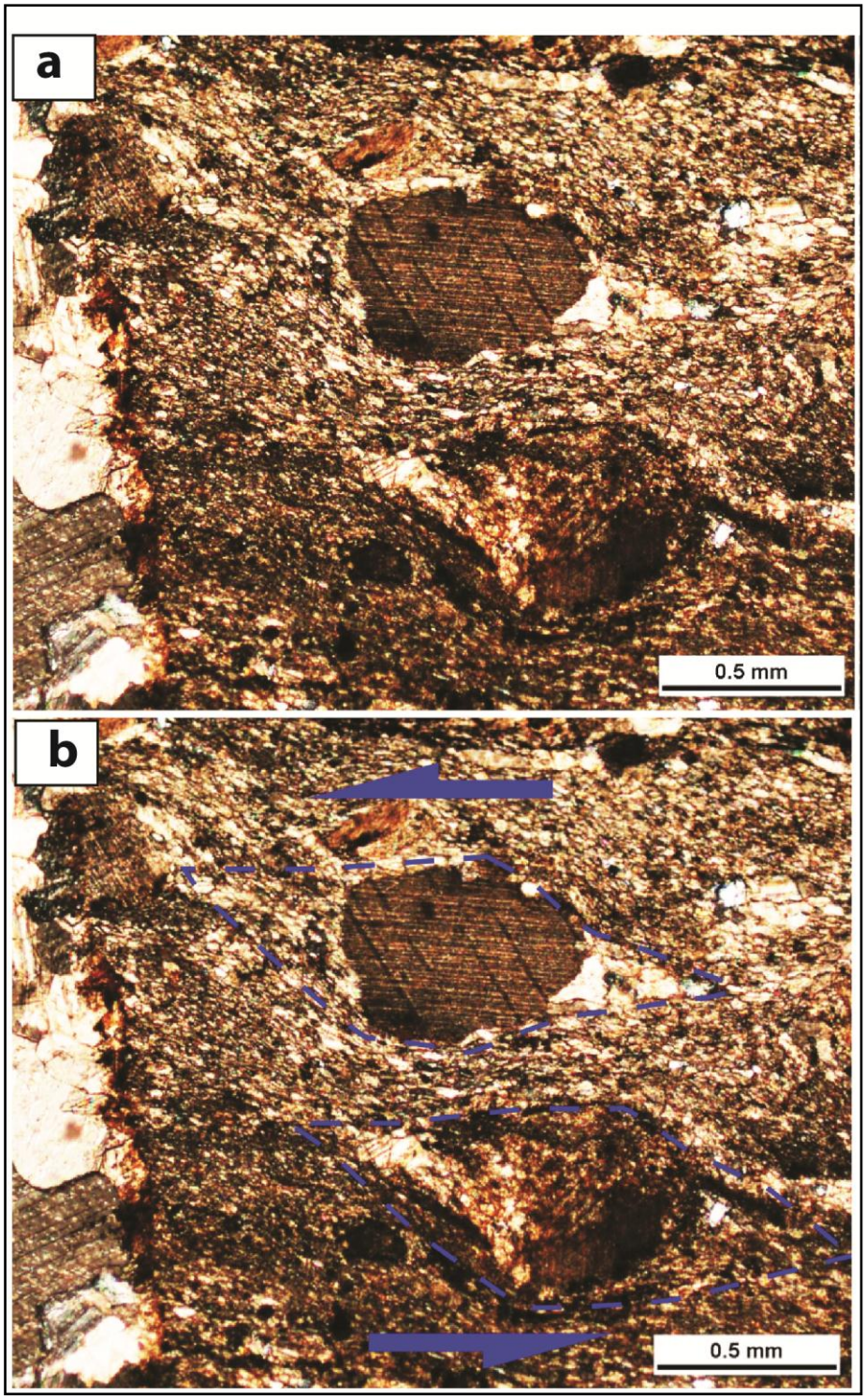


Figure 3.17 Photograph of microstructure shows (a) Feldspar porphyroclasts $\sigma$ type. (b) Drafting strain shadow of porphyroclasts $\sigma$ type in sinistral shear scene. Outcrop ID43, L2, CPL 5×.

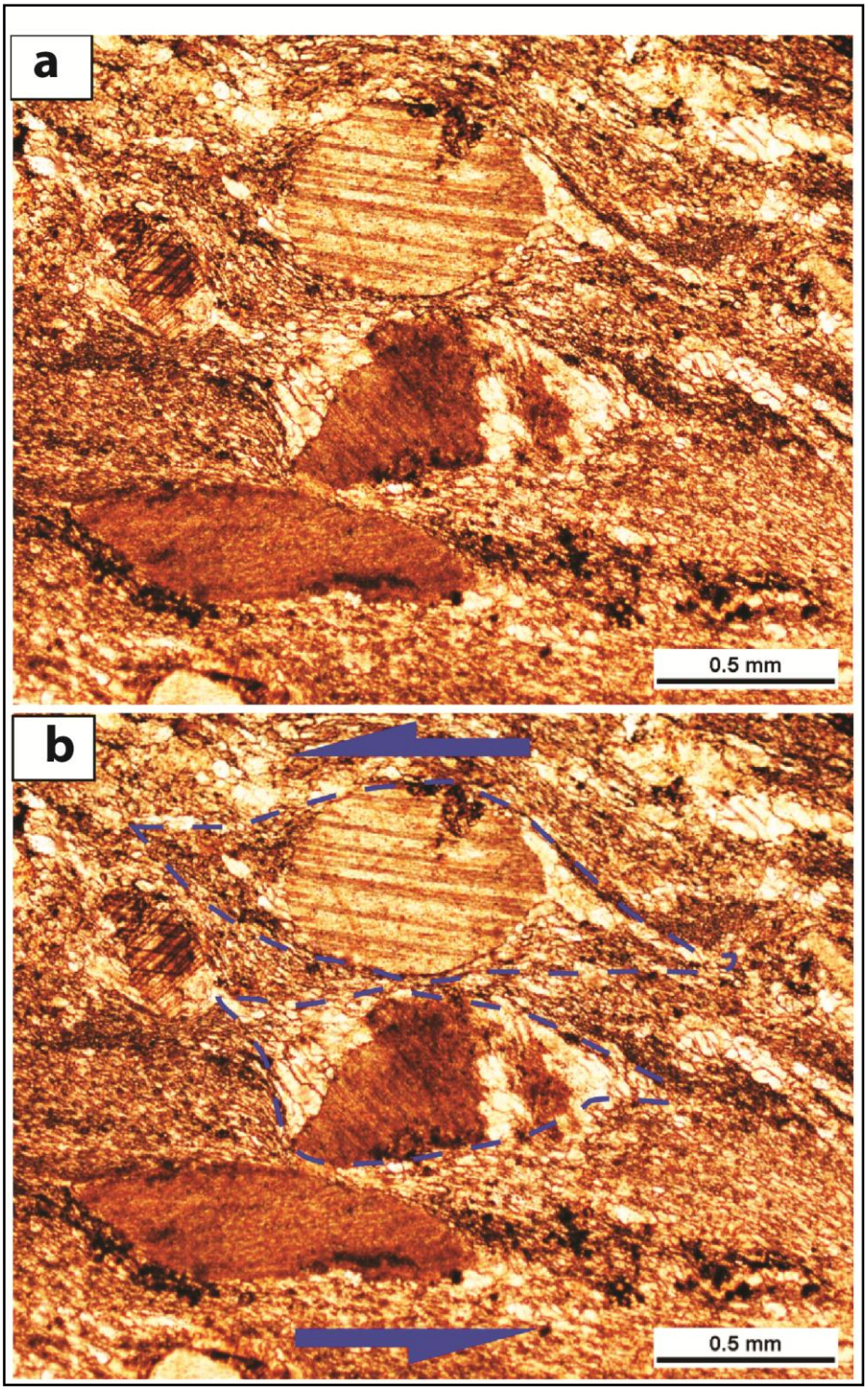


Figure 3.18 Photograph of microstructure shows (a) Feldspar porphyroclasts $\sigma$ type. (b) Drafting strain shadow of porphyroclasts $\sigma$ type in sinistral shear scene. Outcrop ID43, L3, PPL 5×.

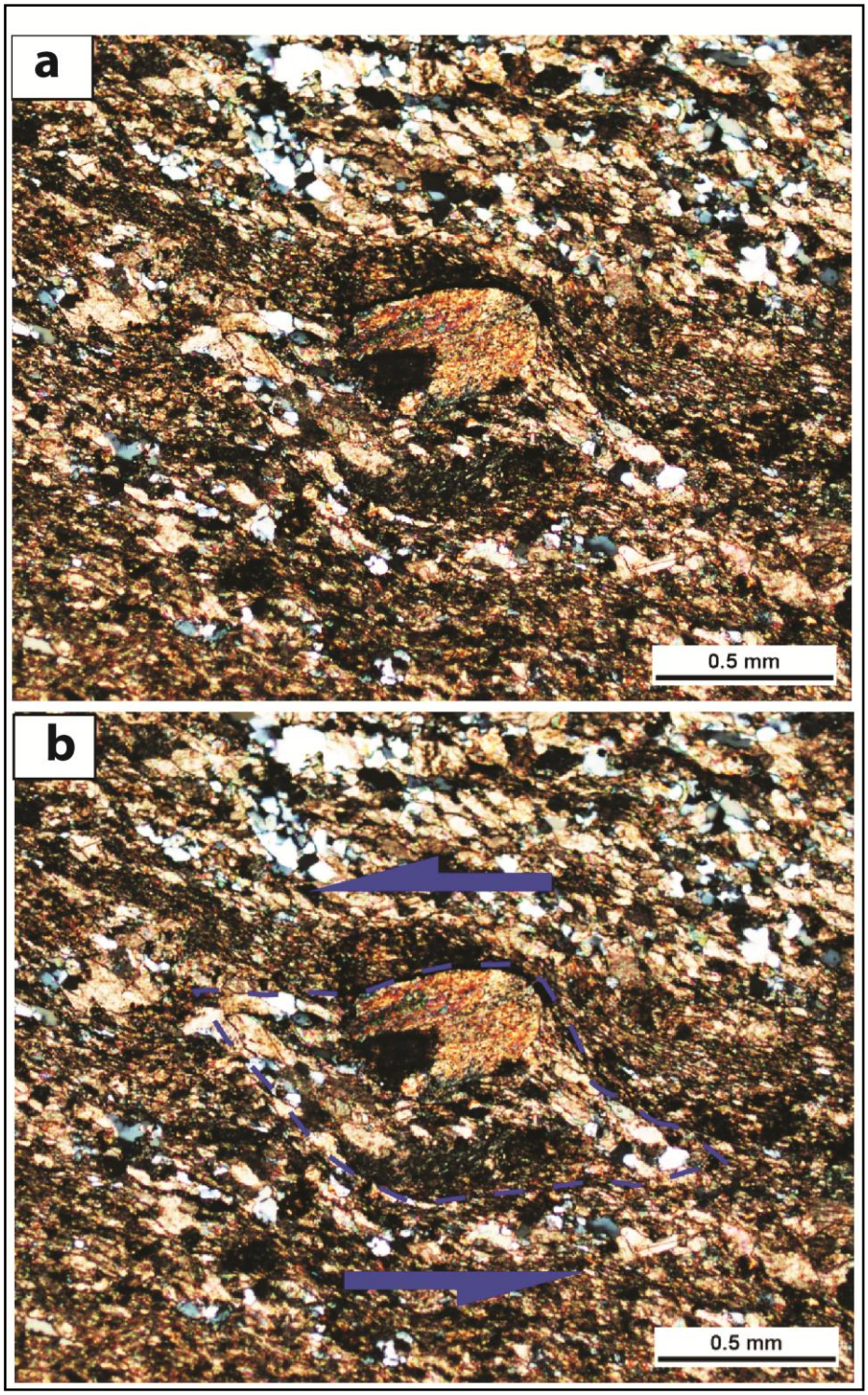


Figure 3.19 Photograph of microstructure shows strain shadow (a) Porphyroclasts $\sigma$ type. (b) Drafting strain shadow of porphyroclasts $\sigma$ type in sinistral shear scene. Outcrop ID43, L4, CPL 5×.

Figure 3.20 Photograph illustrates outcrop of shale and quartz veins ID47 (Looking to W) foliation 068°/52° dip direction to SE. Coordinate 789642E/ 1612082N.

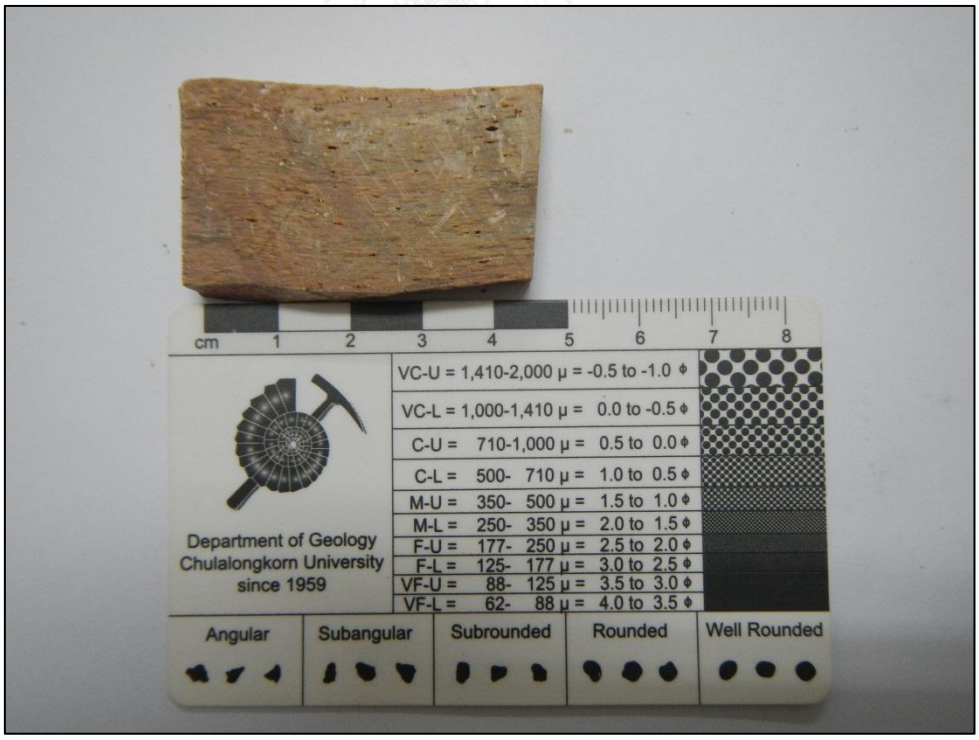


Figure 3.21 Photograph shows slab sample of outcrop ID47.

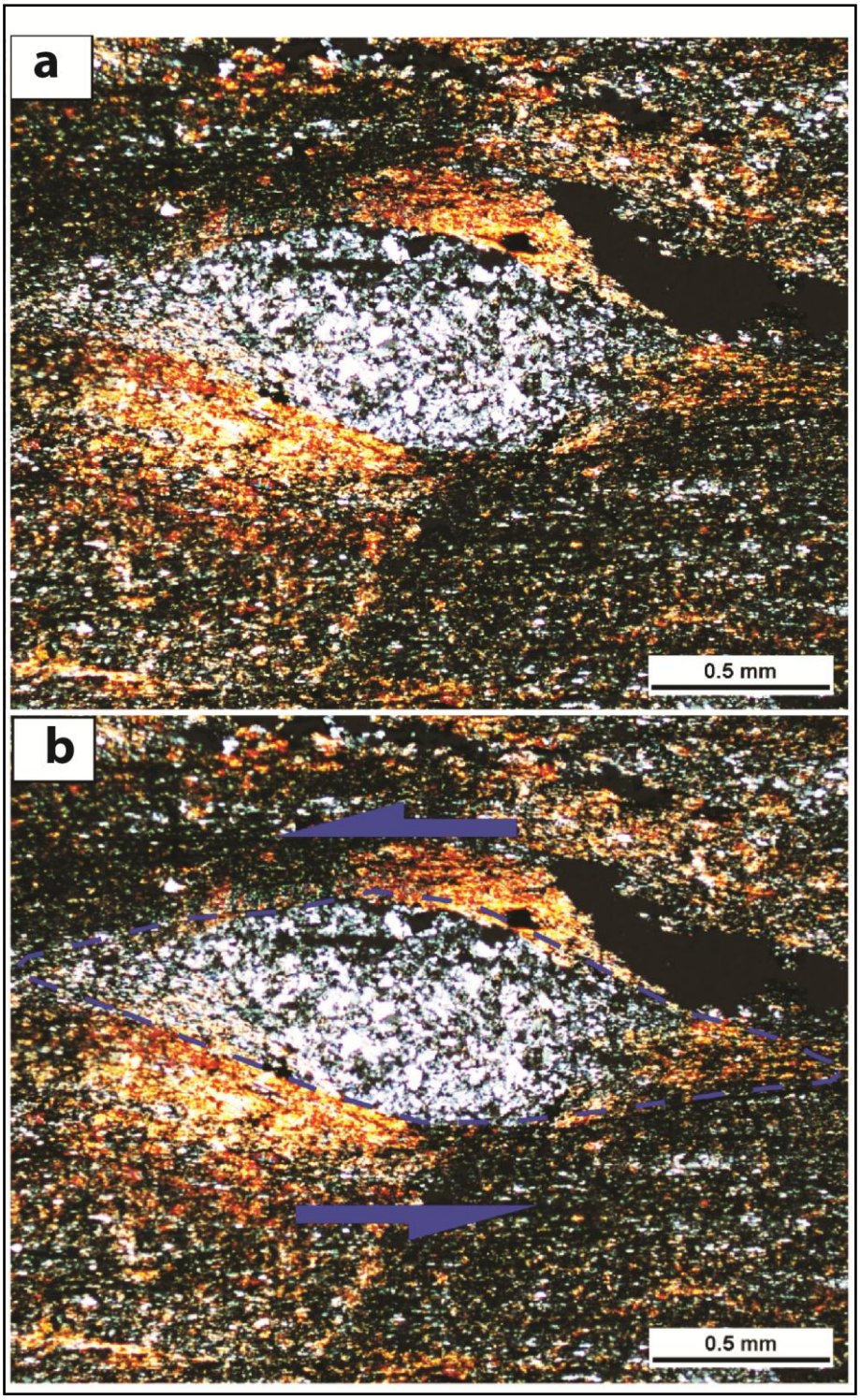


Figure 3.22 Photograph of microstructure appears (a) strain shadow of porphyroclasts $\sigma$ type. (b) Drafting of porphyroclasts $\sigma$ type which indicates sinistral shear scene. Outcrop ID47, L1, CPL 5×.

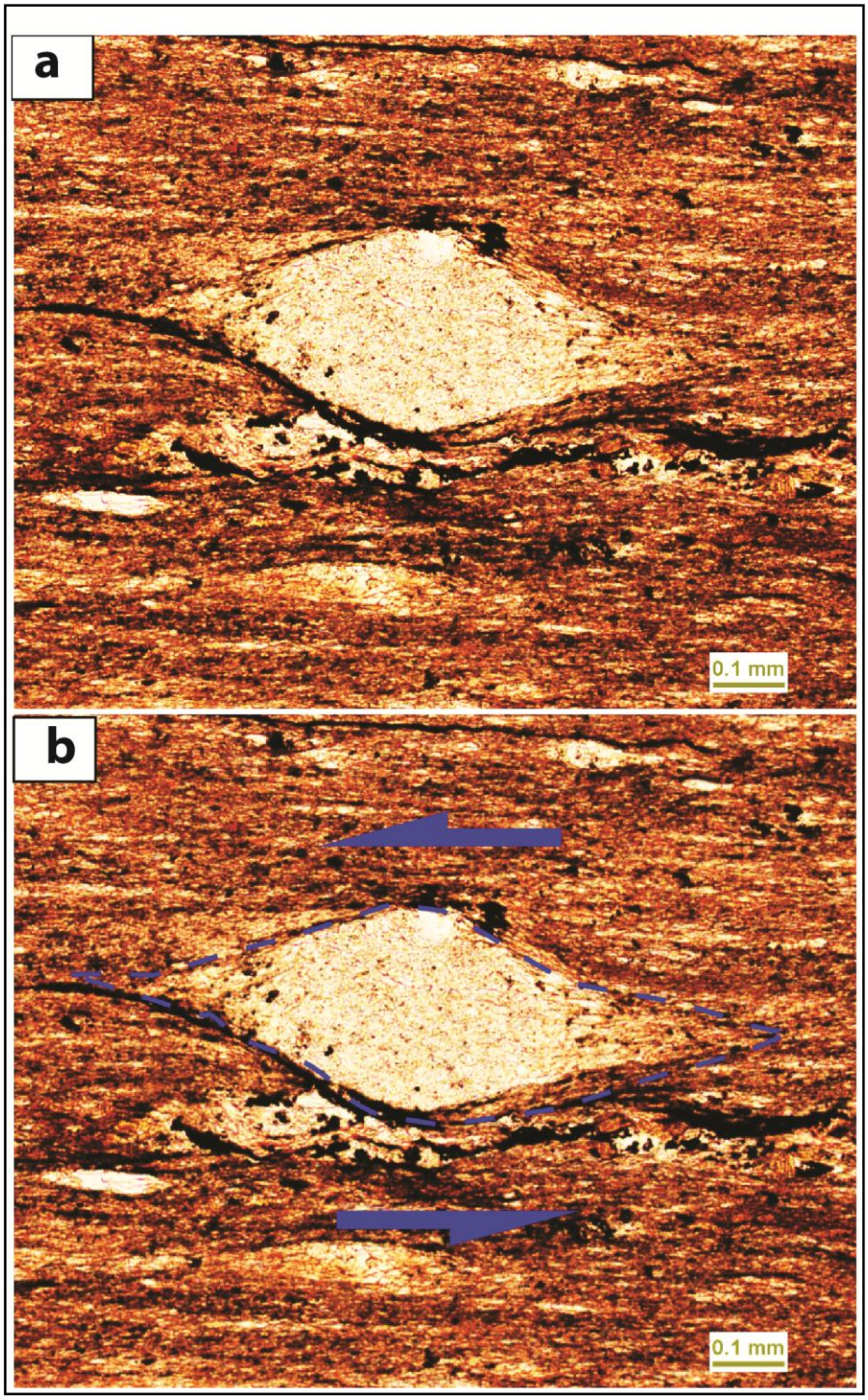


Figure 3.23 Photograph of microstructure shows (a) Strain shadow of porphyroclasts $\sigma$ type. (b) porphyroclasts $\sigma$ type which indicates sinistral shear scene. Outcrop ID47, L2, PPL 10×.

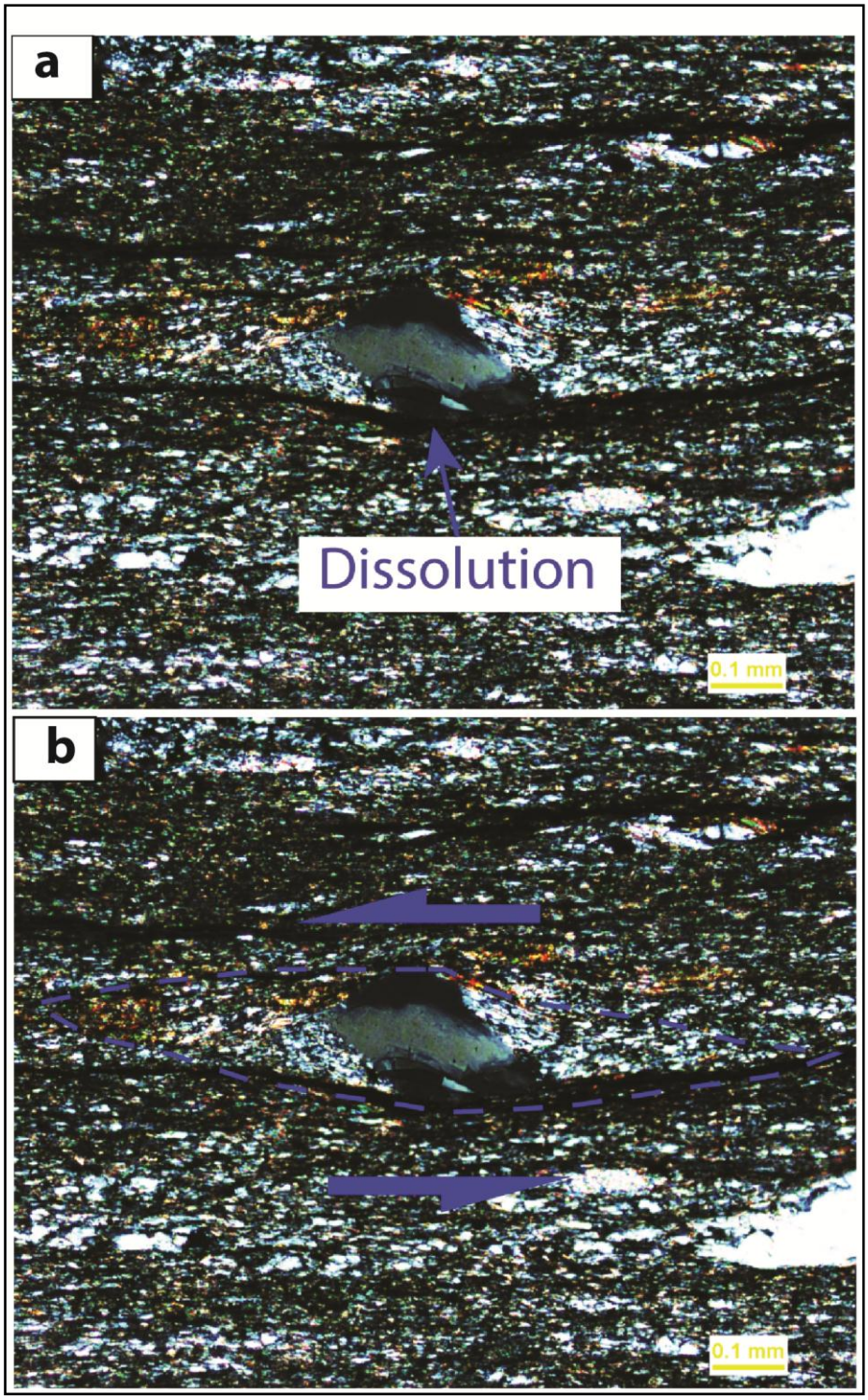


Figure 3.24 Photograph of microstructure illustrates (a) Dissolution (dark horizontal seams). (b) Strain shadow of porphyroclasts $\sigma$ type in sinistral shear scene. Outcrop ID47, L3, CPL 10×.

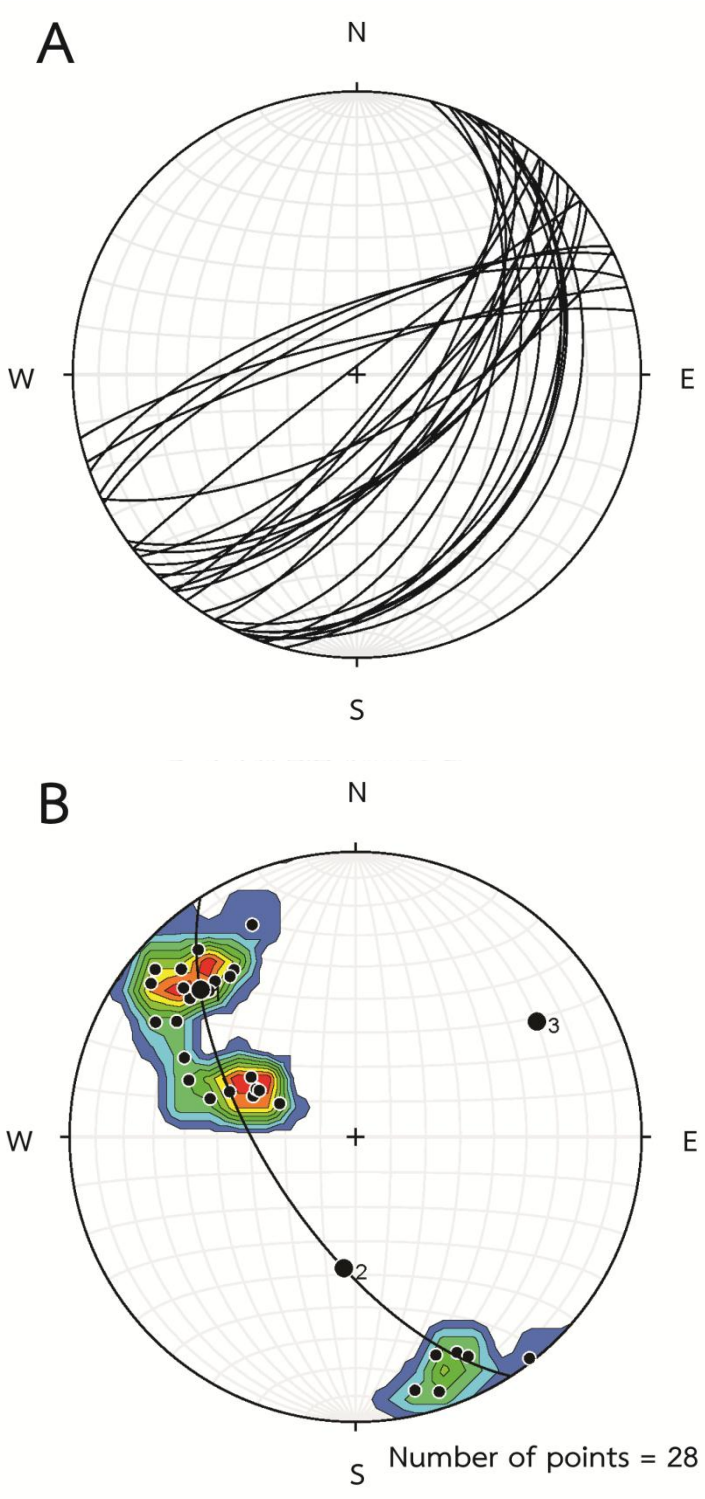


Figure 3.25 Stereonet plot of the Permian rocks (A) Bedding Planes (B) contour pole plot (Contour Int. = 2%; Counting Area = 1% of net area).

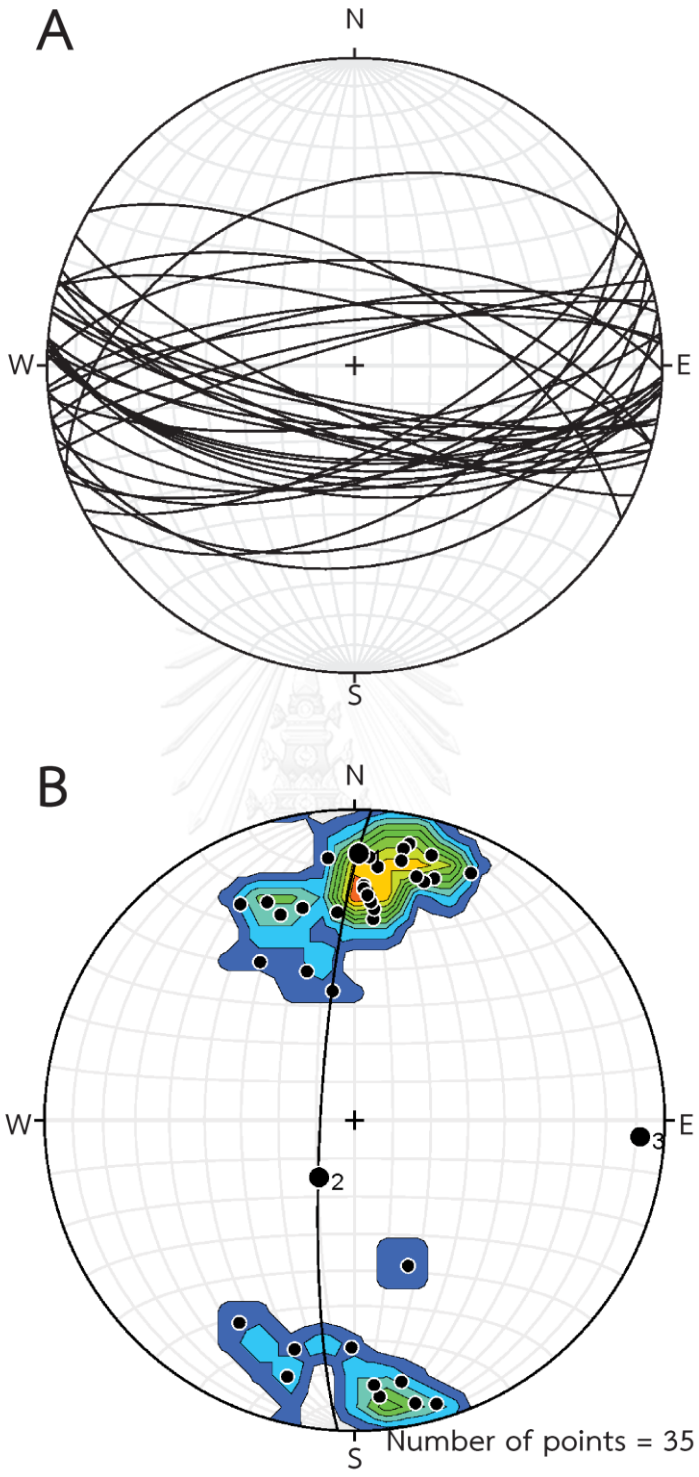


Figure 3.26 Stereonet plot of the Permian rocks (A) Foliation Planes set I (B) contour pole plot (Contour Int. = 2%; Counting Area = 1% of net area).

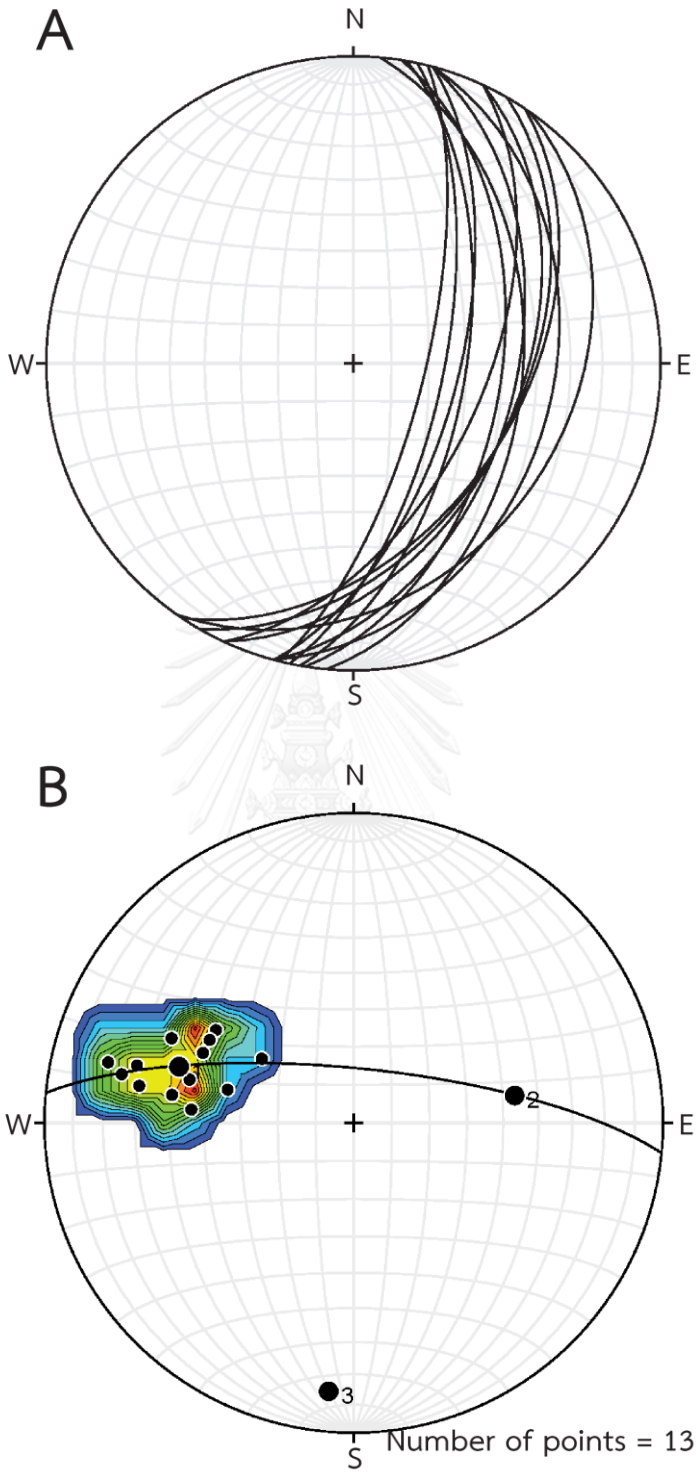


Figure 3.27 Stereonet plot of the Permian rocks (A) Foliation Planes set II (B) contour pole plot (Contour Int. = 2%; Counting Area = 1% of net area).

### 3.2 Permo-Triassic rocks

Permo-Triassic rocks (Figure 3.28) are dominated by the volcanic clastic rocks such as tuff with the color of green to dark green, andesite and rhyolite.

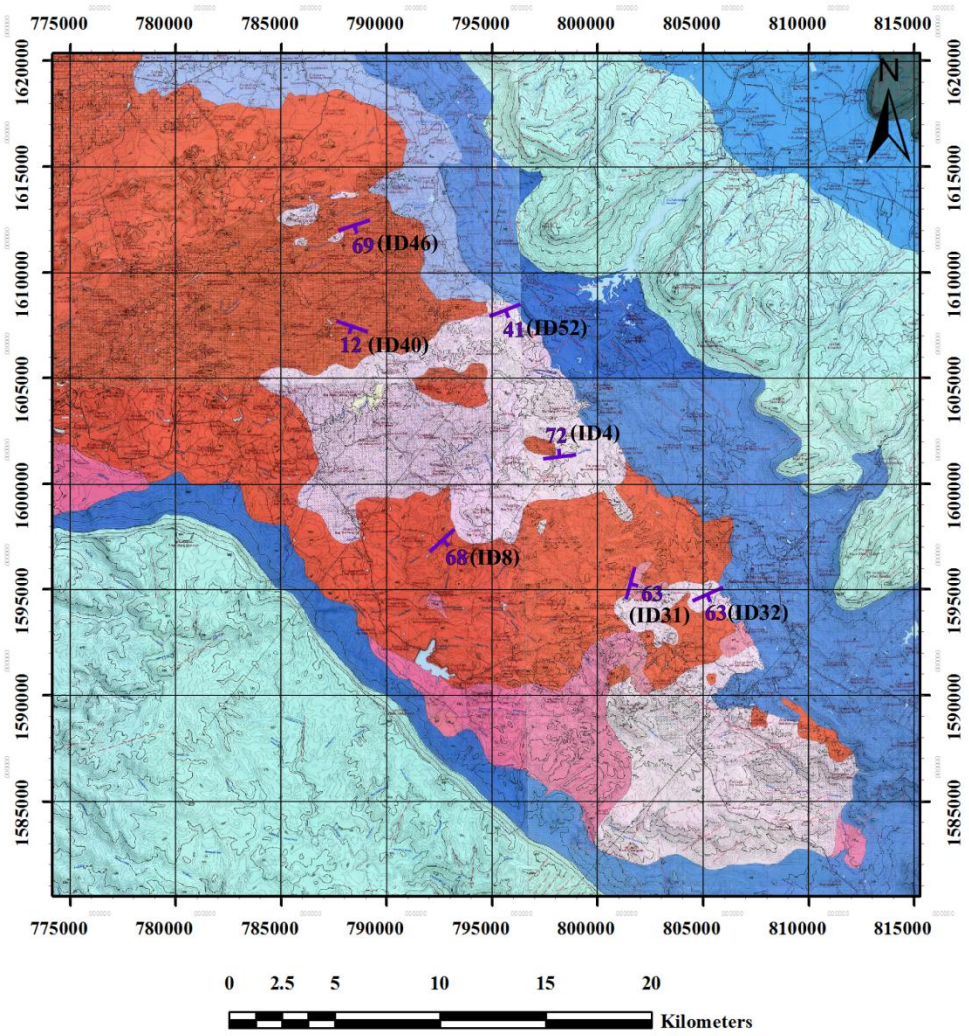


Figure 3.28 Map shows dispersion and foliation of Permo-Triassic outcrops.

Outcrop tuff ID4 (Figure 3.28) illustrated foliation plane 262°/72° dip direction to NW (Figure 3.29). Outcrop Tuff ID32 (Figure 3.28) shows foliation plane 066°/63° dip direction to NW (Figure 3.30). Slab sample low weathered (Figure 3.31) and microstructure appear synthetic micro-fault on crossed polarized light magnificent 5× (Figure 3.32a), drafting porphyroclasts of synthetic micro-fault sinistral shear scene crossed polarized light magnificent 5× (Figure 3.32b). In addition, tuff outcrop ID46 (Figure 3.28) foliation plane 071°/69° dip direction to SE (Figure 3.33) and illustrated kink band dextral thrust scene (Figure 3.34). Besides, microstructure shows micro-folded thrust in dextral scene direction is apparent on plane polarized light magnificent 5× (Figure 3.35a) and drafting of micro-folded in dextral shear scene crossed polarized light magnificent 5× (Figure 3.35b). Hinge layer on crossed polarized light magnificent 5× (Figure 3.36a) and drafting of hinge layer on crossed polarized light magnificent 5× (Figure 3.36b). Not only hinge of layer, but also grains are hinged on crossed polarized light magnificent 5× (Figure 3.37a) and drafting micro-folded shows dextral shear scene on crossed polarized light magnificent 5× (Figure 3.37b). Moreover, micro-folded are extended grains minerals to boudins on plane polarized light magnificent 5× (Figure 3.38a), and drafting of micro-folded shows dextral shear scene on crossed polarized light magnificent 5× (Figure 3.38b). Also, porphyroclasts of tuff outcrop ID46 illustrated strain shadow on crossed polarized light magnificent 5× (Figure 3.39a) and drafting of porphyroclasts $\emptyset$ type on crossed polarized light magnificent 5× (Figure 3.39b) corresponding with kink band in Figure 3.34. Some of porphyroclasts $\sigma$ type showed strain shadow in dextral shear scene are cracked in latter on crossed polarized light magnificent 5×(Figure 3.40a) and drafting porphyroclasts $\sigma$ type shows dextral shear scene on crossed polarized light magnificent 5× (Figure 3.40b), while development of boudins are appeared on crossed polarized light magnificent 5× (Figure 3.41a) and drafting boudins indicated dextral shear scene (Appendix B) on crossed polarized light magnificent 5× (Figure 3.41b). Moreover, extension mechanism are illustrated in both of frank of grains such as Figure 3.42a illustrates porphyroclasts $\sigma$ type and drafting shows dextral shear

scene (Figure 3.42b) but in Figure 3.43a appears porphyroclasts $\emptyset$ type and drafting illustrate not stair steeping (Figure 3.43).

Stereonet plot of 45 plane (Figure 3.44A) illustrated foliations of the Permo-Triassic rocks into two groups are ENE-WSW to NE-SW. Moreover, poles plotted $\pi$ diagram (Figure 3.44B) to determining folding feature demonstrated trend axial plane about NE-SW and $\pi$-axis that imply axial plane plunges to NE.

Figure 3.29 Photograph of tuff outcrop ID4 (Looking to S) orientation 262°/72° dip direction to NW. Coordinate 798106E/1601526N.

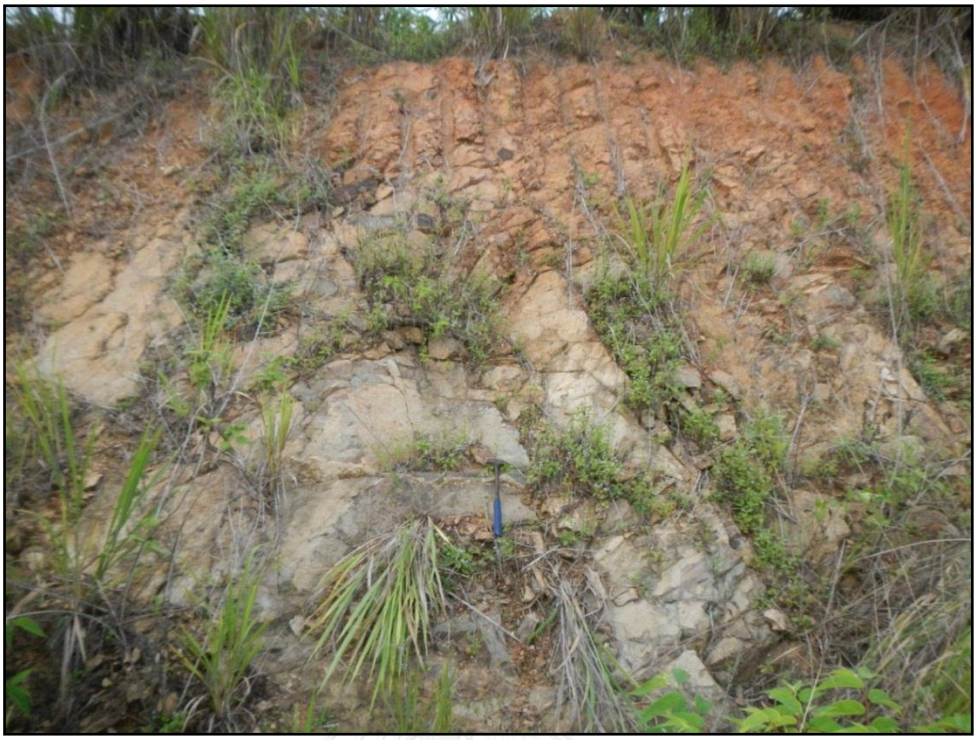

Figure 3.30 Photograph tuff outcrop ID32 (Looking to S) orientation 066°/63° dip direction to NW. Coordinate 805302E/1594530N.

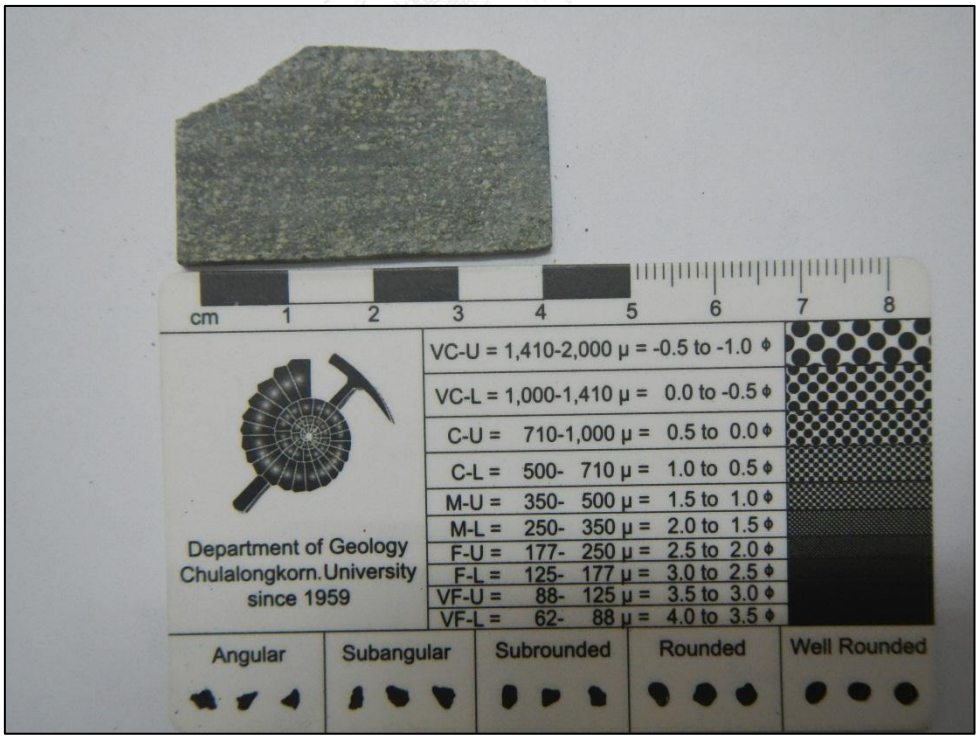


Figure 3.31 Photograph shows slab sample of outcrop ID32.

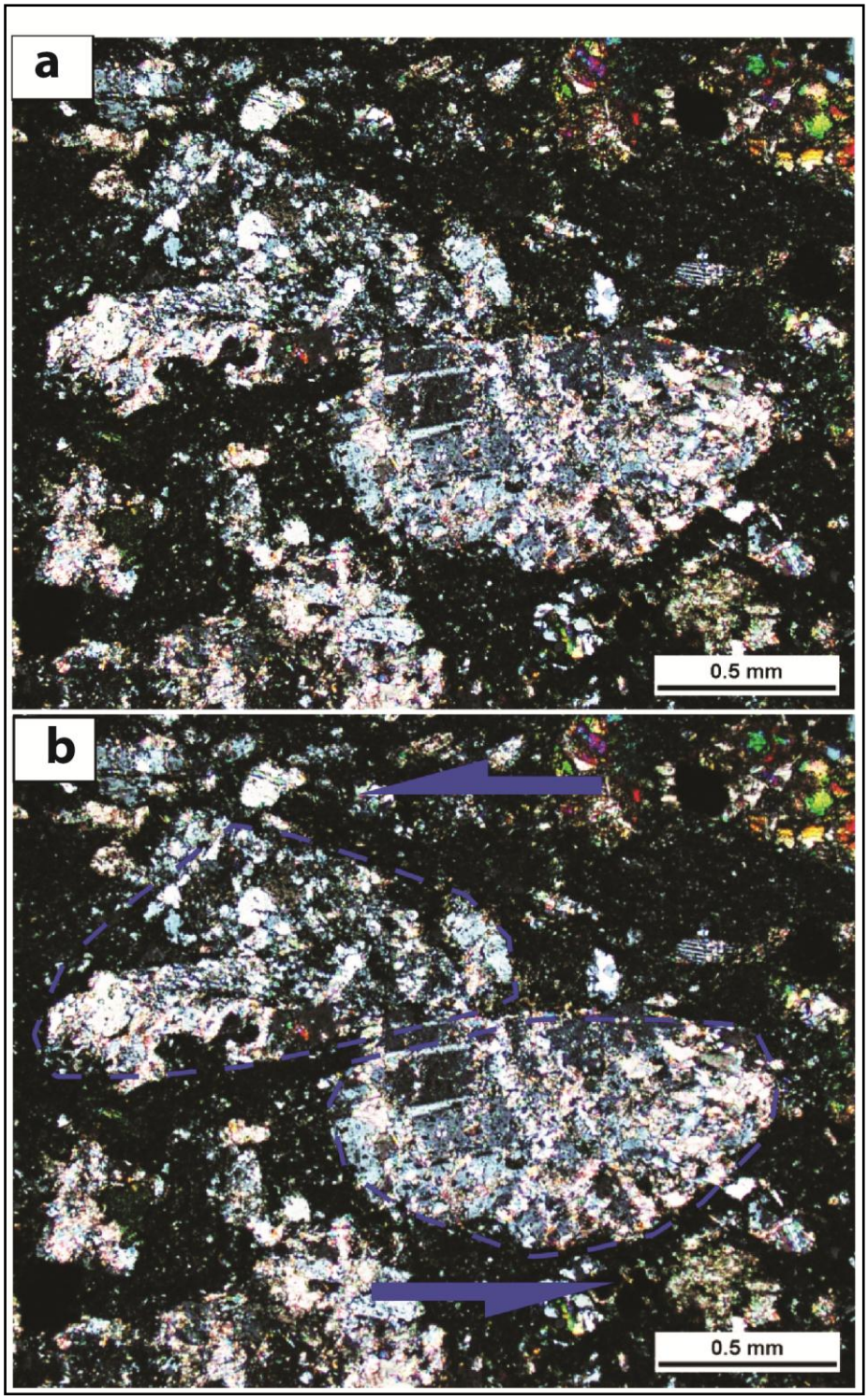


Figure 3.32 Photograph of microstructures shows (a) Synthetic micro-fault. (b) Drafting of synthetic micro-fault in sinistral shear scene. Outcrop ID32, L1, CPL 5×.

Figure 3.33 Photograph Tuff outcrop ID46 (Looking to NE) orientation 071°/69° dip direction to SE. Coordinate 788514E/1611975N.

Figure 3.34 Photograph shows kink bands. Outcrop of Tuff ID46 (close up). Compass has diameter long about 3.1 inches and wide 2.8 inches.

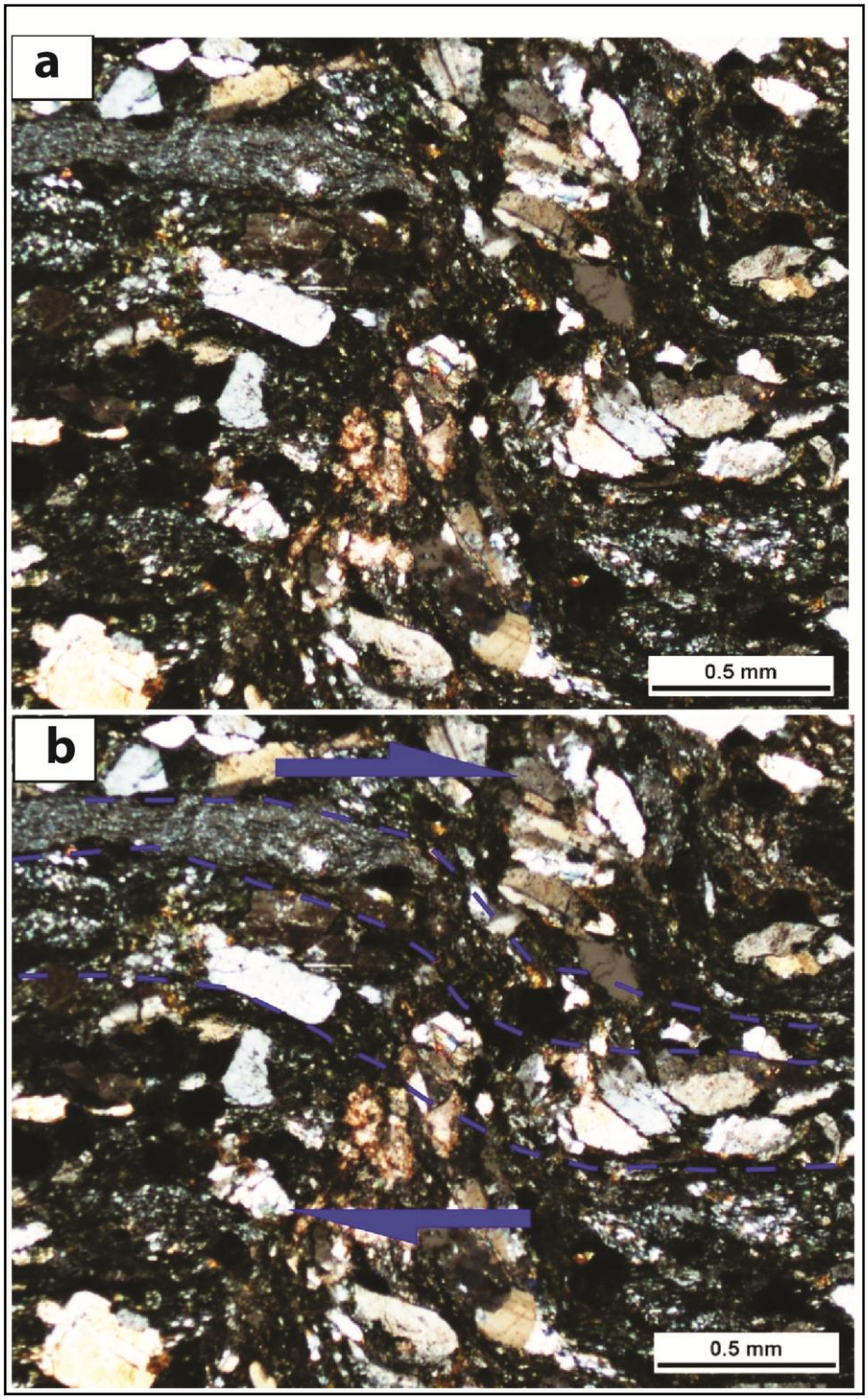


Figure 3.35 Photograph of microstructures shows (a) Micro-folded in tuff. (b) Drafting micro-folded which indicates dextral shear scene. Outcrop ID46, L1, CPL 5×.

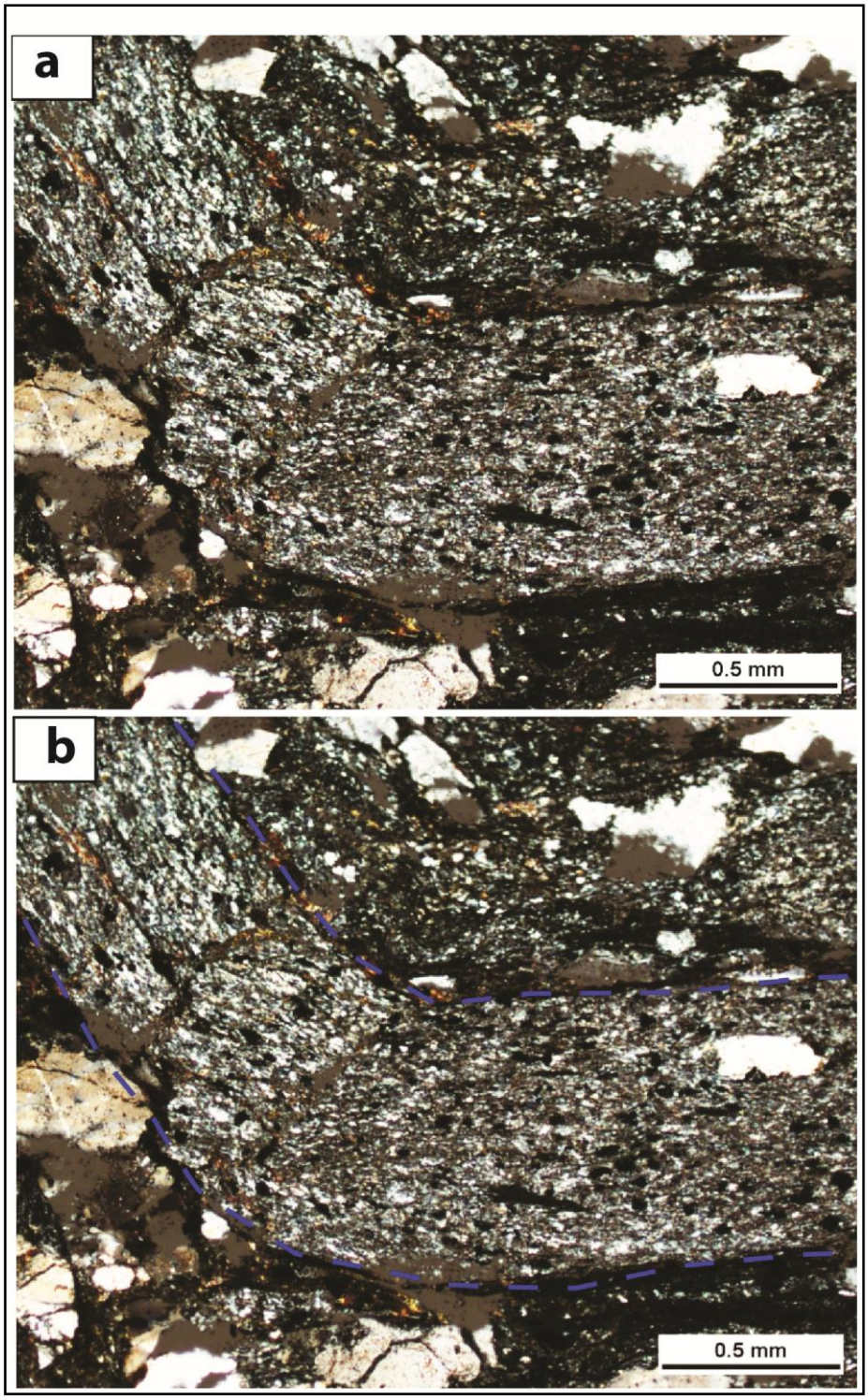


Figure 3.36 Photograph of microstructures shows (a) Hinge layer. (b) Drafting of hinge layer. Outcrop ID46, L2, CPL 5×.

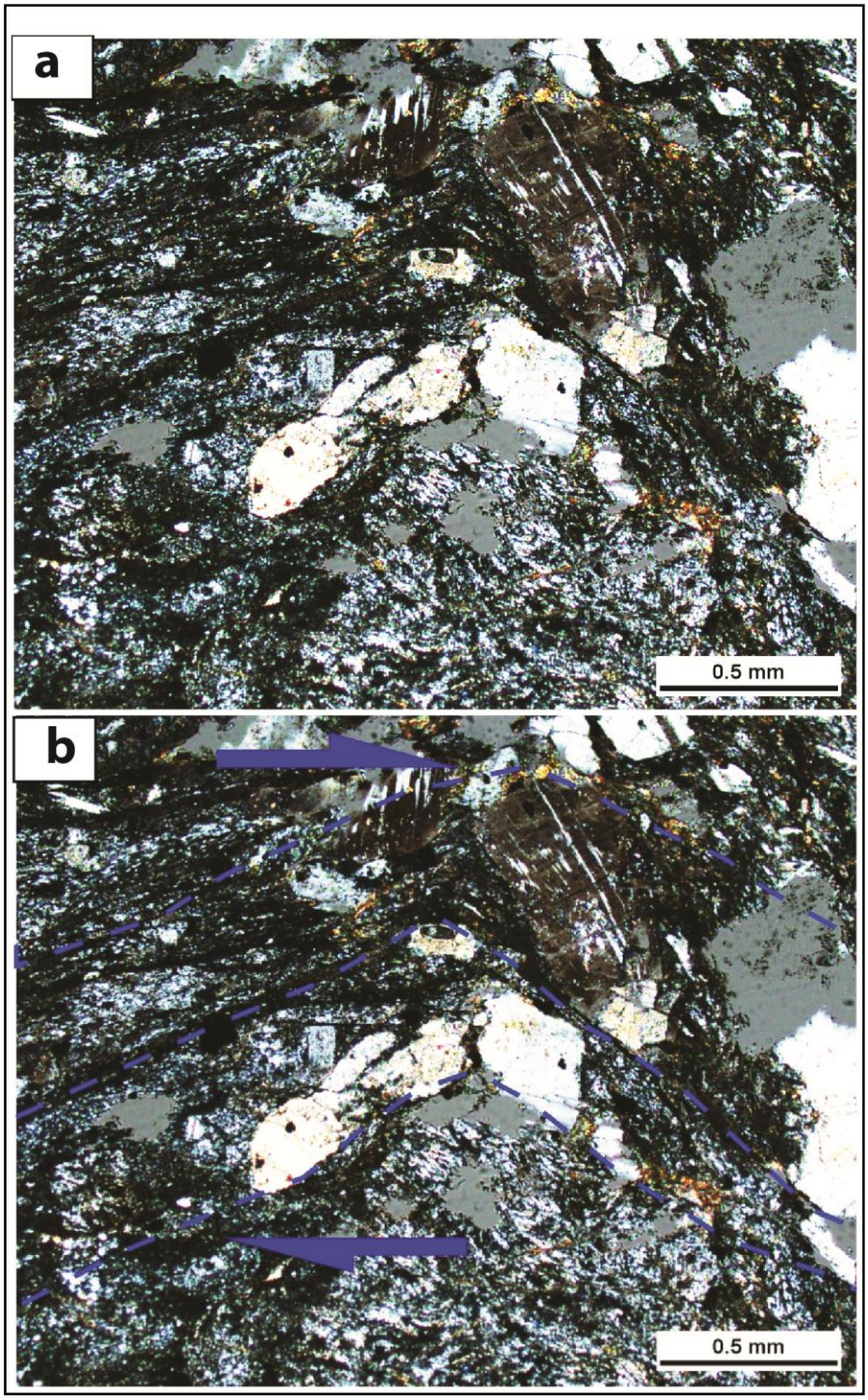


Figure 3.37 Photograph of microstructures shows (a) Micro-folded. (b) Drafting of micro-folded which indicates dextral shear scene. Outcrop ID46, L3, CPL 5×.

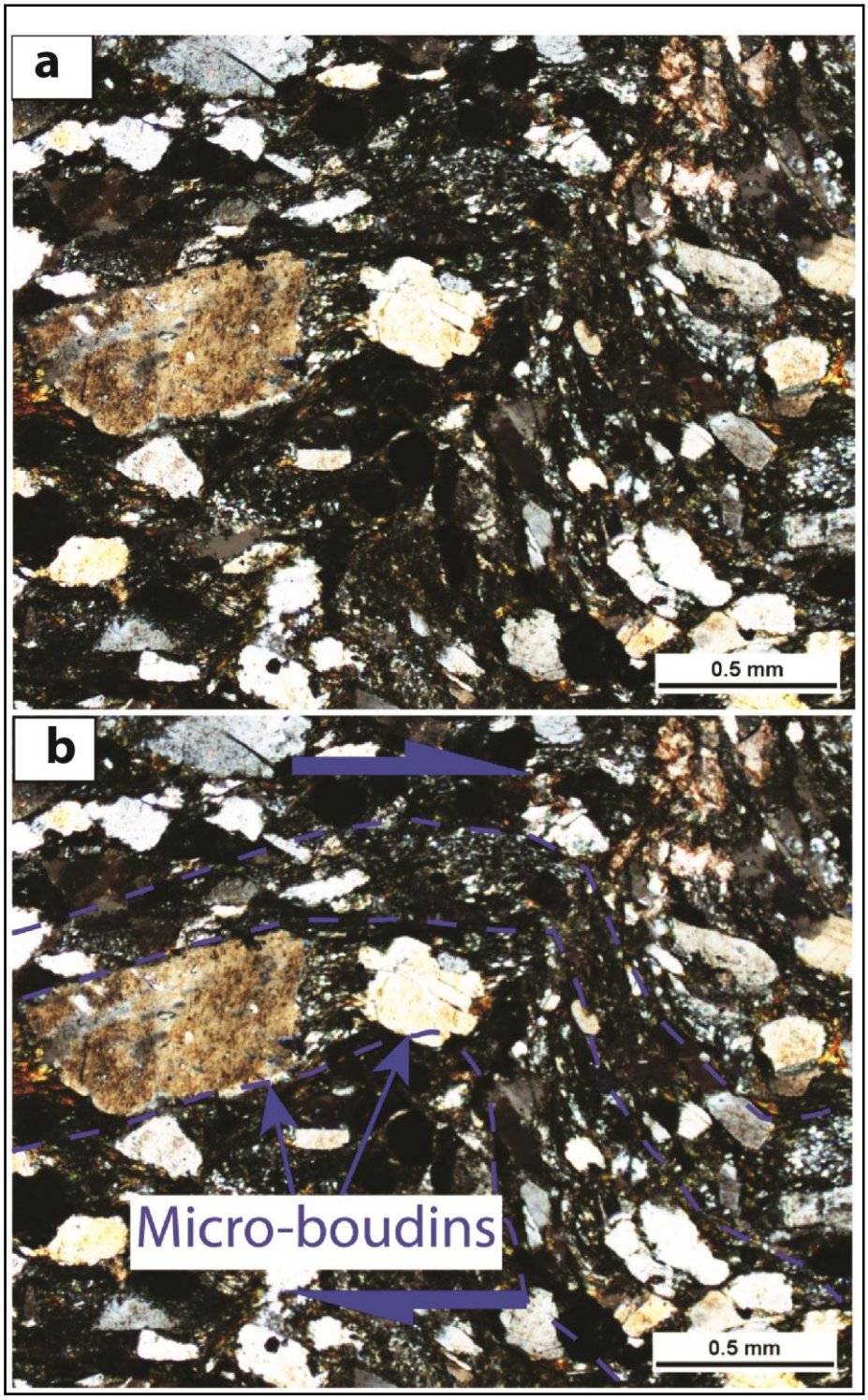


Figure 3.38 Photograph of microstructures shows (a) micro-folded. (b) micro-folded and micro-boudins which indicates dextral shear scene. Outcrop ID46, L4, CPL 5×.

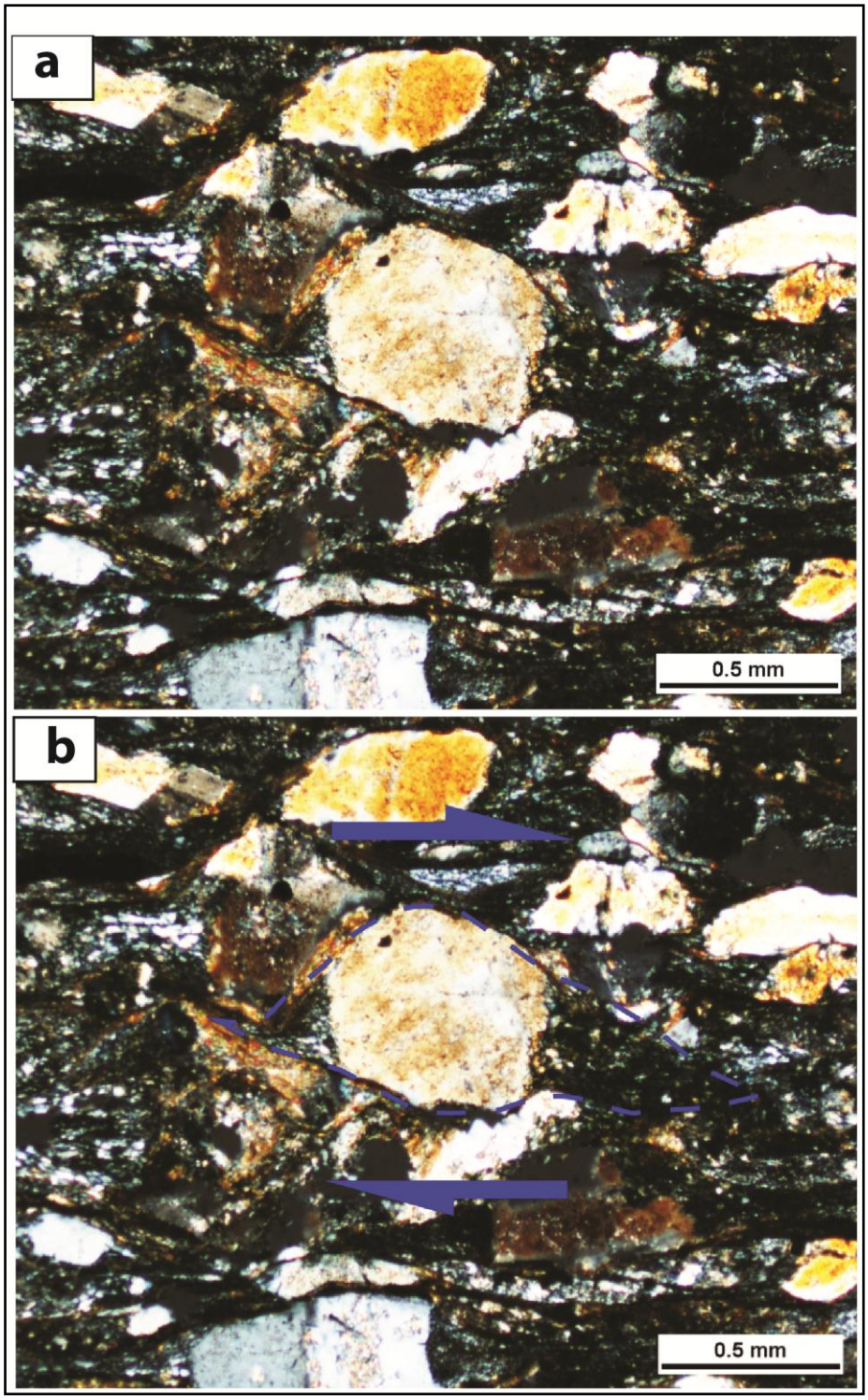


Figure 3.39 Photograph of microstructure shows (a) Strain shadow of porphyroclasts Ø type. (b) Porphyroclasts Ø type indicates no stair stepping Outcrop ID46, L5, CPL 5×.

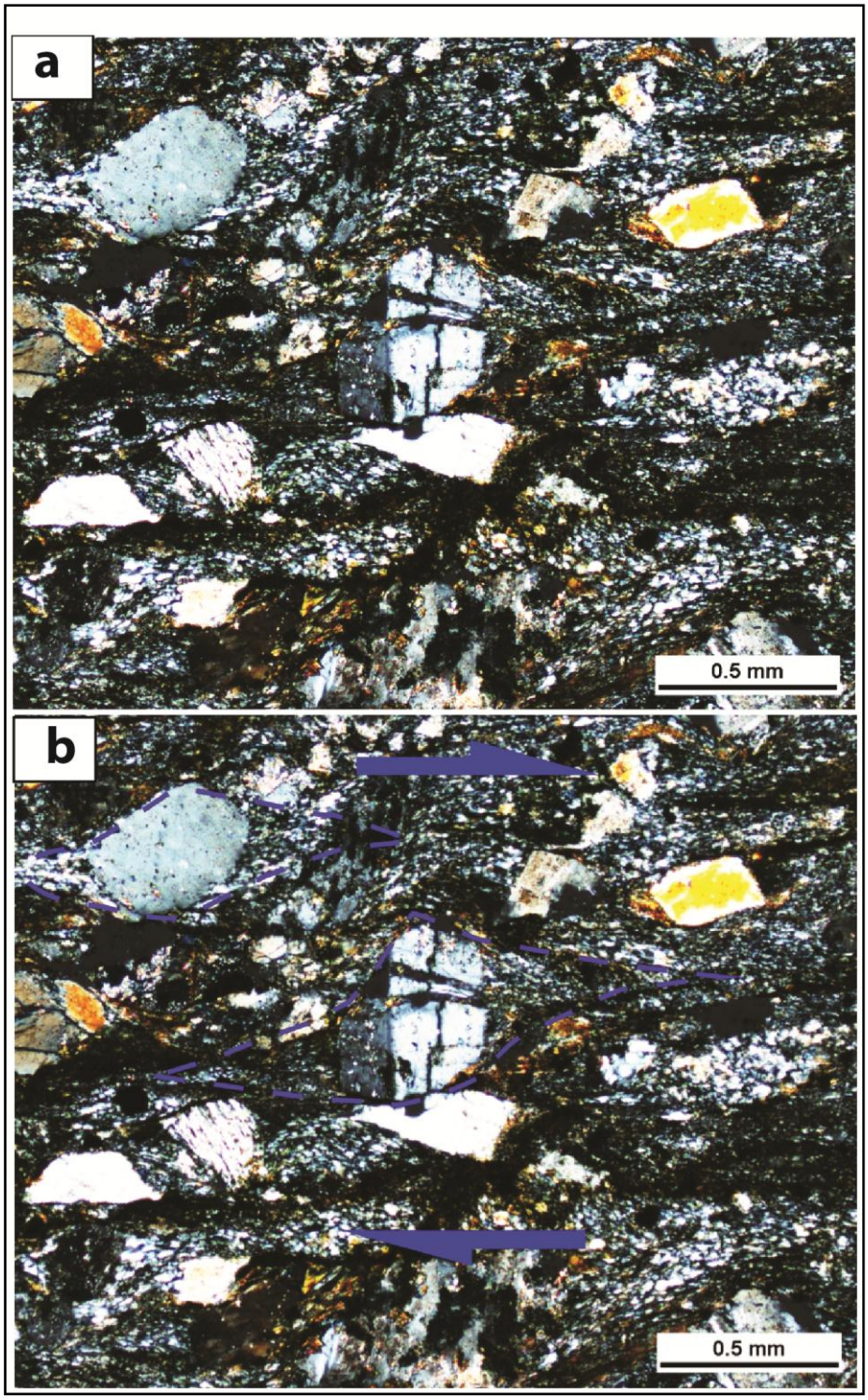


Figure 3.40 Photograph of microstructure shows (a) Strain shadow in porphyroclasts $\sigma$ type. (b) Drafting porphyroclasts $\sigma$ type indicates dextral shear scene Outcrop ID46, L6, CPL 5×.

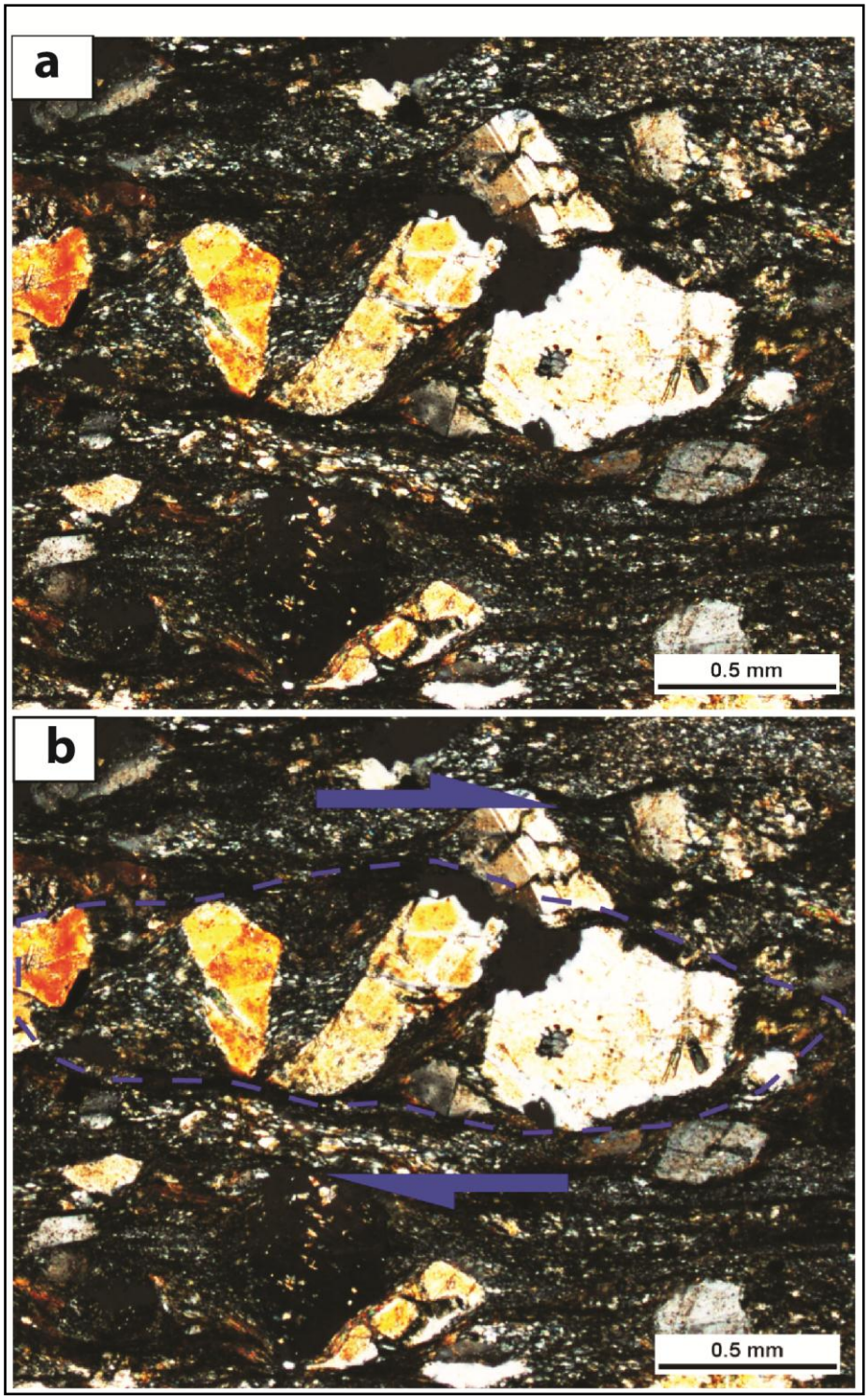


Figure 3.41 Photograph of microstructure Illustrates (a) development of boudins. (b) Drafting of development of boudins which indicates dextral shear scene. Outcrop ID46, L7, CPL 5×.

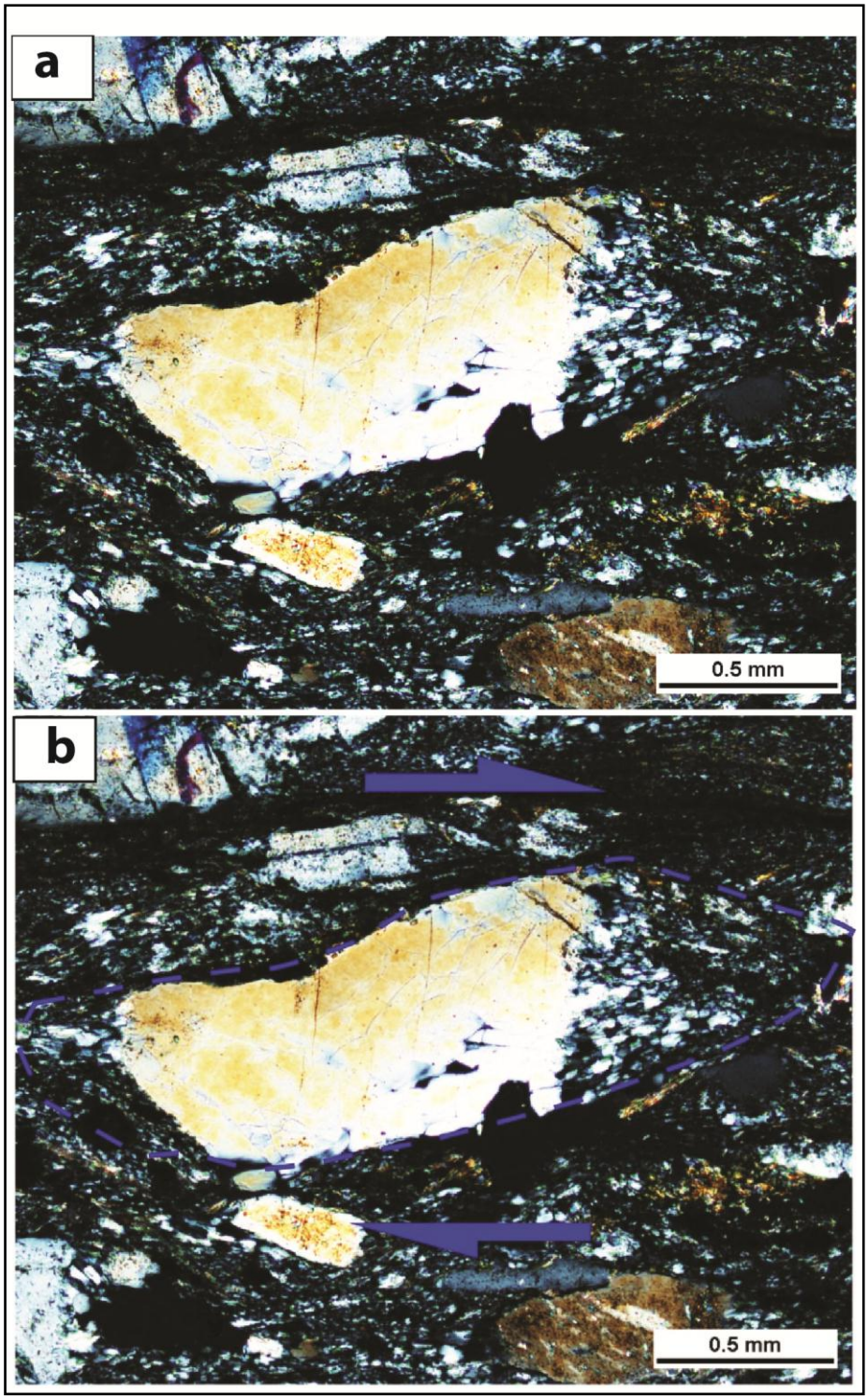


Figure 3.42 Photograph of microstructure Illustrates (a) Porphyroclasts $\sigma$ type. (b) Drafting of porphyroclasts $\sigma$ type indicates dextral shear scene. Outcrop ID46, L8, CPL 5×.

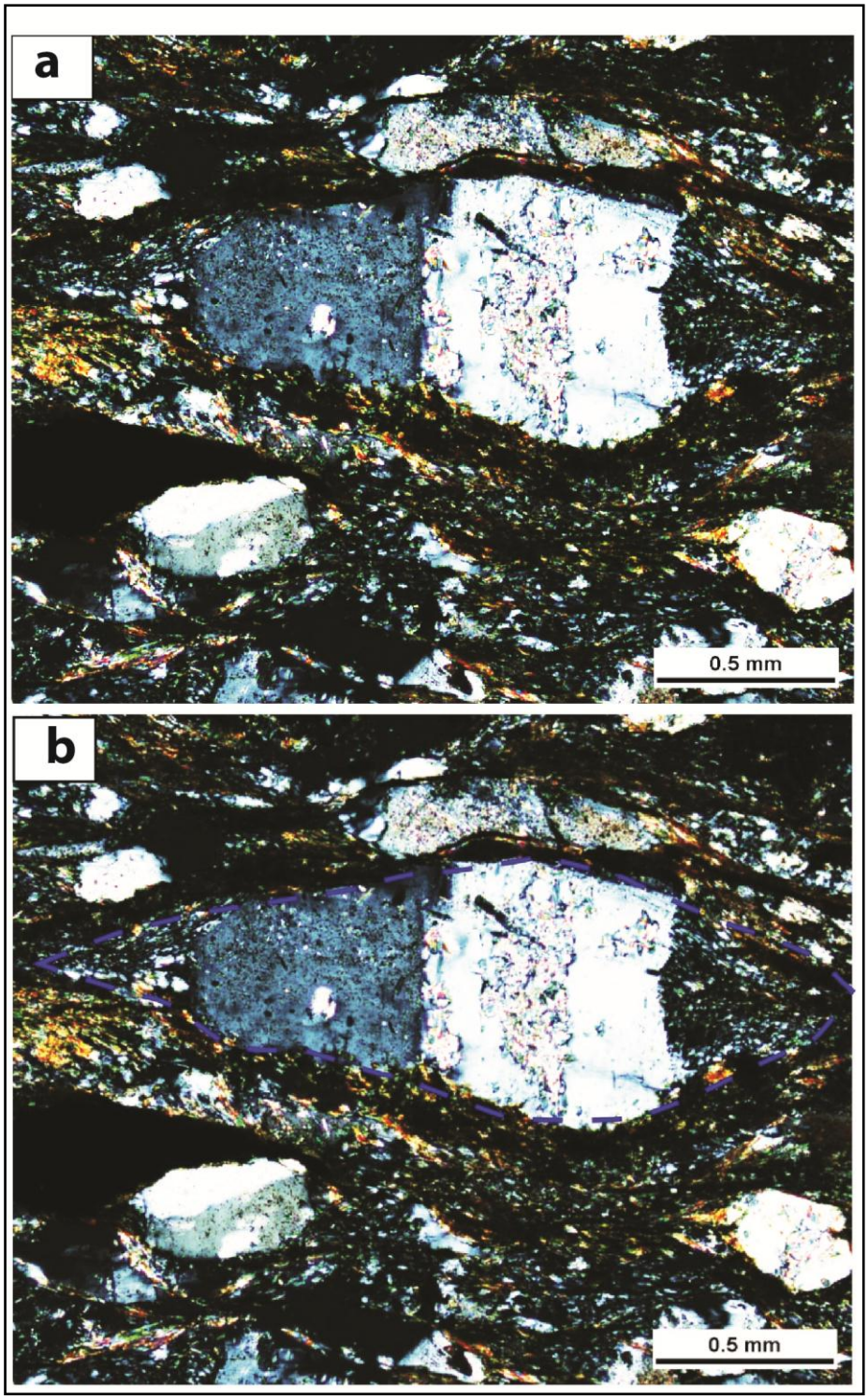


Figure 3.43 Photograph of microstructure Illustrates (a) Porphyroclasts Ø type. (b) Drafting of porphyroclasts Ø type. Outcrop ID46, L9, CPL 5×.

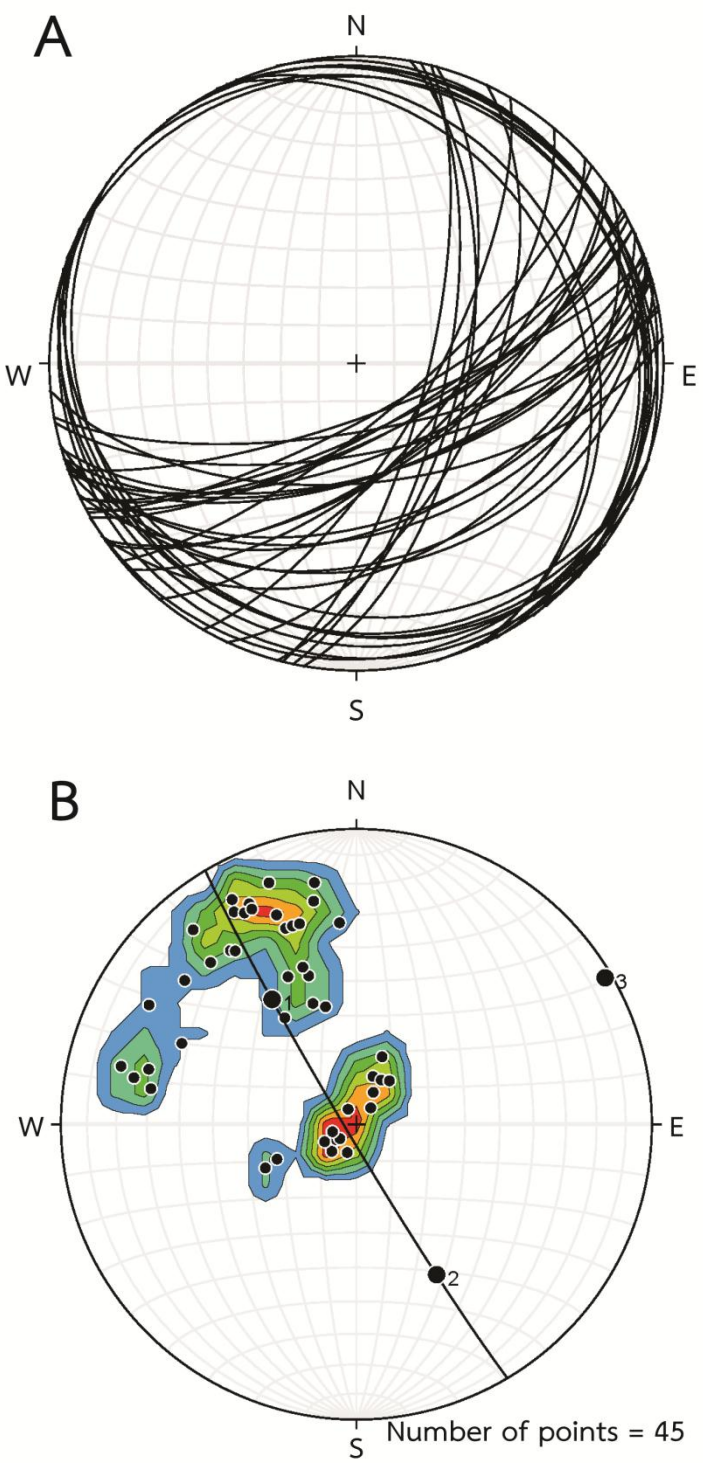


Figure 3.44 Setreonet plot of the Permo-Triassic rocks (A) Foliations Plane (B) contour pole plot (Contour Int. = 2%; Counting Area = 1% of net area).

### 3.3 Triassic rocks

Triassic rocks in the study area (Figure 3.45) are provided in the central part of the study area, that dominant by the intrusive rocks such as granite outcrop (Figure 3.46 and Figure 3.47) and pink granite outcrop (Figure 3.48). Almost of the Triassic intrusive rocks in study area were deformed.

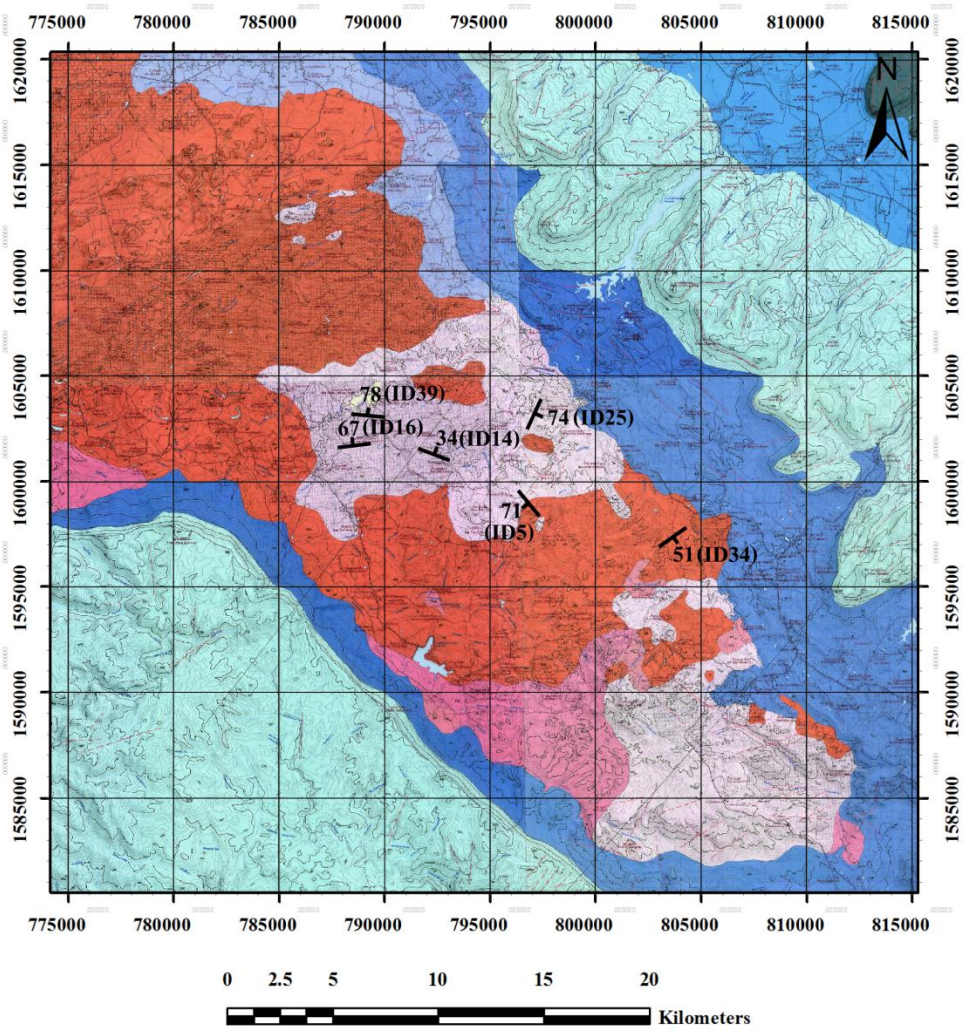


Figure 3.45 Map shows dispersion and foliation of Triassic outcrops.

Station ID14 (Figure 3.45) are illustrated foliation has orientation 292°/34° dip direction to NE (Figure 3.48). Slap sample is very low weathered (Figure 3.49), microstructures are appeared tapering edges of twins in feldspar. Deformation twins can commonly be distinguished from growth twins by their shape. Also, they are commonly tapered, while deformation twins can be concentrated at high strain sites such as the rim of crystals or sites where two crystals touch each other. In feldspar growth and deformation twins occur (Passchier and Trouw, 2005). Tapering edges of twins in feldspar illustrated on crossed polarized light magnificent 5× (Figure 3.50a) and drafting tapering twin crossed polarized light magnificent 5× (Figure 3.50b). In addition, granite outcrop ID39 (Figure 3.45) are showed orientation of foliation trend 277°/78° dip direction to NE (Figure 3.51ผิดพลาด! ไม่พบแหล่งการอ้างอิง). Slab sample is moderately weathered (Figure 3.52) and microstructure are illustrated strain shadow and dissolution (dark seams) in dextral shear scene on crossed polarized light magnificent 5× (Figure 3.53a) and drafting porphyroclasts $\sigma$ type which indicates sinistral shear scene on crossed polarized light magnificent 5× (ผิดพลาด! ไม่พบแหล่งการอ้างอิง). Furthermore, subgrain rotation recrystallization appeared on crossed polarized light magnificent 5× (Figure 3.54a) drafting point to subgrain rotation recrystallization on crossed polarized light magnificent 5× (Figure 3.54b) while in the same thin section of outcrop ID39 shows porphyroclasts $\sigma$ type on crossed polarized light magnificent 5× (Figure 3.55a) and drafting which indicates sinistral shear scene on crossed polarized light magnificent 5× (Figure 3.55bผิดพลาด! ไม่พบแหล่งการอ้างอิง).

The Triassic rocks orientation can be separated to 2 sets are consisted of the first trends are appeared in the NE zone of the study area. Stereonet plot of 29 planes orientation are illustrated in ENE-WSW to NE-SW (Figure 3.56A) and poles plotted $\pi$diagram (Figure 3.56B) folding feature demonstrated trend of axial plane about NE-SW and $\pi$-axis (point 3 in Figure 3.56B) that imply axial plane plunges to NE while the second trend are appeared in SW zone of the study area (Figure 3.1) trend from stereonet plot about NW-SE (Figure 3.57A) Structural analysis of stereonet plot of poles plotted $\pi$ diagram (Figure 3.57B) folding feature demonstrated trend axial plane about NW-SE and also $\pi$-axis that imply axial plane plunges to NW.

Figure 3.46 Photograph of granite outcrop ID16 (Looking to W) orientation 263°/67° dip direction to NW. Coordinate 788496E/1601951N.

Figure 3.47 Photograph granite outcrop ID34 (Looking to W) orientation 055°/51° dip direction to SE. Coordinate 803775E/ 1597165N.

Figure 3.48 Photograph of pink granite outcrop ID14 (Looking to SW) orientation 292°/34° dip direction to NE. Coordinate 792387E/ 1601475N.

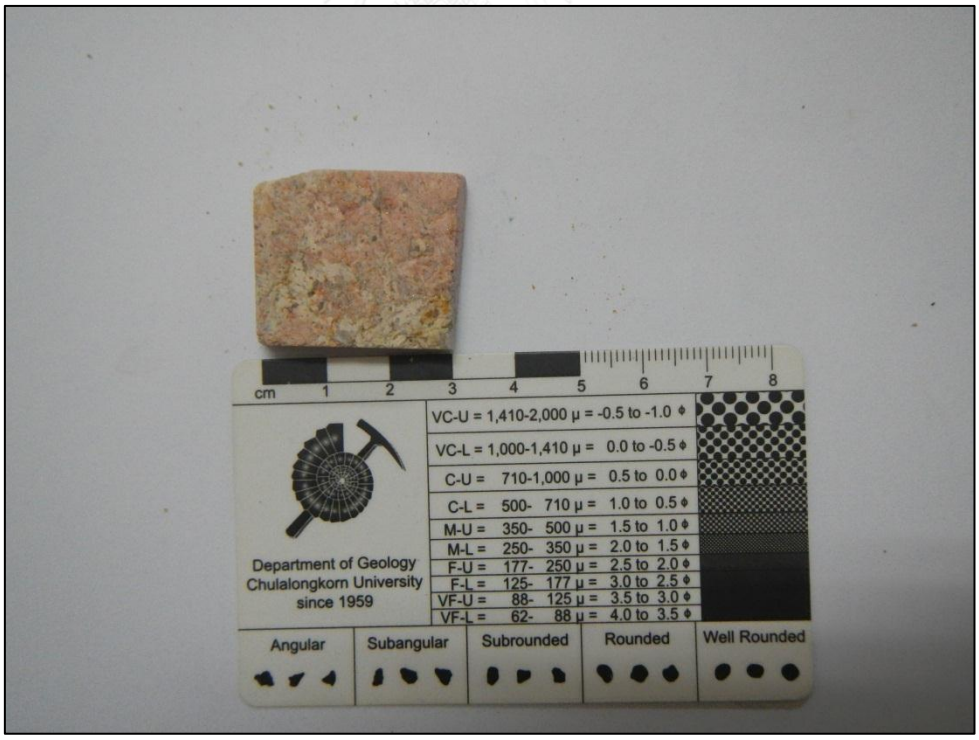


Figure 3.49 Photograph shows slab sample of outcrop ID14.

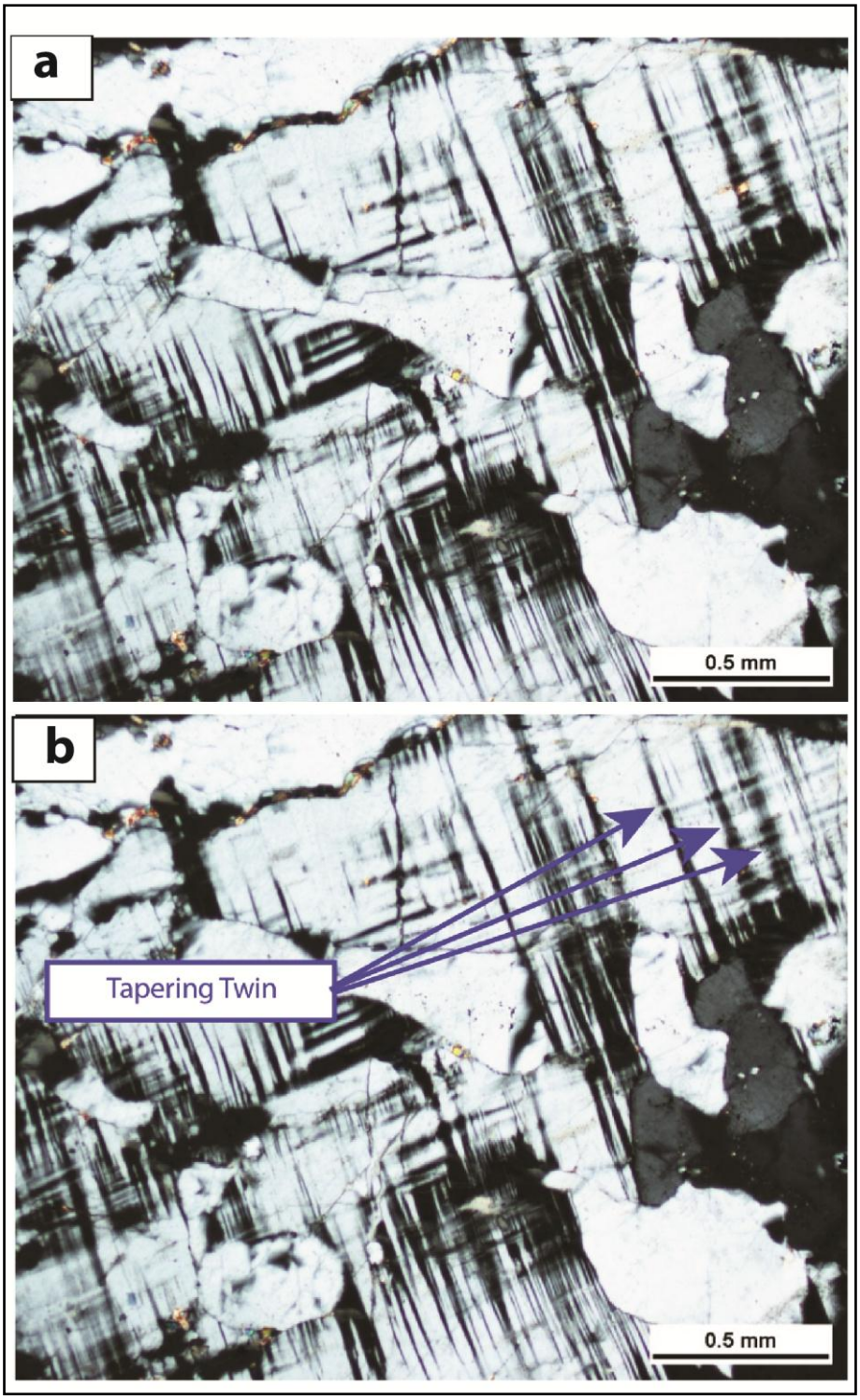


Figure 3.50 Photograph of microstructure shows (a) Tapering twins. (b) Drafting of tapering twins. Outcrop ID14, L1, CPL 5×.

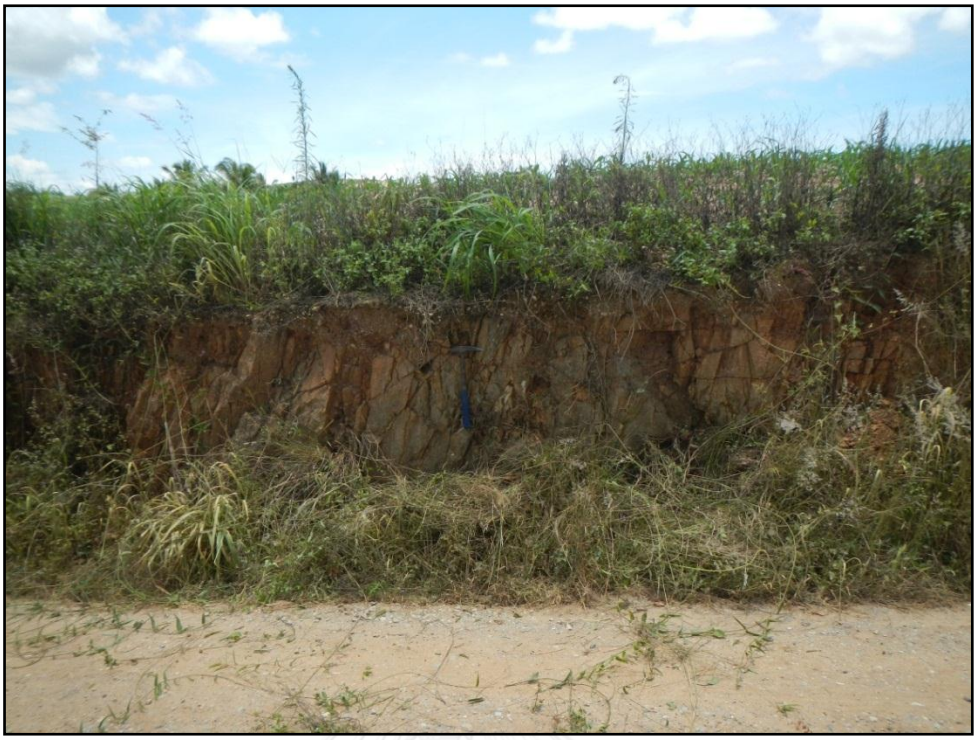

Figure 3.51 Photogtraph of granite outcrop ID39 (Looking to SE) orientation 277°/78° dip direction to NE. Coordinate 789244E/ 1603426N.

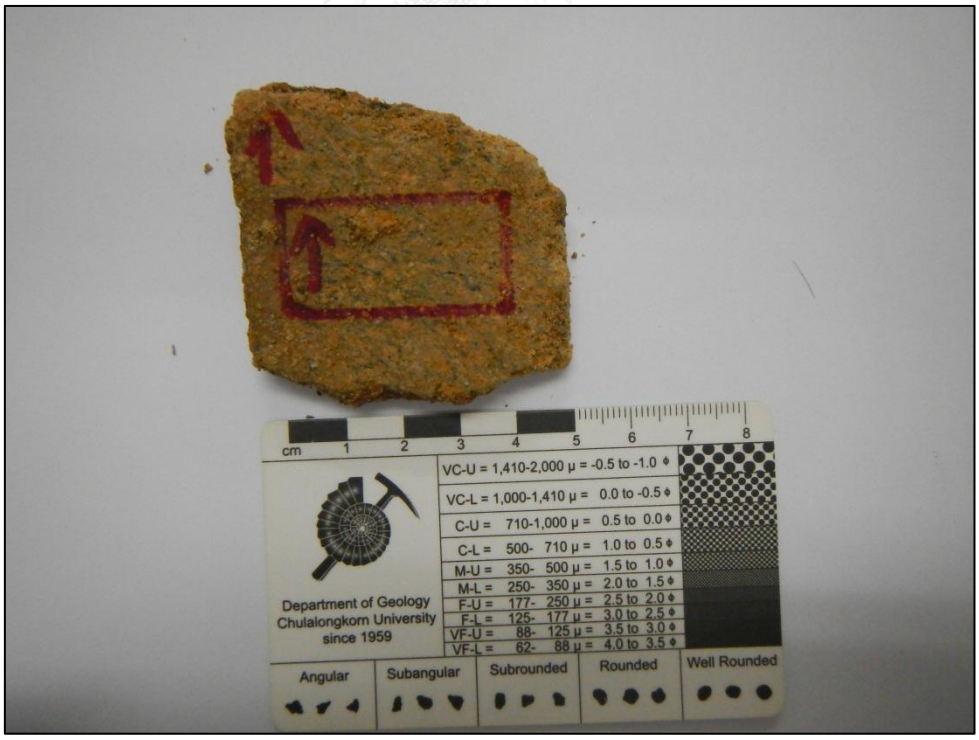


Figure 3.52 Photograph shows slab sample of outcrop ID39.

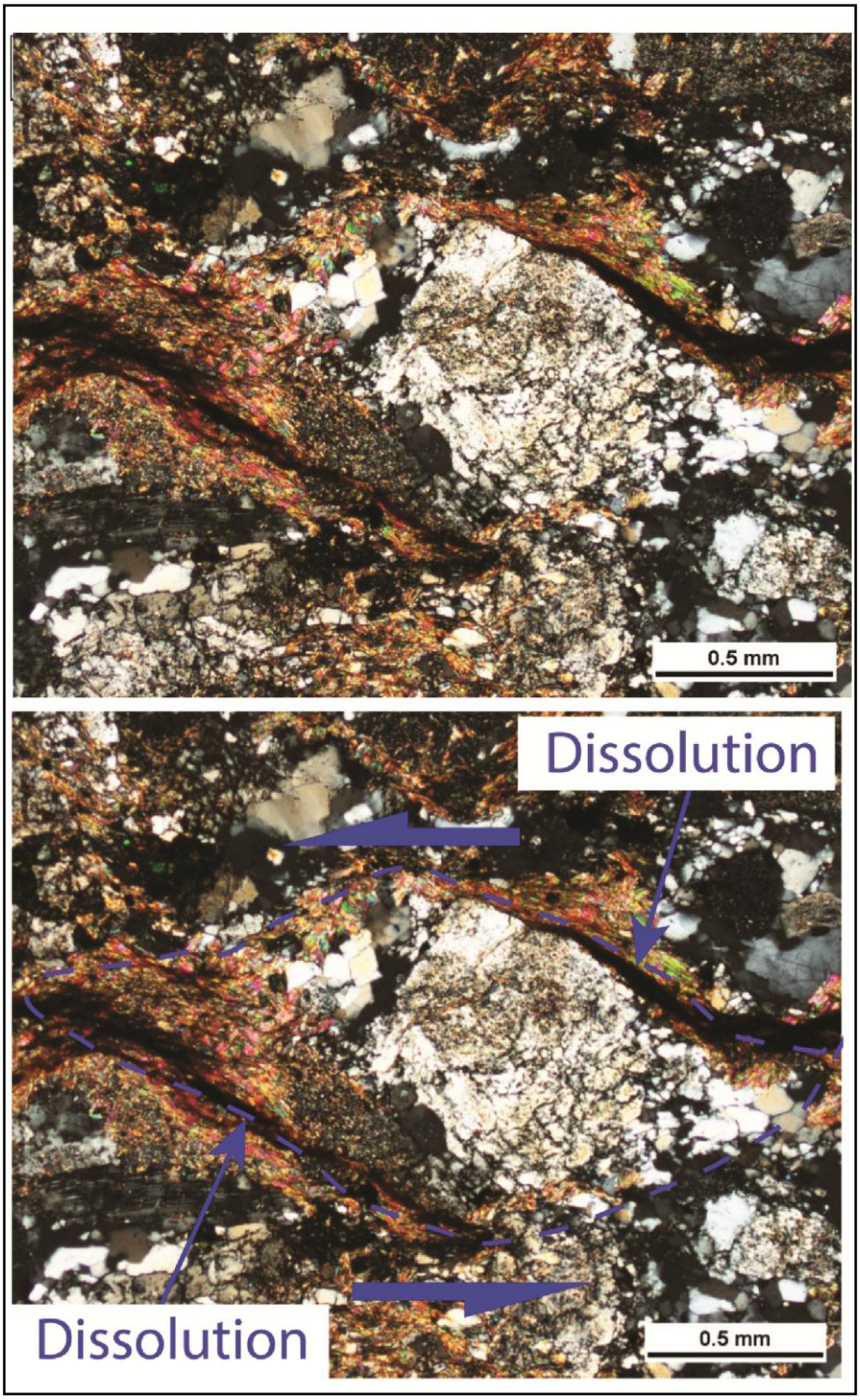


Figure 3.53 Photograph of microstructure illustrates (a) Strain shadow porphyroclasts $\sigma$ type. (b) Drafting of porphyroclasts $\sigma$ type and dissolution (dark seams) indicates sinistral shear scene. Outcrop ID39, L1, CPL 5×.

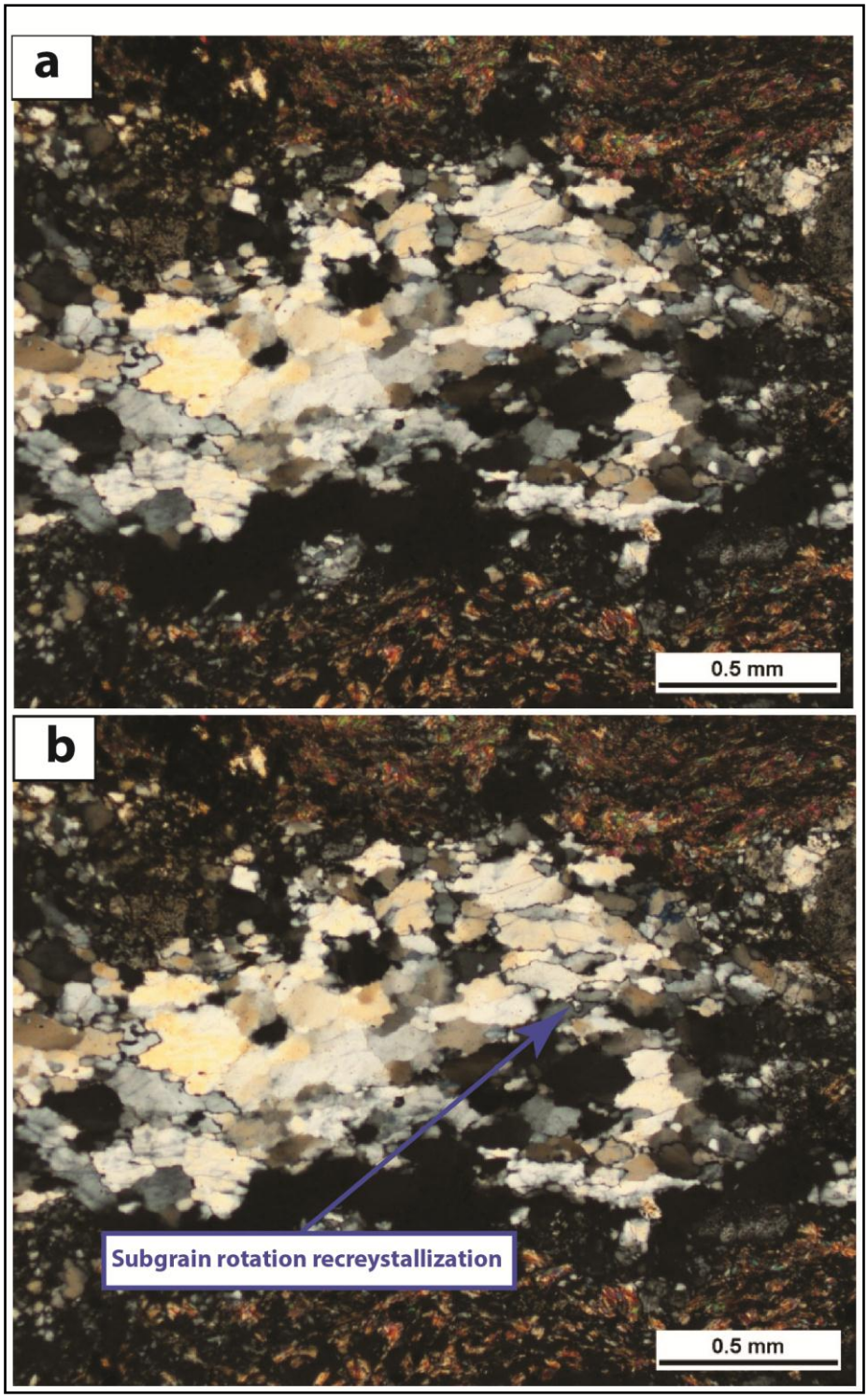


Figure 3.54 Photograph of microstructure illustrates (a) Polycrystal are recrystallization. (b) Point to subgrain rotation recrystallization. Outcrop ID39, L2, CPL 5×.

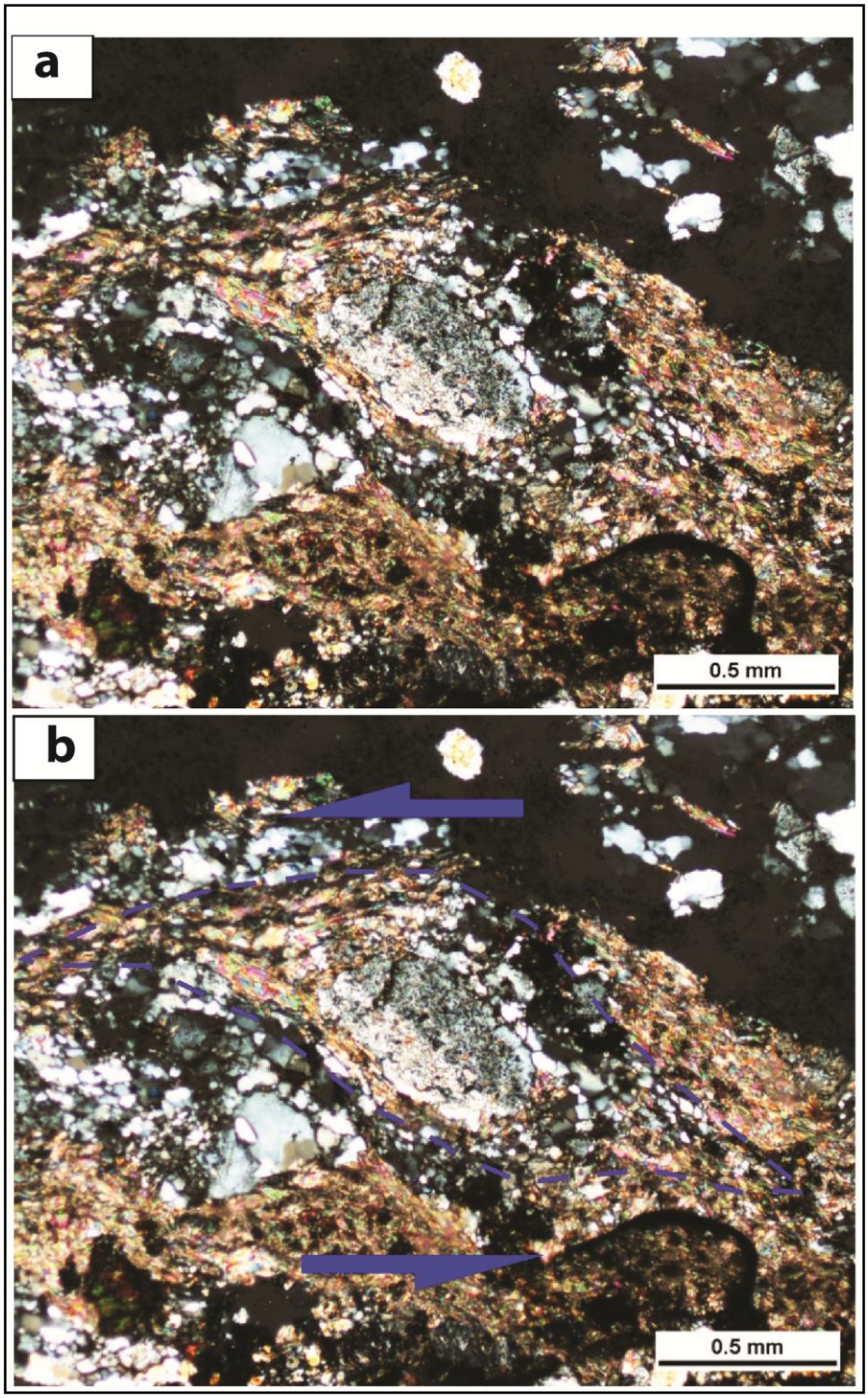


Figure 3.55 Photograph of microstructure (a) Shows strain shadow porphyroclasts $\sigma$ type. (b) Porphyroclasts $\sigma$ type which drafting indicates sinistral shear scene. Outcrop ID39, L3, CPL 5×.

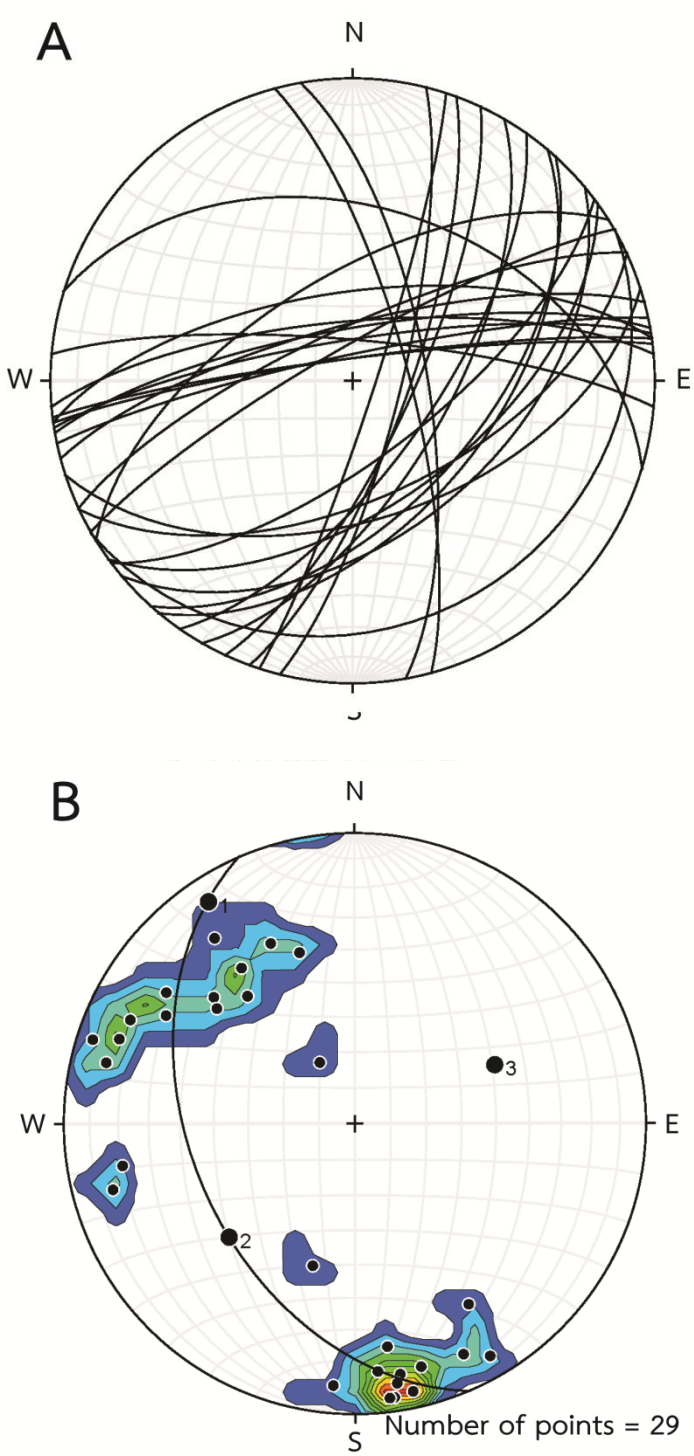


Figure 3.56 The Stereonet plot of the Triassic rocks the first set of foliation (A) the orientation Plane (B) contour pole plot (Contour Int. = 2%; Counting Area = 1% of net area).

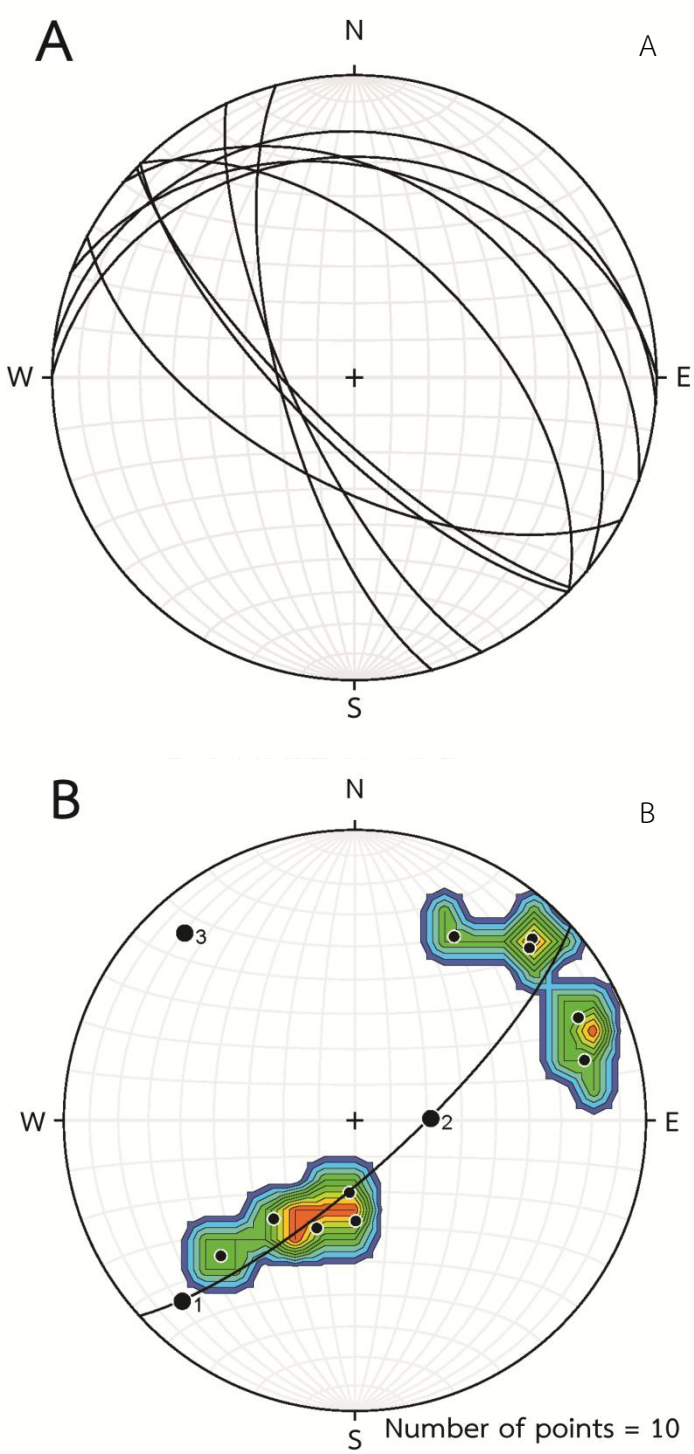


Figure 3.57 The Stereonet plot of the Triassic rocks the second set foliation (A) the orientation Plane (B) contour pole plot (Contour Int. = 2%; Counting Area = 1% of net area).

### 3.4 Triassic hornblende granite rocks

Triassic hornblende granite in the study area can be separated from the Triassic granite (Granite and pink granite). Also the Triassic hornblende granites are found in the central part of the study area (Figure 3.58).

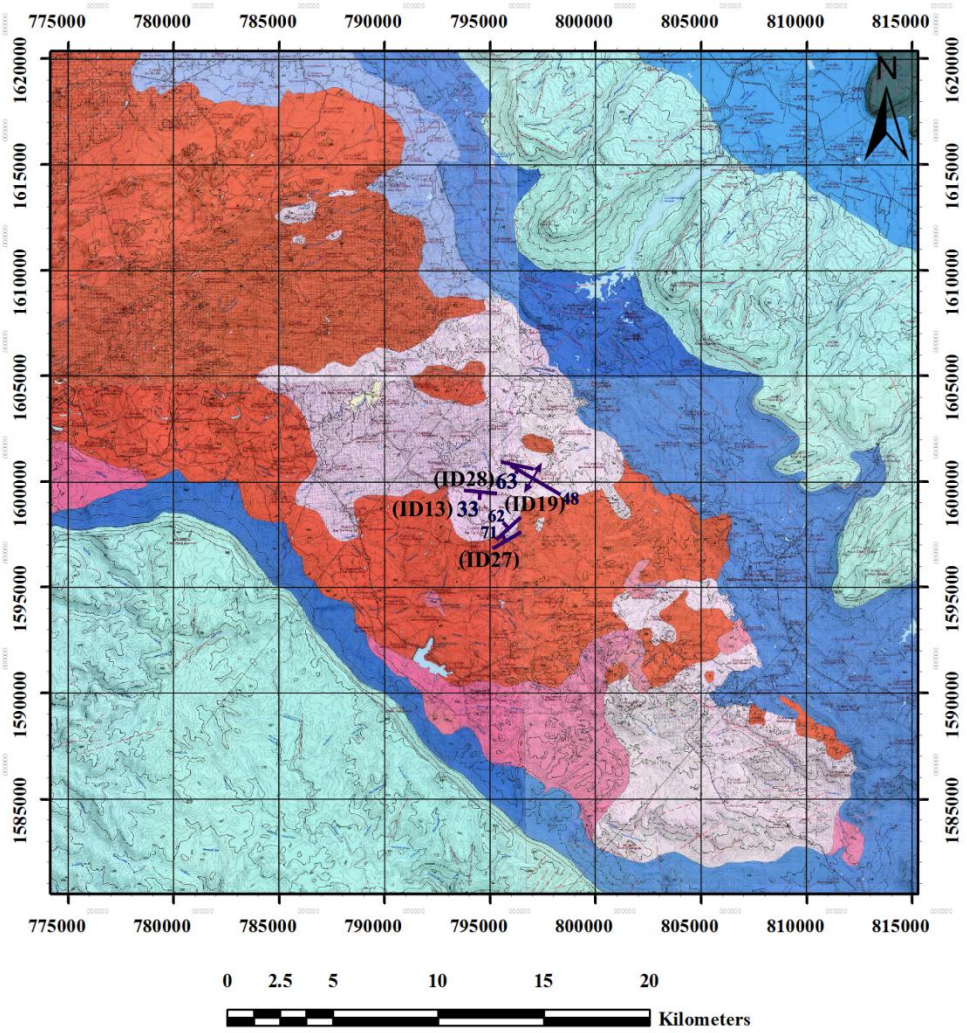


Figure 3.58 Map shows dispersion and foliation of Triassic hornblende granite outcrops.

Hornblende granite outcrop ID13 (Figure 3.58) illustrates dyke foliation plane 097°/33° dip direction to SW (Figure 3.59). Microstructures are not deformation on plane polarized light magnificent 5× (Figure 3.60a), on crossed polarized light magnificent 5× (Figure 3.60b). Hornblende granite outcrop ID19 (Figure 3.58) shows layered feature (Figure 3.61) foliation plane 226°/62° dip direction to NW. Besides, outcrop ID28 (Figure 3.58) illustrates foliation plane 105°/63° dip direction to SW (Figure 3.62), while microstructure is deformed in contact between felsic rocks and mafic rocks on plane polarized light magnificent 5× (Figure 3.63), on crossed polarized light magnificent 5× (Figure 3.63).

Orientation of structural geology in hornblende granites are illustrate in stereonet plot of 46 planes are ENE-WSW and ESE-WNW (Figure 3.64A) poles plotted $\pi$ diagram (Figure 3.64B) folding feature demonstrated trend axial plane about ENE-WSW and also $\pi$-axis that imply axial plane plunges to WSW.

Figure 3.59 Photograph hornblende granite outcrop ID13 (Looking to SW) foliation plane 097°/33° dip direction to SW. Coordinate 794498E/1599317N.

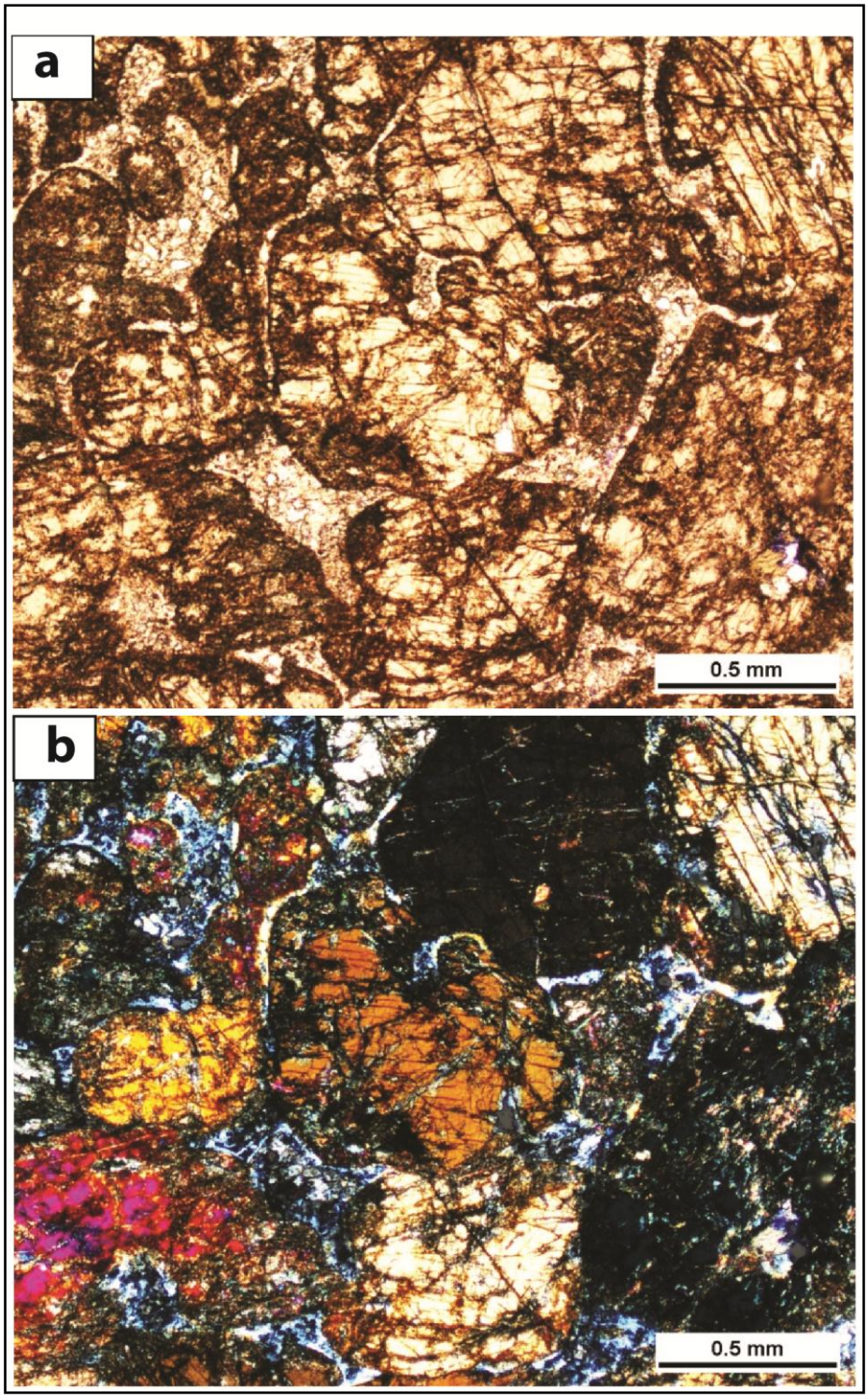


Figure 3.60 Photograph of microstructure shows (a) Hornblende are not deformation. Outcrop ID13, L1, PPL 5×.(b) hornblende are not deformation. Outcrop ID13, L1, CPL 5×.

Figure 3.61 Photograph of hornblende granite outcrop ID19 (Looking to NE) foliation plane 226°/62° dip direction to NW. Coordinate 795707 E/ 1597962 N.

Figure 3.62 Photograph of hornblende granite in abandon mine ID28 (Looking to SE) foliation plane 105°/63° dip direction to SW. Coordinate 796216E/ 1600554N.

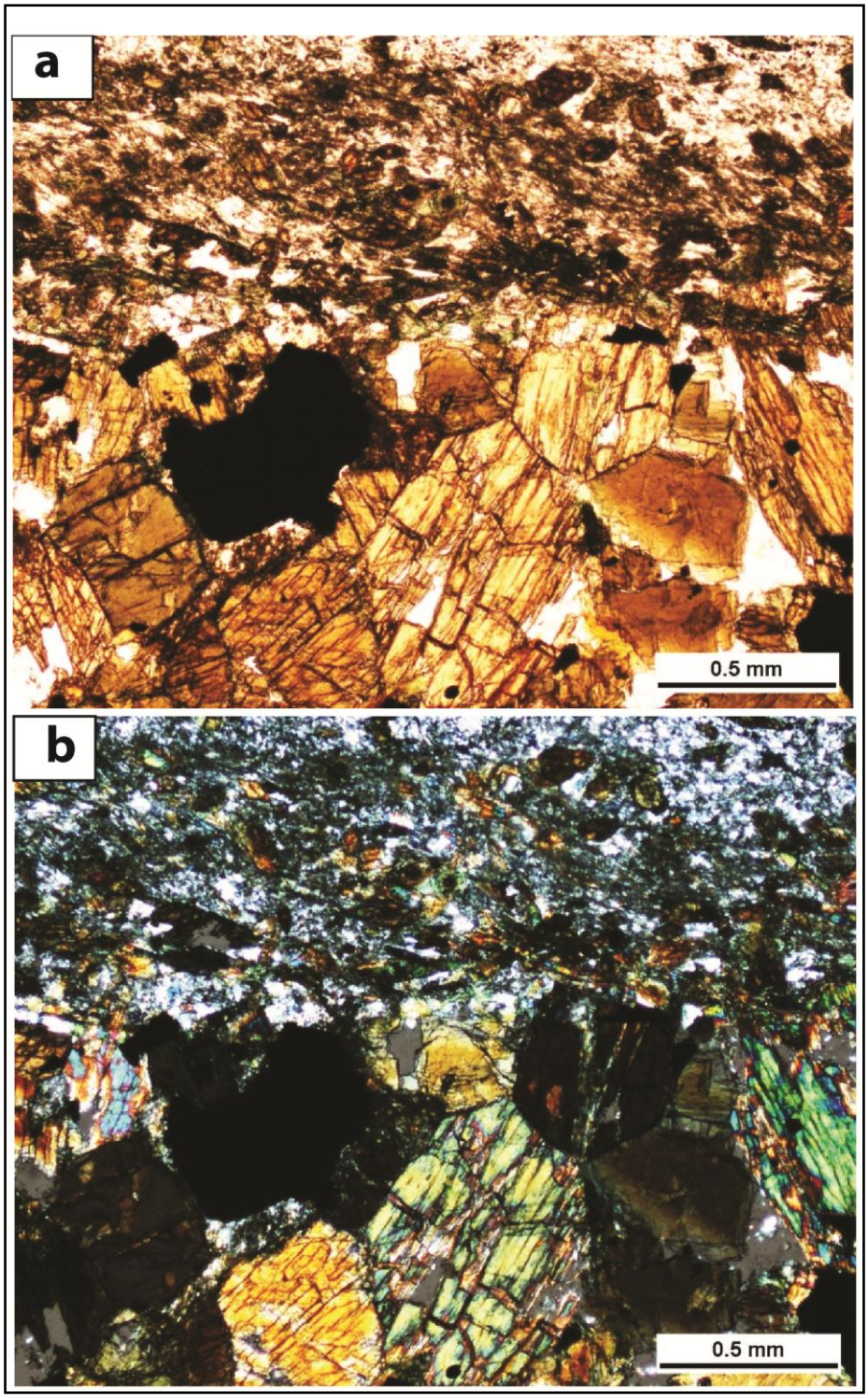


Figure 3.63 Photograph of microstructures shows (a) Hornblende granite of outcrop ID28, L1, PPL 5×. b) Hornblende granite. Of outcrop ID28, L1, CPL 5×.

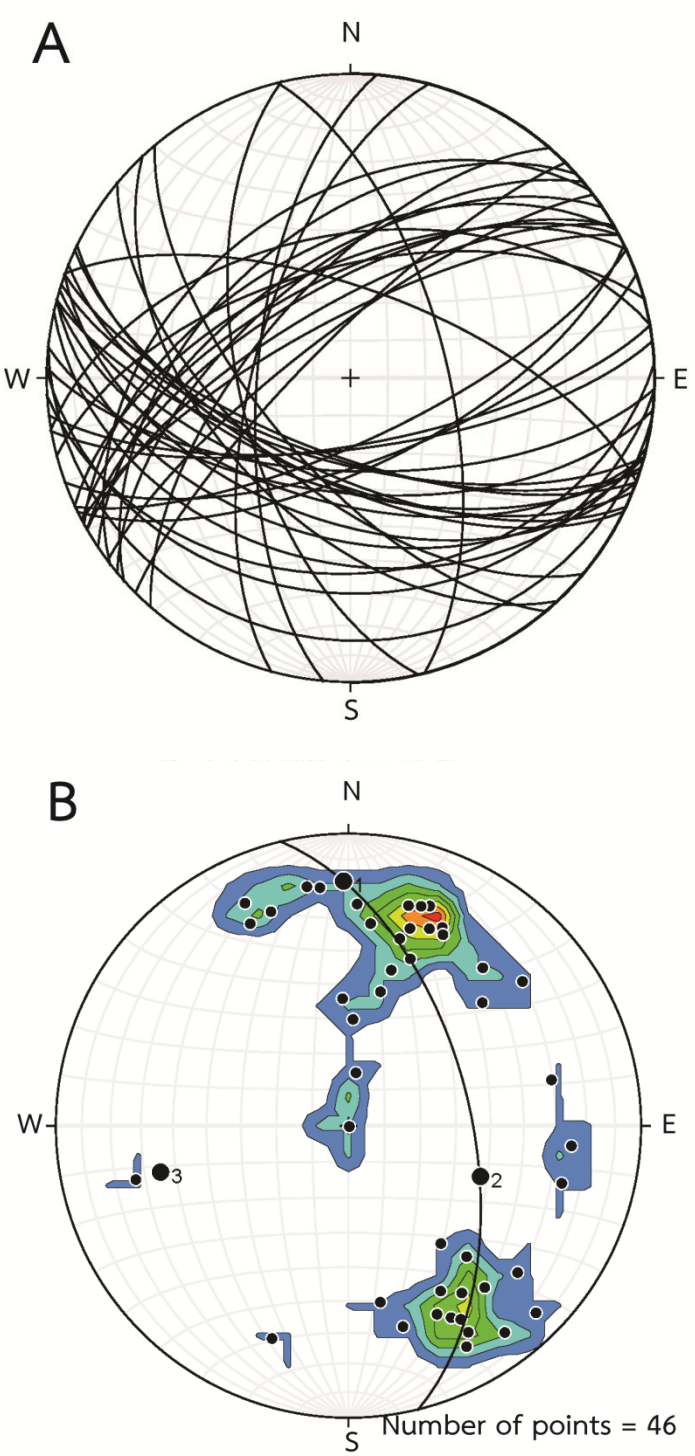


Figure 3.64 The Stereonet plot of the hornblende granite (A) the foliation Plane (B) contour pole plot (Contour Int. = 2%; Counting Area = 1% of net area).

### 3.5 Mesozoic Khorat group

Mesozoic Khorat group in the study area are showed in both frank of rim in the study area (Kemlheg and Vichidchalermpong, 1992a, b; Putthapiban et al., 1989a, b) in the northern part and southern part which are unconformities with the Triassic intrusive rocks. The Khorat group is dominated by non-marine sedimentary rocks. Rocks In the study area are found in the northeastern part of the study area (Figure 3.65).

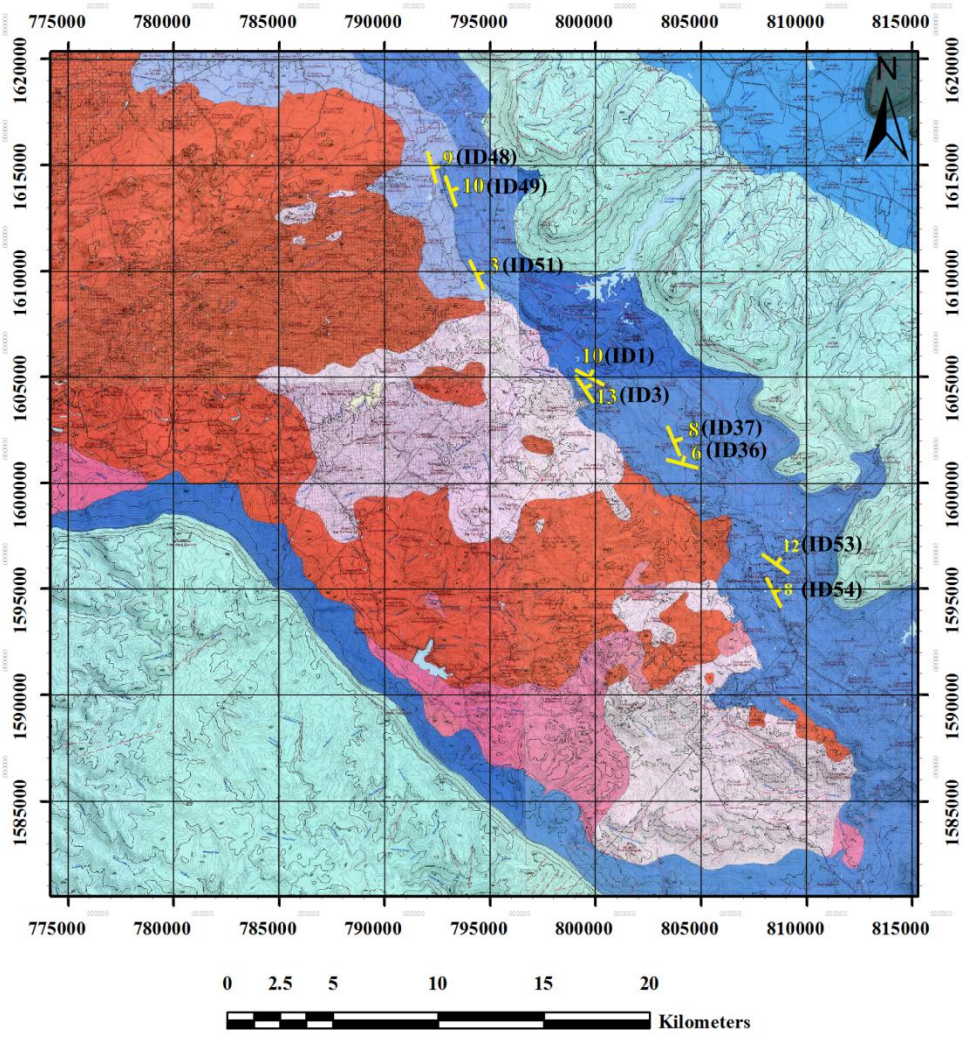


Figure 3.65 Map showing dispersion and bedding of Mesozoic Khorat group outcrops.

The Mesozoic Khorat group in the study area is consisted by of conglomerate outcrop ID1 (Figure 3.65) bedding plane 298°/10° dip direction to NE (Figure 3.66) and sandstone ID37 (Figure 3.65) bedding plane 337°/8° dip direction to NE (Figure 3.67) and sandstones of outcrop ID51 (Figure 3.65) bedding plane 333°/3° dip direction to NE (Figure 3.68) are very fine grained colored dark brown to dark purple and some of mica detrital in sandstone. All outcrops are not deformed by the Triassic intrusive rocks.

Bedding planes are illustrated in stereonet plot of 54 planes are ENE-WSW and WNW-ESE (Figure 3.69A). Also, poles plotted $\pi$ diagram (Figure 3.69B) structural feature demonstrated trend of plane are about NW-SE. $\pi$-axis implies the structural plunges to SE.

Figure 3.66 Photograph shows conglomerate outcrop ID1 (Looking to SE) bedding plane 298°/10° dip direction to NE. Coordinate 799824E/ 1605200N.

Figure 3.67 Photograph exhibits outcrop of sandstone ID37 (Looking to SE) bedding plane 337°/8° dip direction to NE. Coordinate 803935E/ 1602099N.

Figure 3.68 Photograph illustrates outcrop of sandstone ID51 (Looking to SW) bedding plane 333°/3° dip direction to NE. Coordinate 794560E/ 1609883N.

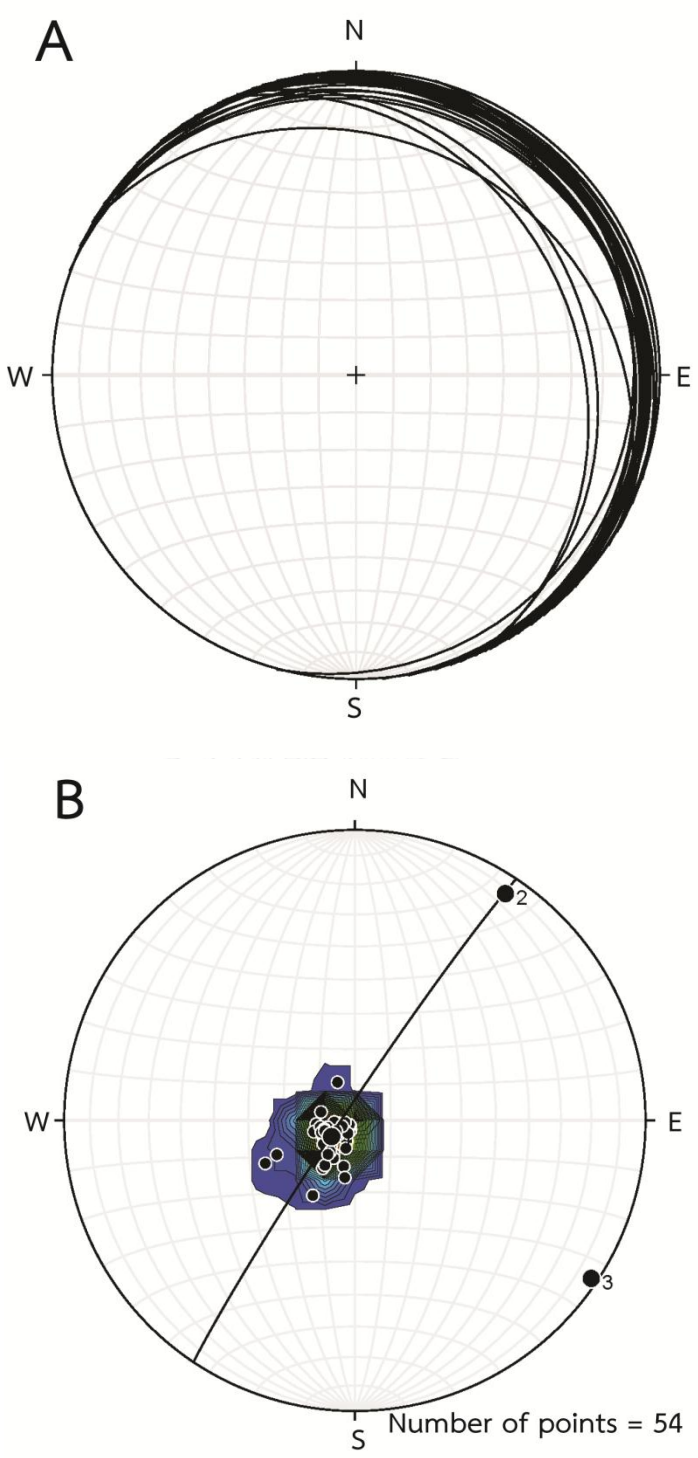


Figure 3.69 The Stereonet plot of the Mesozoic Khorat group (A) the bedding Plane (B) Contour pole plot (Contour Int. = 2%; Counting Area = 1% of net area).

**3.6 Summary structural analysis.**

Structural analysis in study area recognizes to five groups such as Permian rocks, Permo-Triassic rocks, Triassic granite rocks, Triassic hornblende granite rocks and Mesozoic of Khorat (Figure 3.70).

Permian rocks are recognized to two groups, first group is bedding planes plot and second group is foliation planes plot. Bedding planes plot shows orientation in NE-SW. $\pi$ diagram trend axial plane about NE-SW and axial plane plunges to NE.
And Foliation planes plot illustrates the orientation of the Permian rocks recognizes to two set such as set I foliation plane shows trend in ENE-WSW to ESE-WNW trend axial plane about E-W axial plane plunges to E. Set II foliation planes orientates trend in NE-SW. The orientation of folding feature demonstrated axial plane about N-S and axial plane plunges to S.

Permo-Triassic rocks illustrated foliations into two groups are ENE-WSW to NE-SW. $\pi$ diagram illustrates trend axial plane about NE-SW, axial plane plunges to NE.

Triassic rocks recognize foliation two set. first trends are appeared in the NE zone of the study area where illustrates in ENE-WSW to NE-SW and $\pi$diagram folding feature shows trend of axial plane about NE-SW, axial plane plunges to NE while the second trend are appeared in SW zone of the study area trend shows NW-SE. $\pi$ diagram shows axial plane about ENE-WSW to NE-SW and axial plane plunges to NW.

Triassic hornblende granite rocks illustrate ENE-WSW and ESE-WNW. $\pi$ diagram shows trend axial plane about ENE-WSW and axial plane plunges to WSW.

Mesozoic Khorat group shows bedding planes in about NW-SE and plunges to SE.

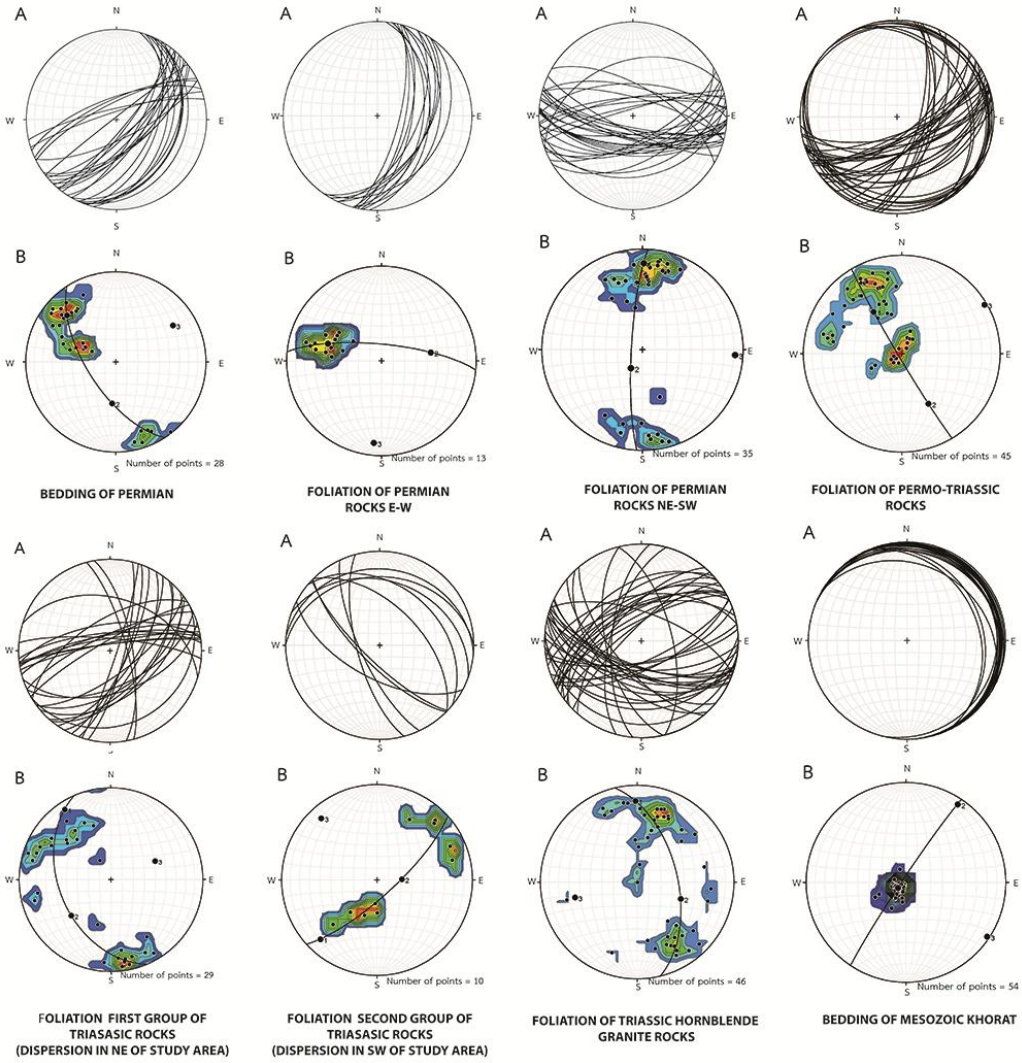


Figure 3.70 The summary of planes and contour plot of rock units in study area.

# CHAPTER IV

# THE STRUCTURAL EVOLUTIONARY MODEL

Rusults from chapter three are used in order to construct the structural evolutionary model of study area (Figure 4.1). Also, rocks units in study area can be divided into five units which are Permian clastic sedimentary rocks, the Permo-Triassic volcanic rocks, the Triassic intrusive rocks, the Triassic hornblende granite rocks, and the Mesozoic Khorat group. Detail of rock member in each rock units and the orientation are fits into, the Permian clastic sedimentary rocks. They have ESE-WNW, which can be swing to ENE-WSW and NE-SW and determining the orientation of folding feature demonstrated trend axial plane about E-W and axial plane plunges to E. The Permo-Triassic volcanic rocks are illustrated their orientation in ENE-WSW to NE-SW. Moreover, determining folding feature demonstrated trend axial plane about NE-SW and axial plane plunges to NE. the Triassic intrusive rocks can be divided orientation into two groups such as the first group appears in the NE zone of the study area and orientation are illustrated in ENE-WSW to NE-SW folding feature demonstrated trend of axial plane about NE-SW and axial plane plunges to NE, while trend of the second group, in SW of the study area are showed trend about NW-SE and folding feature and trend axial plane about NW-SE and axial plane plunges to NW. the Triassic Hornblende granite rocks are dominant by dykes of hornblende granites are appeared in the central part of the study area and are illustrated orientation in ENE-WSW and ESE-WNW folding with axial plane about ENE-WSW and plunges to WSW. The Mesozoic of the Khorat group show orientations in ENE-WSW and ESE-WNW. Also, structural feature demonstrated trend of plane are about NW-SE and also structural plunges to SE.

Therefore, the orientations of rock units in the study area can be recognized to two episodes of folding from trend of rock units, the first group consisted of the Permian clastic sedimentary rocks, the Permo-Triassic volcanic rocks, the Triassic intrusive rocks appeared in the NE of study area and the Triassic hornblende granite are illustrated trend of orientation in ENE-WSW, ESE-WNW and NE-SW and the second

rock unit groups are composed of the Triassic intrusive rock in the SW part of the study area and the Mesozoic rocks of the Khorat group are illustrated trend of orientation in NW-SE direction. Ramsay (1976) recognizes superposition of fold to be four types. Include Type0, Type1, Type2 and Type3 base on fold geometry and displacement, the kinematic superposition of two phases of fold forming deformation produce a variety of three-dimensional and differently oriented two-dimensional section (Appendix A). Subsequently, Grasemann et al. (2004) classification of refold structures in three-dimensional geometry of six end-member refold structures by built up Type0 of Ramsay (1976) to be three type are $Type0_1$, $Type0_2$ and $Type0_3$ (Appendix A). Therefore, Two trends of the orientation data and rock units in the study area suggests that two episode is a kind of Type1 of the superposition of folding, Because of the first trend are illustrated ENE-WSW, ESE-WNW and NE-SW and the second trends is showed NW-SE that imply two set of orientations together with deformation are perpendicular and corresponding with Type1 the classification of refolded (Grasemann et al., 2004; Ramsay, 1976).

The structural evolution model in the study area (Figure 4.2) can be divided into four stages. The first stage (Figure 4.2a) rocks are formed and rocks were deformed ($D_1$) by forces direction about N-S to NW-SE directions this event was generated first trend of fold ($F_1$) illustrated in the Permian clastic sedimentary rocks, the Permo-Triassic volcanic rocks, The Triassic intrusive rocks in the NE part of the study area and the Triassic hornblende granite are showed ENE-WSW, ESE-WNW and NE-SW directions (Figure 4.2b). Afterward, first trend of fold ($F_1$) appeared orientations in ENE-WSW, ESE-WNW and NE-SW directions are effected from the second deformation ($D_2$) by force direction about NE-SW (Figure 4.2c) this event was generated trend of second fold ($F_2$) are appeared in the Triassic intrusive rocks in the SW part of the study area trend of second fold ($F_2$) are illustrated in NW-SE. Resulting from two deformations stage were illustrated geometry in a dome and basin (egg carton) interference pattern (Figure 4.2d) while the Mesozoic of the Khorat group were deposited after second deformation, because of sedimentary rocks of the Khorat group are not deformation structure.

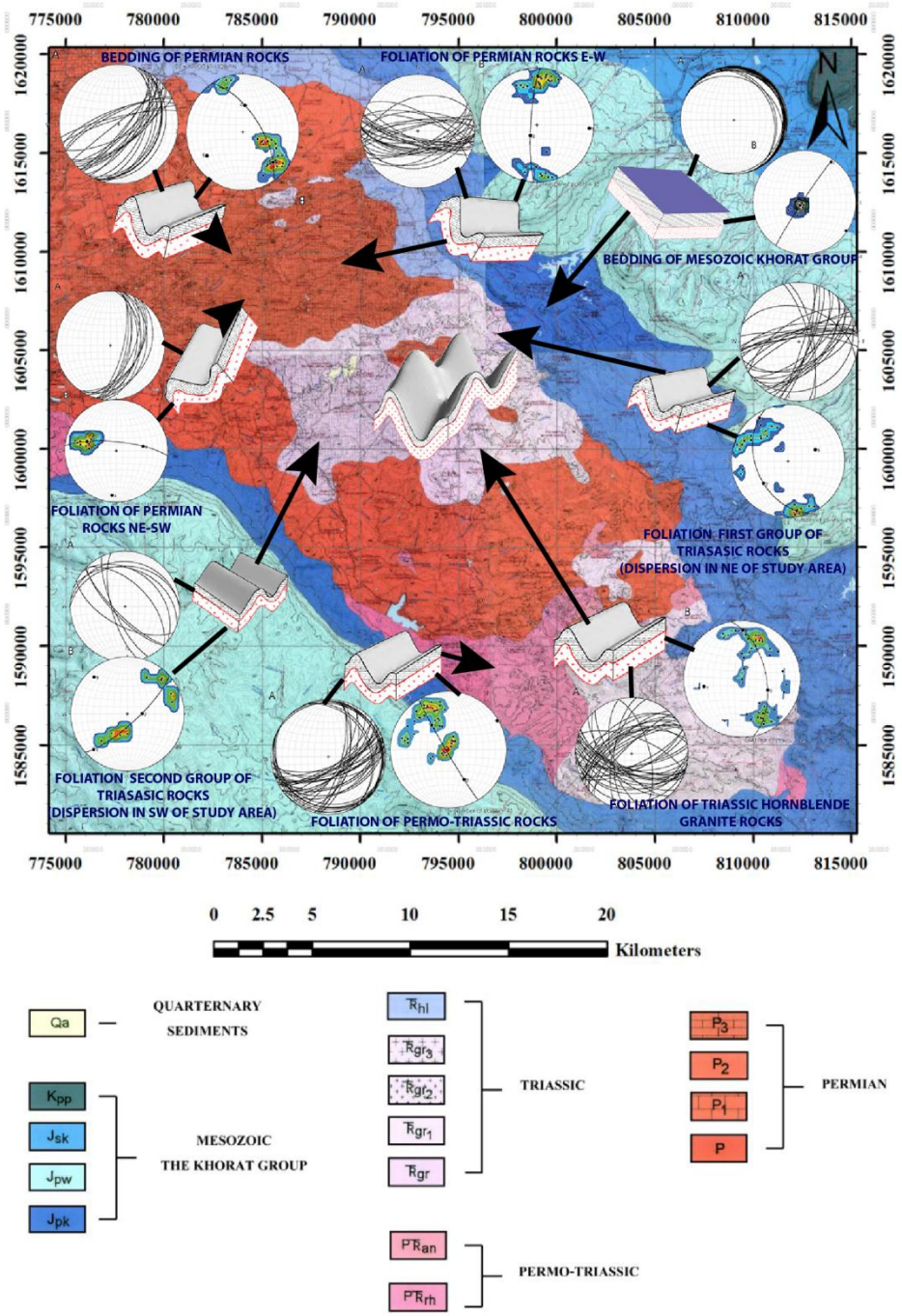


Figure 4.1 Map Illustates structural analysis in the study area.

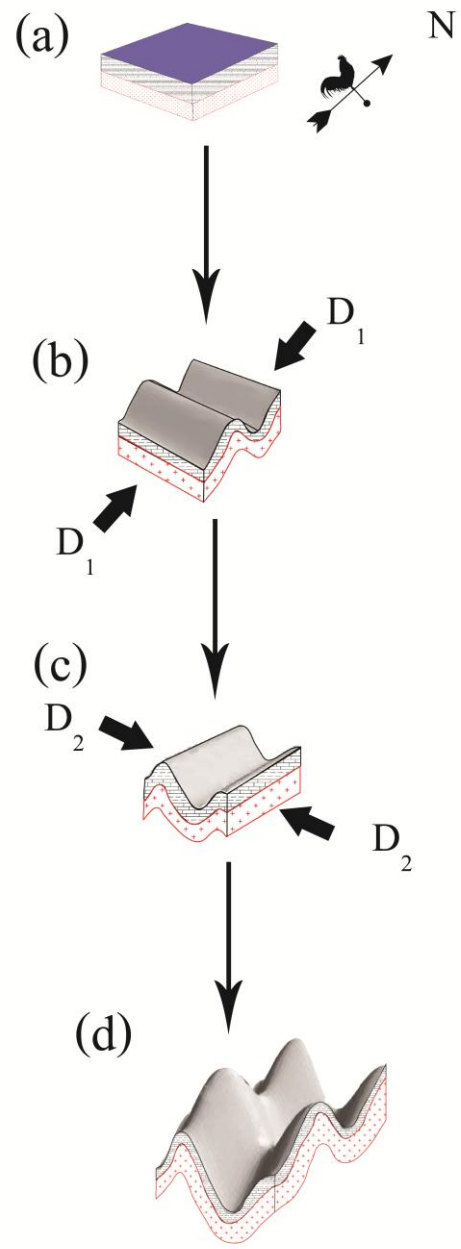


Figure 4.2 Illustration the structural evolutionary model in Amphoe Wang Nam Khiao area. (a) Before the first deformation. (b) The resulting from the first deformation ($D_1$) generated the first folding ($F_1$). (c) The second deformation ($D_2$) generate the second folding ($F_2$) (d) Resulting geometry in a dome and basin (egg carton) interference pattern for two sets folding. (After Grasemann et al., 2004; Ramsay, 1976)

# CHAPTER V
# DISCUSSION AND CONCLUSION

## 5.1 Discussion

### 5.1.1 Structural geology

Structural geology recognizes to five groups which follow rock units. Permian structure separates two bedding plane analysis and foliation plane analysis. Bedding plane of Permian units shows strike trend in NE-SW. Foliation plane of Permian illustrates two sets foliation trend. Set I is ENE-WSW to ESE-WNW and set II foliation shows in NE-SW (Figure 5.1). Results indicate foliation of Permian units in study area exhibit two events which compose of first generate foliation trend in E-W to be Set I and second event generates foliation trend in NW-SE to be Set II. While foliation trends corresponding with Permian of Khao Khwang (Arboit et al., 2014; Morley et al., 2013) in northern part of study area, but study area disappear thrust fault.

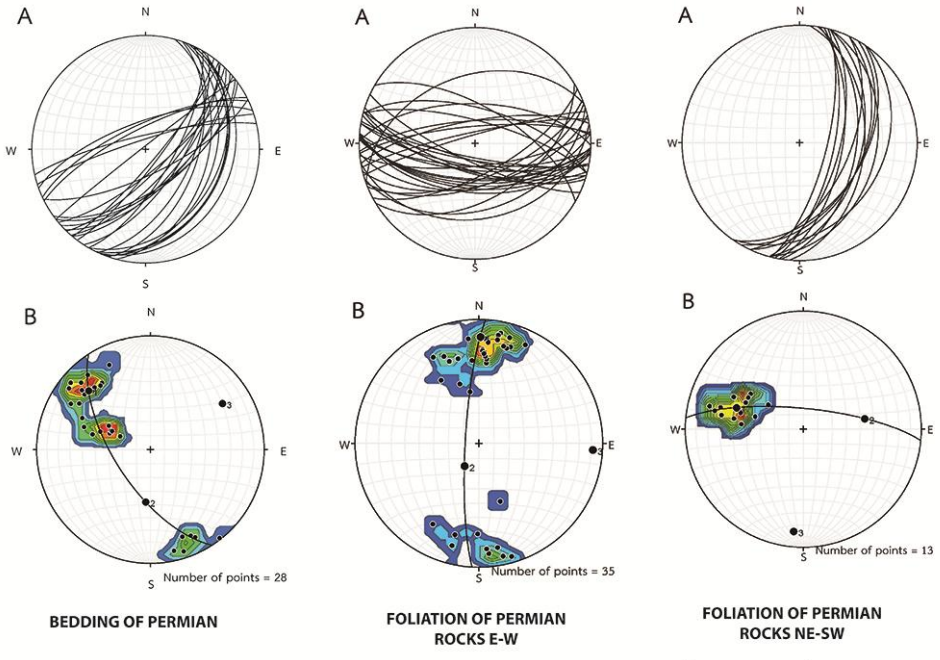


Figure 5.1 The orientation of bedding planes and foliation planes of Permian unit.

Permo-Triassic rocks in study area show foliation plane in ENE-WSW to NE-SW which corresponding with foliation in Permian unite.

Triassic rocks recognize the foliation plane to two groups that first group compose of foliation trend in ENE-WSW to NE-SW (Figure 5.2). This group were found in NE of study area. Second group illustrates foliation trend in NW-SE that appear in SW of study area. Foliations in first group trends are corresponding with foliation in Permian unit and Permo-Triassic unit. Second trend may be deformed later first trend, because the western zone of study area deformed in the last times. Last deformation from Indosinian orogeny (Booth and Sattayarak, 2011)

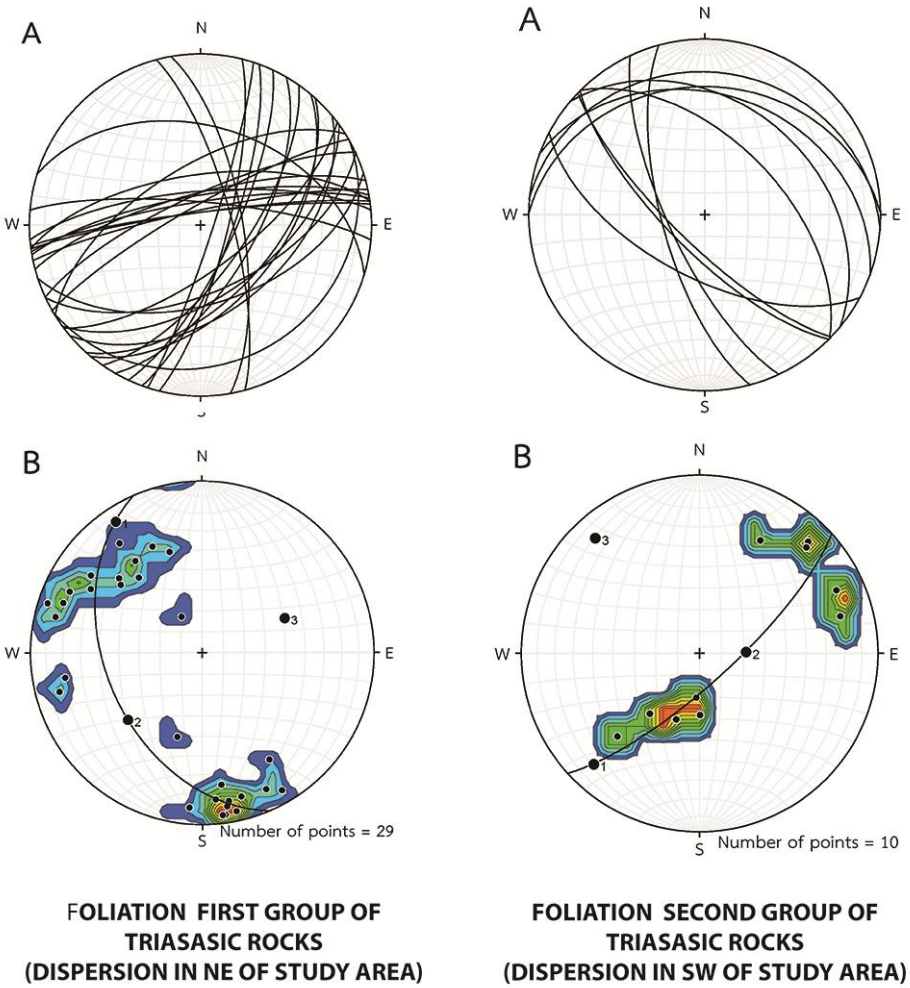


Figure 5.2 The orientation of bedding planes and foliation planes of Triassic unit.

Triassic hornblende granites are separated from Triassic granite, because structure shows dyke and found only in central part of the study area. Foliations trend of hornblende granite shows ENE-WSW and ESE-WNW which correspond with foliation trend in Permian unit, Permo-Triassic unit and Triassic granite in NE of study area.

Mesozoic Khorat group (Kemlheg and Vichidchalermpong, 1992a, b; Putthapiban et al., 1989a, b) disperse in NE and SW of study area. Bedding plane in NE part of study area shows NE-SE plunge to SE. SW of study area are not access to correct data, because SE area is part of Khao Yai national park.

5.1.2 Microstructures

Deformation of microstructures determines four groups except Mesozoic Khorat group, Deformation are flexural flow fold (Figure 5.3).

The Permian rocks illustrate grains shape of euhedral to subhedral with foam structure, and S-C shear bands. Also, develop of porphyroclasts show dissolution in strain caps. Porphyroclasts recognize two types which composed of porphyroclasts $\emptyset$ type indicate porphyroclasts no stair stepping and porphyroclasts $\sigma$ type which indicate stair stepping direction of shear scene. Microstructure deformation in Permian unit shows ductile style.

The Permo-Triassic rocks show subhedral to anhedral and inequigranular interlobate to seriate interlobate. Also, microstructures are illustrated synthetic of micro-fault. As well, micro-folded kinking, boudins and porphyroclasts show strain in the texture, which indicated the brittle and ductile deformation in tuff. Permo-Triassic deformation indicate shallow deformation which microstructure shows brittle deformation such as micro-fault,

Triassic rocks under the microscopic present subhedral to anhedral and equigranular interlobate. Triassic rocks illustrate tapering edges of twins, strain shadow of porphyroclasts, and subgrain rotation recrystallization. Deformation of microstructures indicates ductile deformation.

Triassic hornblende granite rocks are subhedral to anhedral and equigranular interlobate, Hornblende granite in abandon mine showed grain shape and hardly deformation. May be dyke of Triassic hornblende extruded later.

Porphyroclasts show strain shadow in the Permian rocks, the Permo-Triassic rocks and the Triassic rocks, but are not illustrated in the Triassic hornblende granite rocks. The tapering edges of twins are illustrated in the Triassic rocks. The brittle deformation such synthetic micro-fault is found in the Permo-Triassic volcanic rocks. The ductile deformation such as micro-folded, kinking and boudins are found. Thus, the brittle and ductile deformations were found only the Permo-Triassic rocks. While, only the ductile deformations were dominated in the Permian rocks, the Triassic rocks that confirm the deformation in the micro scale.

5.1.3 Structural evolution.

Structural evolution in Amphoe Wang Nam Khiao area explains by orientation in each rock unit. Permian unit shows bedding plane in NE-SW which direction is primary structure. Permian deposits in NE-SW direction. Foliations trend in ENE-WSW to ESE-WNW and NE-SW which from Indosinian I (Booth and Sattayarak, 2011). Foliation trend imply verging in perpendicular force about SSE-NNW, WWS-NNE to NE-SW directions. Permo-Triassic volcanic rock in study area illustrates foliation trend in ENE-WSW to NE-SW. Foliation trend imply that still effected from Indosinian I. Triassic unit was deformed two period. Foliation trend in NE part of study area shows ENE-WSW to NE-SW trend which still Indosinian I event but foliations in second group illustrated trend in NW-SE direction which different from Indosinian I force direction. Foliations trend NW-SE direction may be from Indosinian II (Booth and Sattayarak, 2011). Indosinian II dominant by closed palaeo suture between Sibumasu Terrane, Sukhotiai Terrane and Indochina terrane (Booth and Sattayarak, 2011; Metcalfe, 2013). Foliation of Triassic hornblende granite shows trend in ENE-WSW and ESE-WNW which indicate effected from Indosinian I. After Indosinian II marker by Hui Hin Lat Formation of Khorat group (Figure 1.3), Mesozoic Khorat unit deposited.

Indosinian events can conclude effected in study area to; The structural evolution of Amphoe Wang Nam Khiao begins with the Permian rifting in E-W to NE-SW direction that generate orientation trend in ENE-WSW, ESE-WNW and NE-SW direction. The first north verging deformation ($D_1$) (may be from Indosinian I) generated the first folds ($F_1$) and closed the Permian rifting, while the second deformation (may be from Indosinian II) generated trend in NW-SE in the Triassic intrusive rocks in the SW part of the study area is started in the Indosinian II in the Late Triassic the second deformation ($D_2$) east verging and generated the second fold ($F_2$). The two events are produced a dome and basin (egg carton) in Figure 5.3. In the last stage, the Mesozoic non-marine clastic sedimentary rocks of the Khorat group were deposited later from evidences constructed landforms and morphology in the Wang Nam Khiao area in the present.

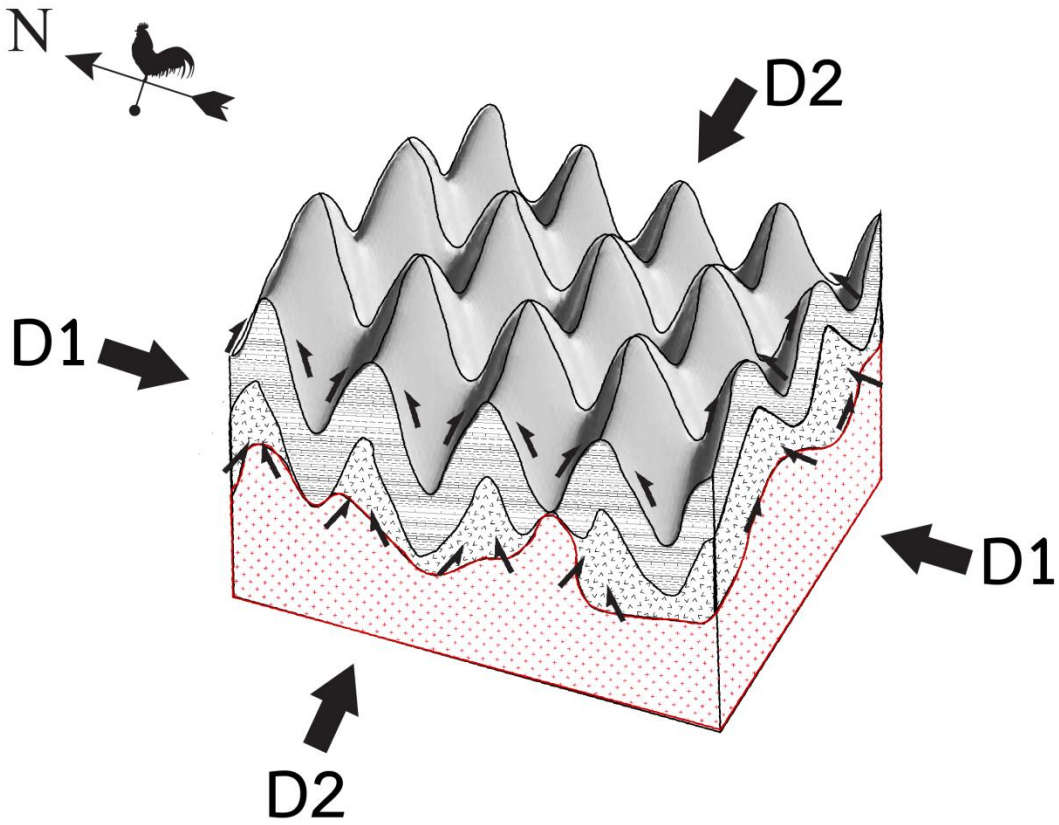


Figure 5.3 Structural model in Study area show flexural flow fold in domes and basins.

## 5.2 Conclusion

The structural geology in Amphoe Wang Nam Khiao can be separated to be two groups, and are composed of the Permian clastic rocks, the Permo-Triassic volcanic rocks, and the Triassic intrusive rocks in the NE part of the study area. The Triassic hornblende granite is orientated in ENE-WSW, ESE-WNW and NE-SW direction in contrast to the Triassic granite in the SW part of the study area, and the Mesozoic of the Khorat group that has an orientation in NW-SE direction. The microstructures are separated by the deformation. The Permian clastic rocks and the Triassic intrusive rock illustrate ductile deformation such as strain shadow, boudins, tapering edges of twins, and subgrain rotation. The Permo-Triassic volcanic rocks show brittle deformation and ductile deformation. Thus, the deformations in volcanic rocks are illustrated micro-folded, micro-fault, and kink bands. While, the Triassic hornblende granites have less deformation, the Mesozoic of the Khorat group are undeformed. Microstructure in the study area illustrated deformation except in the Khorat group. The structural evolution in Amphoe Wang Nam Khiao area began with the rifting in the Permian of the Indosinain I and thrust to north direction generated the structural orientation trend in the Permian clastic rocks in ENE-WSW, ESE-WNW and NE-SW. These structures are determined to be the first deformation ($D_1$) produced the first fold ($F_1$) and the second scenario during the Indosinian II in late Triassic. The second deformation ($D_2$) generated the second fold ($F_2$) in two evident, which were produced a dome and basin (egg carton) and the Mesozoic Khorat group deposited after late Triassic generated landform and structural geology in a present day.

## REFERENCES


Arboit, F., Collins, A.S., King, R., Morley, C.K., and Hansberry, R. 2014. Structure of the Sibumasu–Indochina collision, central Thailand: A section through the Khao Khwang Fold and thrust belt. Journal of Asian Earth Sciences 95: 182-191.

Barr, S.M., and Macdonald, A.S. 1987. Nan River suture zone, northern Thailand. Geology 15: 907–910.

Blenkinsop, T.G. 2000. Deformation Microstructures and Mechanisms in Minerals and Rocks Trans.). In (Ed.),^(Eds.), (ed., Vol. 1, pp. XII, 150). Springer Netherlands. (Reprinted from.

Booth, J.E., and Sattayarak, N. 2011. Subsurface Carboniferous – Cretaceous geology of Northeast Thailand. In Ridd, M.F., Barber, A.J., and Crow, M.J. (eds.), The Geology of Thailand, pp. 184–222. Geological Society, London: Geological Society.

Bunopas, S. 1981. Paleogeographic History of Western Thailand and Adjacent Parts of Southeast Asia: A Plate Tectonic Interpretation PARTII. Ph.D. thesis, Victoria University of Wellington Victoria University of Wellington, New Zealand, Victoria University of Wellington, New Zealand.

Chakraborty, K.R., and Metcalfe, I. 1995. Structural evidence for a probable Paleozoic unconformity at Kg Kuala Abang, Trengganu. Warta Geologi 21: 141-146.

Grasemann, B., Wiesmayr, G., Draganits, E., and Fusseis, F. 2004. Classification of Refold Structures. The Journal of Geology 112: 119-125.

Hada, S., Bunopas, S., Ishii, K., and Yoshikura, S. 1999. Rift-drift history and the amalgamation of Shan-Thai and Indochina/East Malaya blocks. In Metcalfe, I. (ed.), Gondwana Dispersion and Asian Accretion, pp. 7-87. A.A. Balkema, Rotterdam: A.A. Balkema, Rotterdam.

Kemlheg, S., and Vichidchalermpong, A. 1992a. Geological Map of Thailand BAN SAP NOI QUADRANGLE Trans.). In 2 (Ed.),^(Eds.), F5338 3 Sheet 5338 III (2 ed., Vol. pp.). Department of Mineral Resources, Bangkok, Thailand. (Reprinted from: 2013).

Kemlheg, S., and Vichidchalermpong, A. 1992b. Geological Map of Thailand BAN SUKHANG QUADRANGLE Trans.). In 2 (Ed.),^(Eds.), F5338 2 Sheet 5338 II (2 ed., Vol. pp.). Departmentof Mineral Resources, Bangkok, Thailand. (Reprinted from: 2013).

Metcalfe, I. 2002. Permian tectonic framework and palaeogeography of SE Asia. Journal of Asian Earth Sciences 20: 551-566.

Metcalfe, I. 2013. Gondwana dispersion and Asian accretion: Tectonic and palaeogeographic evolution of eastern Tethys. Journal of Asian Earth Sciences 66: 1-33.

Morley, C.K., Ampaiwan, P., Thanudamrong, S., Kuenphan, N., and Warren, J. 2013. Development of the Khao Khwang Fold and Thrust Belt: Implications for the geodynamic setting of Thailand and Cambodia during the Indosinian Orogeny. Journal of Asian Earth Sciences 62: 705-719.

Nakhonratchasima. 2016. general information of Changwat Nakhon Ratchasima. [Online]. Available from: www.nakhonratchasima.go.th/service/sammary.doc

Passchier, C.W., and Trouw, R.A.J. 2005. Microtectonics. Germany: Springer-Verlag Berlin Heidelberg.

Putthapiban, P., Vichidchalermpong, A., and Boonprasert, T. 1989a. Geological Map of Thailand AMPHOE WANG NAM KHIAO QUADRANGLE Trans.). In (Ed.),^(Eds.), F5337 1 Sheet 5337 I (2 ed., Vol. pp.). Department of Mineral Resources, Bangkok, Thailand. (Reprinted from: 2013).

Putthapiban, P., Vichidchalermpong, A., and Boonprasert, T. 1989b. Geological Map of Thailand BAN THA WANG SAI QUADRANGLE Trans.). In 2 (Ed.),^(Eds.), F5337 4 Sheet 5337 IV (2 ed., Vol. pp.). Department of Mineral Resources, Bangkok, Thailand. (Reprinted from: 2013).

Ramsay, J.G. 1976. Folding and Fractureing of Rocks. New York: McGraw-Hill.

Ramsay, J.G., and M.I., H. 1987. The techniques of modern structural geology volume2: Fold and Fractures. Academic press: Academic press.

Ridd, M.F. 2012. The role of strike-slip faults in the displacement of the Palaeotethys suture zone in Southeast Thailand. Journal of Asian Earth Sciences 51: 63-84.

Ridd, M.F., and Morley, C.K. 2011. The Khao Yai Fault on the southern margin of the Khorat Plateau, and the pattern of faulting in Southeast Thailand. Proceedings of the Geologists' Association 122: 143-156.

Roger, F., Maluski, H., Leyreloup, A., Lepvrier, C., and Truong Thi, P. 2007. U–Pb dating of high temperature episodes in the Kon Tum Massif (Vietnam). Journal of Asian Earth Sciences 30: 565–572.

Rowland, S.M., Duebendorfer, E.M., and Schiefelbein, I.M. 2007. Structural Analysis and Synthesis: A laboratory Course in Structural Geology. Blackwell Publishing Ltd.

RTSD. 1999a. Topographic Map AMPHOE WANG NAM KHIAO Trans.). In 7018, L. (Ed.),^(Eds.), Sheet 517-5337I (2nd–RTSD ed., Vol. pp.). Royal Thai Survey Department. (Reprinted from.

RTSD. 1999b. Topographic Map BAN SAP NOI Trans.). In 7018, L. (Ed.),^(Eds.), Sheet 448-5338III (2nd–RTSD ed., Vol. pp.). Royal Thai Survey Department. (Reprinted from.

RTSD. 1999c. Topographic Map BAN SUKHANG Trans.). In 7018, L. (Ed.),^(Eds.), Sheet 449-5338 (2nd–RTSD ed., Vol. pp.). Royal Thai Survey Department. (Reprinted from.

RTSD. 1999d. Topographic Map BAN THA WANG SA Trans.). In 7018, L. (Ed.),^(Eds.), Sheet 516-5337IV (2nd–RTSD ed., Vol. pp.). Royal Thai Survey Department. (Reprinted from.

Saesaengseerung, D., Agematsu, S., Sashida, K., and Sardsud, A. 2008a. A PreliminaryStudy of Lower Permian Radiolarians and Conodonts from the Bedded Chert along the Sra Kaeo Suture Zone, Eastern Thailand. in International Symposia on Geoscience Resources and Environments of Asian Terranes (GREAT 2008). pp. 189-191. Bangkok. Department of Geology, Chulalongkorn University, Bangkok.

Saesaengseerung, D., Sashida, K., and Sardsud, A. 2008b. Discovery of Middle Triassic radiolarian fauna from the Nan area along the Nan-Uttaradit suture zone, northern Thailand. Paleontological Research 12: 397-409.

Sashida, K., Adachi, S., Igo, H., Nakornsri, N., and Ampornmaha, A. 1997. Middle to Upper Permian and Middle Triassic radiolarians from eastern Thailand Trans.). In (Ed.),^(Eds.), Geological Sciences (ed., Vol. 18, pp. 1-17). University of Tsukuba: Science Reports of the Institute of Geoscience, University of Tsukuba. (Reprinted from.

Trouw, R.A.J., Passchier, C.W., and Siersma, D. 2009. Atlas of Mylonites - and related microstructures. Springer-Verlag Berlin Heidelberg.

Ueno, K., and Hisada, K. 1999. Closure of the Paleo-Tethys caused by the collision of Indochina and Sibumasu. Chikyu Monthly 21: 832–839

Wang, X.F., Metcalfe, I., Jian, P., He, L.Q., and Wang, C.S. 2000. The Jinshajiang-Ailaoshan Suture Zone, China: tectonostratigraphy, age and evolution. Journal of Asian Earth Sciences 18: 675-690.

# APPENDIX

# APPENDIX A
# SUPERPOSITION OF FOLDS

A region that has experienced more than one episode of deformation may show complex fold interference patterns in the field and on a geologic map. Consider the simple case shown in Figure A-1.The first generation of folding, $F_1$, produced folds with east–west-striking axial surfaces (Figure A-1(a)).The second generation of folding, $F_2$, produced folds with north–south-striking axial surfaces (Figure A-1(b)). It is clear that the east–west axial surfaces, $S_1$, developed before the north–south axial surfaces, $S_2$, because the $S_1$ traces have been folded while the $S_2$ traces are straight. Various fold interference patterns can occur, depending on the initial orientation of the $F_1$ fold hinge and its axial surface relative to the $F_2$ fold. Figure A-2 shows the four basic patterns that result from fold superposition. In each case the $F_2$ fold has a vertical axial surface and a horizontal hinge line. In type 0 interference pattern (Figure A-2(a)), both fold generations have parallel hinge lines and axial surfaces. Type 0 is so named because this type of superposed folding does not produce a recognizable interference pattern in the field; from the fold geometry alone, you would not know that two episodes of folding had occurred. Type 1 involves two sets of upright folds; the $F_1$ hinge lines and axial surfaces are perpendicular to the $F_2$ hinge lines and axial surfaces, resulting in a dome-and-basin (sometimes called ‘‘egg-carton’’) interference pattern (Figure A-2(b)). In type 2 interference folding, the $F_1$ folds have sub horizontal axial surfaces (recumbent folds); the $F_2$ hinge lines are oriented perpendicular to the $F_1$ hinge lines. This type of fold superposition results in complex mushroom-shaped and boomerang-shaped map patterns (Figure A-2(c)). In type 3 interference folding, the $F_1$ folds are also recumbent; however, in this case the $F_2$ hinge lines are parallel to the $F_1$ hinge lines (Figure A-2(d))(Rowland et al., 2007)

Grasemann et al. (2004) described Six end members of refold structures are distinguished, two of which are newly defined (Figure A-3): Type 1: Identical to the existing type1 refold structure frequently leading to dome-basin interference

patterns. Type 2: Identical to the existing type 2 refold structure frequently leading to domecrescent-mushroom interference patterns. Type 3: Identical to the existing type 3 refold structure frequently leading to convergent-divergent interference patterns. Type $0_1$: Newly defined refold structure, the shearing direction of the superposed fold is the direction of the initial fold axis. The shear planes are perpendicular to the axial plane of the initial fold. Neither the axial planes nor the folds axes of the initial and the superposed folds appear deformed, and the resulting refold structure is identical to the shape of the initial fold. However, a passive marker on the layer surface of the initial fold perpendicular to the fold axis, which is deformed by the second fold generation, clearly demonstrates the superposition of heterogeneous deformation. Type $0_2$: Newly defined refold structure. The shearing direction and the shear plane of the superposing fold are parallel to the initial fold axis and axial plane respectively. The resulting refold structure is identical to the shape of the initial fold. A linear passive marker on the initial fold surface normal to fold axis reveals the superposition of heterogeneous deformation. However, the deformation of the linear marker is clearly different from the finite deformation of type $0_1$. Type $0_3$: Renamed refold structure, which is identical to the traditional type 0 redundant superposition.

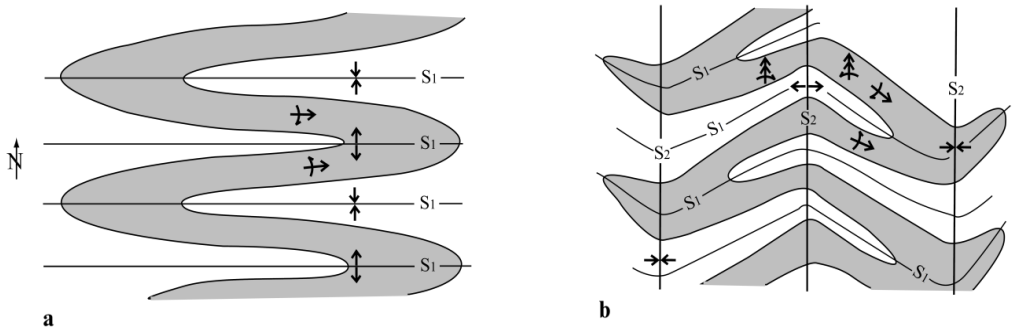


Figure A-1 Superposition of folding (top view). (a) First generation of folding ($F_1$). $S_1$ is the axial-surface trace of the $F_1$ folds; the symbols show the $F_1$ parasitic folds. (b) Map pattern after two generations of folding ($F_1$ and $F_2$). $S_2$ is the axial-surface trace of the $F_2$ folds, and double-headed arrows denote $F_2$ parasitic folds. (Modified after Rowland et al. (2007))

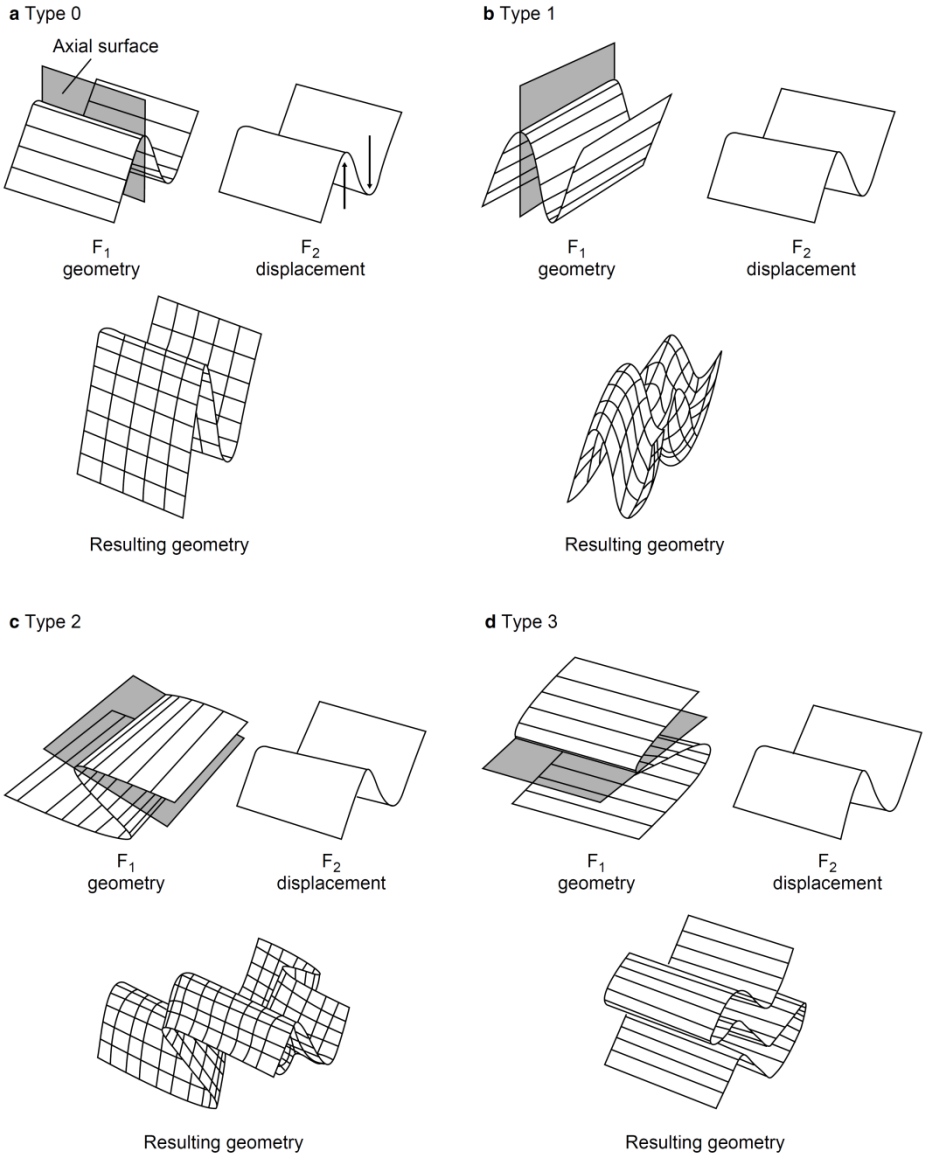


Figure A-2 Four basic pattern resulting the superposition of folds. In each case the orientation of the $F_2$ fold is the same, superimposed on variously oriented $F_1$ folds. (After Ramsay (1976))

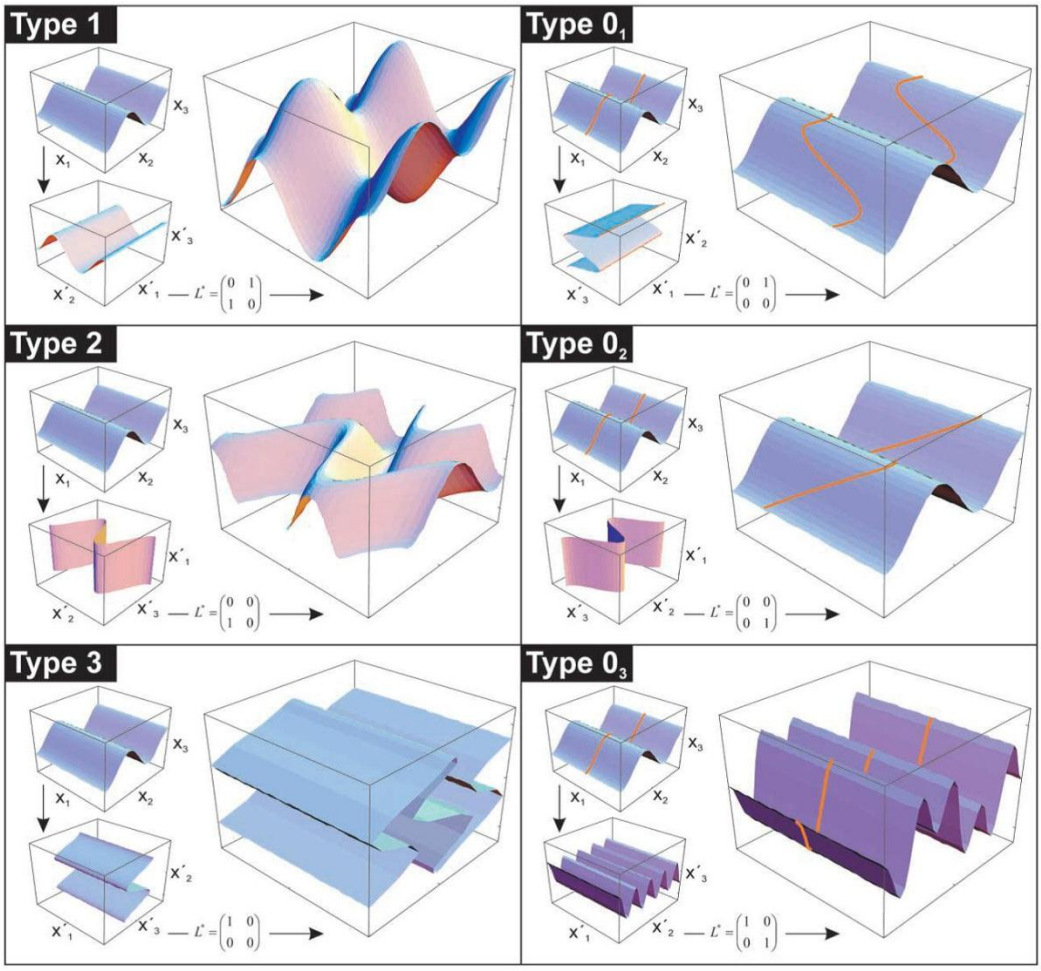


Figure A-3 Three-dimensional geometry of the six end-member refold structures. Marker lines on type $0_1$–$0_3$ refolds clearly reveal the different finite deformation recorded by the structures. In order to highlight the geometry of type $0_3$ refolds, the superposed fold has a three times shorter wavelength responsible for the second-order folds of the finite structure. (Grasemann et al., 2004)

# APPENDIX B

## MICROSTRUCTURES

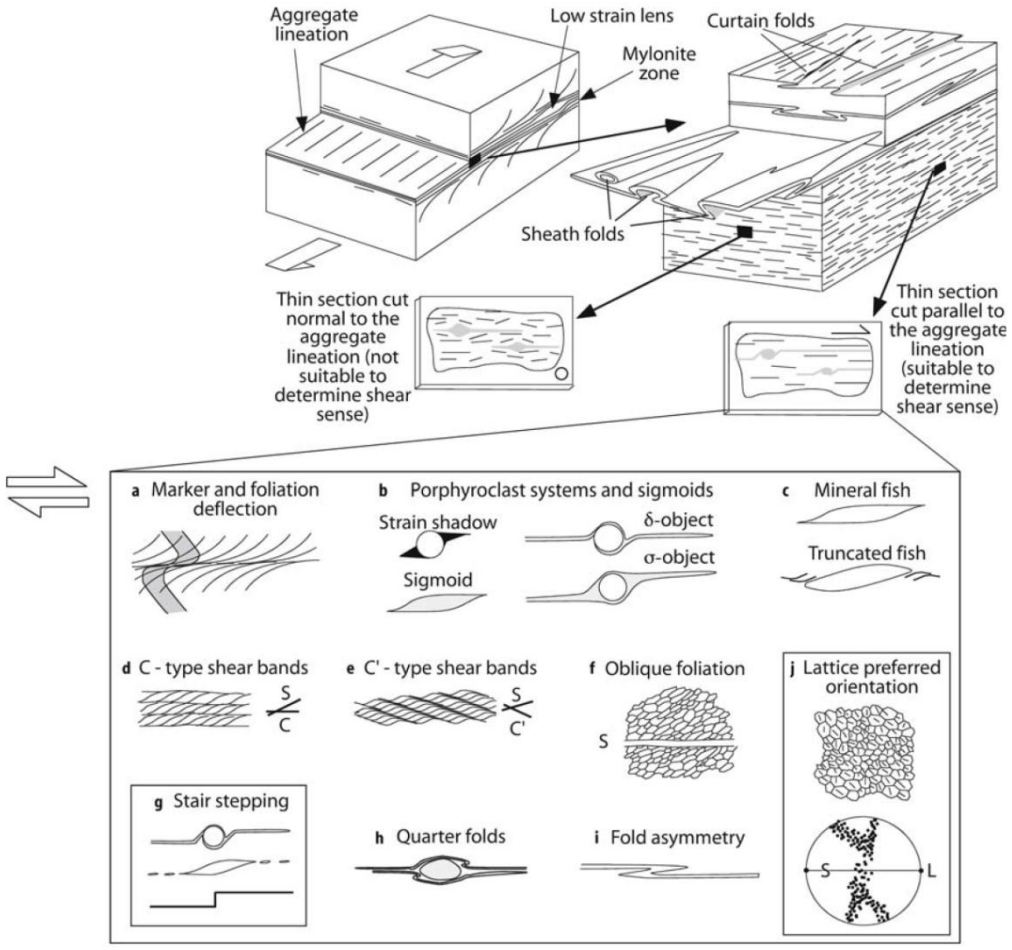


Figure B-1 Schematic diagram showing the geometry of a mylonite zone and the nomenclature used. For thin sections parallel to the aggregate lineation, the most common types of shear sense indicators are shown. (Modified after Passchier and Trouw (2005))

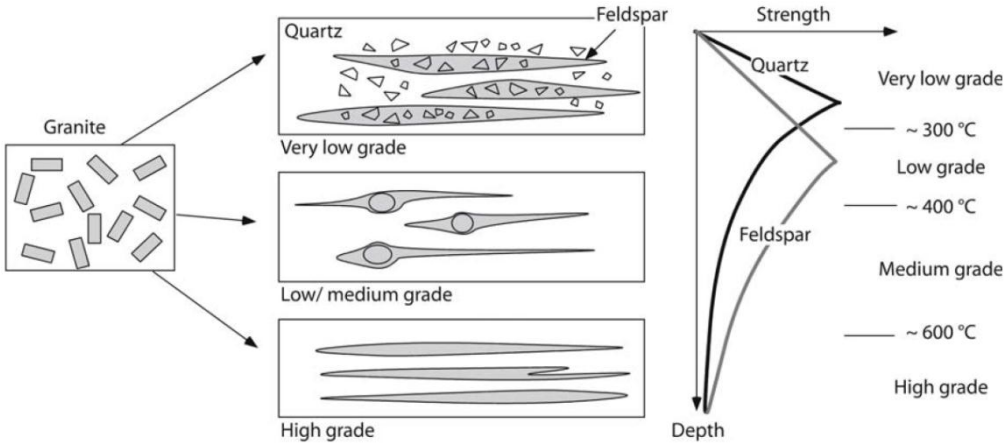


Figure B-2 Changes in the deformation behavior of quartz-feldspar aggregates with depth. At right, a depth-strength graph with brittle (straight line) and ductile (curved line) segments of quartz and feldspar is shown. At very low grade, both quartz and feldspar are brittle, but feldspar is the weaker mineral. At low to medium-grade conditions, quartz deforms by dislocation creep and feldspar is the stronger mineral, developing core-and-mantle structure and mantled porphyroclasts. At high grade, feldspar and quartz deform by dislocation creep and have similar strength.(Modified after Passchier and Trouw (2005))

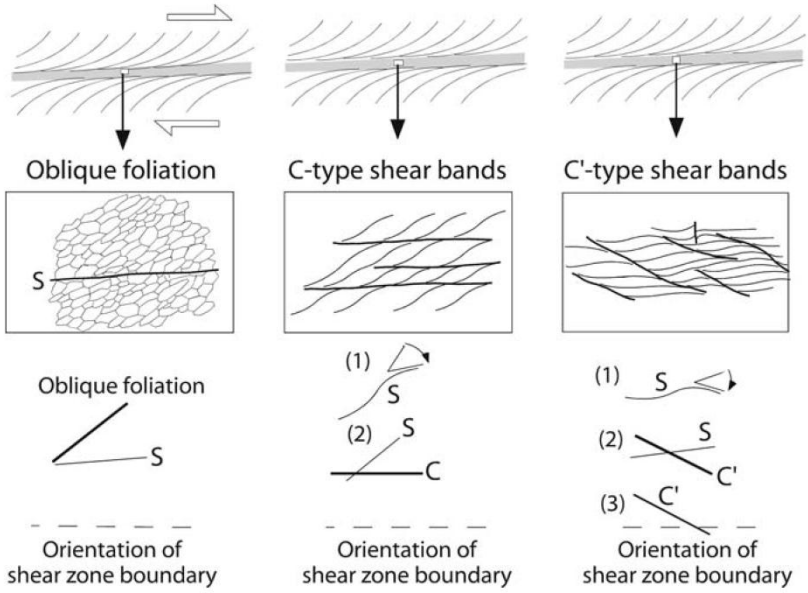


Figure B-3Three types of foliation pairs that are common in ductile shear zones. (Modified after Passchier and Trouw (2005))

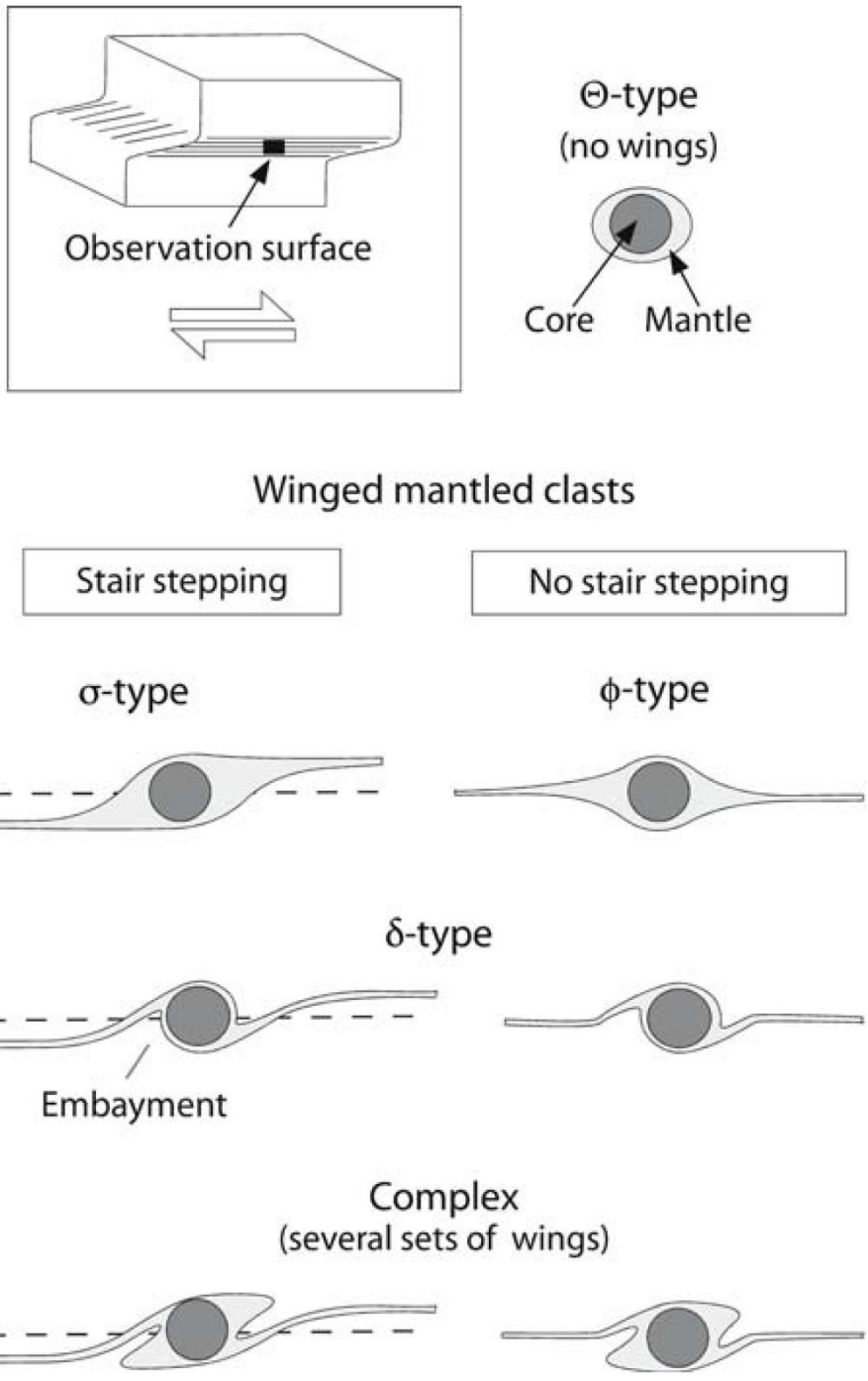


Figure B-4 Classification of mantled porphyroclasts. Dextral sense of shear. .(Modified after Passchier and Trouw (2005))

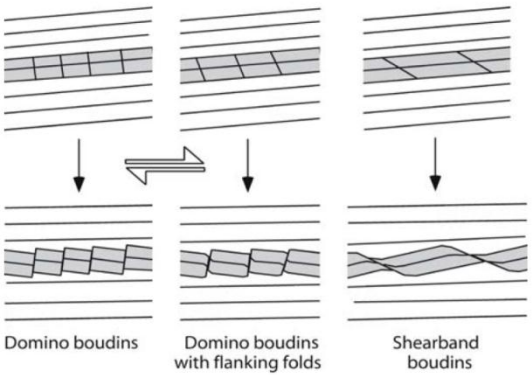


Figure B-5 Schematic presentation of the development of asymmetric boudins. (Modified after Passchier and Trouw (2005))

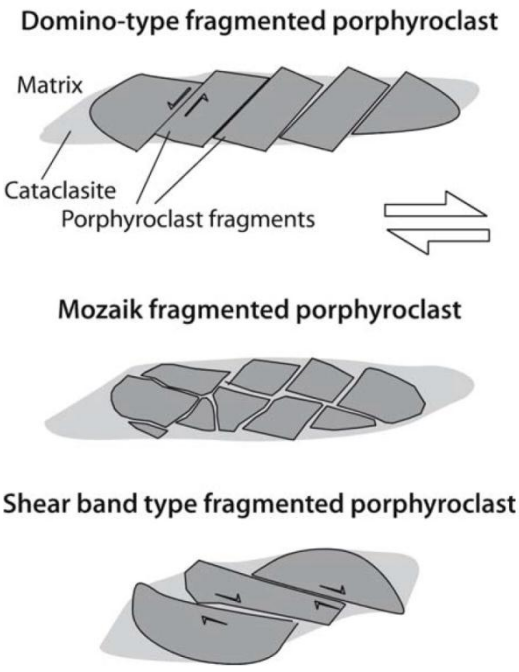


Figure B-6 Illustration of three types of fragmented porphyroclasts, and their interpretation in terms of bulk shear sense (large arrows) (Modified after Passchier and Trouw (2005)).

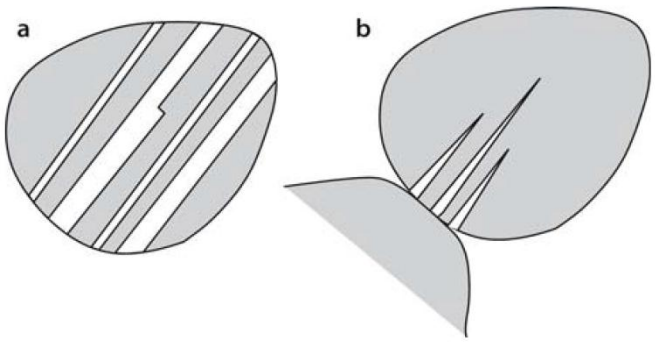


Figure B-7 (a) Growth twins in plagioclase with steps. (b) Deformation twins in plagioclase, with tapering edges nucleated on a high stress site at the edge of the crystal. (Modified after (Passchier and Trouw (2005)))

Deformation twins can commonly be distinguished from growth twins by their shape; deformation twins are commonly tapered, while growth twins are commonly straight and stepped. Twins may be restricted to certain parts of a crystal. Growth twins are commonly bounded by zoning, while deformation twins can be concentrated at high strain sites such as the rim of crystals or sites where two crystals touch each other. In plagioclase, growth and deformation twins occur. Deformation twins commonly taper towards the crystal center.

# APPENDIX C

## ATTITUDE OF STRUCTURAL DATA

Location system in sampling data is WGS84 UTM and orientation of foliations (f) and bedding planes (b)

1. Permian outcrops.

| ID | Longtitude (E) | Lattitude(N) | Strike | Dip | Dip direction | type |
|---|---|---|---|---|---|---|
| 9 | 796969 | 1591247 | 247° | 78° | 337° | b |
| 11 | 795973 | 1592226 | 181° | 75° | 271° | f |
| 12 | 795544 | 1593082 | 267° | 68° | 357° | f |
| 18 | 792801 | 1597160 | 48° | 68° | 138° | b |
| 29 | 803347 | 1592682 | 83° | 59° | 173° | f |
| 30 | 803465 | 1592946 | 96° | 72° | 186° | f |
| 31 | 801732 | 1595209 | 15° | 63° | 105° | f |
| 33 | 804242 | 1595104 | 96° | 63° | 186° | f |
| 41 | 788804 | 1608429 | 23° | 41° | 113° | f |
| 42 | 789880 | 1608813 | 9° | 50° | 99° | f |
| 43 | 789830 | 1609385 | 22° | 38° | 112° | b |
| 44 | 787959 | 1611504 | 38° | 64° | 128° | b |
| 47 | 789642 | 1612082 | 68° | 52° | 158° | f |

2. Permo-Triassic outcrops.

| ID | Longtitude (E) | Lattitude(N) | Strike | Dip | Dip direction | type |
|---|---|---|---|---|---|---|
| 4 | 798106 | 1601526 | 262° | 72° | 352° | f |
| 8 | 792801 | 1597160 | 48° | 68° | 138° | f |
| 31 | 801732 | 1595209 | 15° | 63° | 105° | f |

| ID | Longtitude (E) | Lattitude(N) | Strike | Dip | Dip direction | type |
|---|---|---|---|---|---|---|
| 32 | 805302 | 1594530 | 66° | 63° | 156° | f |
| 40 | 788293 | 1607218 | 109° | 12° | 199° | f |
| 46 | 788514 | 1611975 | 71° | 69° | 161° | f |
| 52 | 795707 | 1607935 | 68° | 41° | 158° | f |

3. Triassic outcrops.

| ID | Longtitude (E) | Lattitude(N) | Strike | Dip | Dip direction | type |
|---|---|---|---|---|---|---|
| 5 | 796647 | 1598844 | 141° | 71° | 231° | f |
| 14 | 792387 | 1601475 | 292° | 34° | 22° | f |
| 16 | 788496 | 1601951 | 263° | 67° | 353° | f |
| 25 | 797316 | 1603073 | 24° | 74° | 114° | f |
| 34 | 803775 | 1597165 | 55° | 51° | 145° | f |
| 39 | 789244 | 1603426 | 277° | 78° | 7° | f |

4. Triassic hornblende granite outcrops.

| ID | Longtitude (E) | Lattitude(N) | Strike | Dip | Dip direction | type |
|---|---|---|---|---|---|---|
| 13 | 794498 | 1599317 | 97° | 33° | 187° | f |
| 19 | 795707 | 1597962 | 226° | 62° | 316° | f |
| 27 | 795636 | 1597431 | 239° | 71° | 329° | f |
| 28 | 796216 | 1600554 | 105° | 63° | 195° | f |

5. Mesozoic Khorat group

| ID | Longtitude (E) | Lattitude(N) | Strike | Dip | Dip direction | type |
|---|---|---|---|---|---|---|
| 1 | 799824 | 1605200 | 298° | 10° | 28° | b |
| 3 | 799662 | 1604569 | 325° | 13° | 55° | b |
| 36 | 804108 | 1601160 | 286° | 6° | 16° | b |

| ID | Longtitude (E) | Lattitude(N) | Strike | Dip | Dip direction | type |
|---|---|---|---|---|---|---|
| 37 | 803935 | 1602099 | 337° | 8° | 67° | b |
| 48 | 792495 | 1614929 | 344° | 9° | 74° | b |
| 49 | 793346 | 1613838 | 341° | 10° | 71° | b |
| 51 | 794560 | 1609883 | 333° | 3° | 63° | b |
| 53 | 808682 | 1596294 | 305° | 12° | 348° | b |
| 54 | 808612 | 1595056 | 334° | 8° | 64° | b |

# VITA

Mr.Tirawut Na Lampang was born on April 29, 1984 in Chiang Mai province in the northern of Thailand. He graduated B.Sc. in geology from Department of Geology, Faculty of Science, Chiang Mai University in 2007. His experience after graduated, the first year he worked in ThungKum gold mine at Loei province. Afterwards, he had worked for the mineral exploration and Geophysics companies until year 2010. He has been worked in the Royal Irrigation Department in position a geologist in geology division, office of topographical and geotechnical survey. Then, He studies in Master's degree with thesis topic in "Structural Geology in Amphoe Wang Nam Khiao Area, Changwat Nakhorn Ratchasima" department of geology, faculty of science, Chulalongkorn University.